MELTING and SOLIDIFICATION
of
ZINC-ALUMINIUM ALLOYS

submitted by

LEONARD WALTER CRANE

for the degree of

Doctor of Philosophy

THE UNIVERSITY OF ASTON IN BIRMINGHAM

March 1997

SUMMARY

Following a scene-setting introduction are detailed reviews of the relevant scientific principles, thermal analysis as a research tool and the development of the zinc-aluminium family of alloys.

A recently introduced simultaneous thermal analyser, the STA 1500, its use for differential thermal analysis (DTA) being central to the investigation, is described, together with the sources of support information, chemical analysis, scanning electron microscopy, ingot cooling curves and fluidity spiral castings.

The compositions of alloys tested were from the binary zinc-aluminium system, the ternary zinc-aluminium-silicon system at 30%, 50% and 70% aluminium levels, binary and ternary alloys with additions of copper and magnesium to simulate commercial alloys and five widely used commercial alloys. Each alloy was shotted to provide the small, 100mg, representative sample required for DTA.

The STA 1500 was characterised and calibrated with commercially pure zinc, and an experimental procedure established for the determination of DTA heating curves at 10°C per minute and cooling curves at 2°C per minute. Phase change temperatures were taken from DTA traces, most importantly, liquidus from a cooling curve and solidus from both heating and cooling curves.

The accepted zinc-aluminium binary phase diagram was endorsed with the added detail that the eutectic is at 5.2% aluminium rather than 5.0%. The ternary eutectic trough was found to run through the points, 70% Al, 7.1% Si, 545°C; 50% Al, 3.9% Si, 520°C; 30% Al, 1.4% Si, 482°C. The dendrite arm spacing in samples after DTA increased with increasing aluminium content from 130μm at 30% to 220μm at 70%. The smallest dendrite arm spacing of 60μm was in the 30% aluminium 2% silicon alloy. A 1kg ingot of the 10% aluminium binary alloy, insulated with Kaowool, solidified at the same 2°C per minute rate as the DTA samples. A similar sized sand casting was solidified at 3°C per minute and a chill casting at 27°C per minute. During metallographic examination the following features were observed: heavily cored α phase which decomposed into α' and α'' on cooling; needles of the intermetallic phase $FeAl_4$; copper containing ternary eutectic and copper rich T phase.

Differential thermal analysis (DTA); Scanning electron microscope (SEM); Cooling curves; Fluidity; Zn-Al-Si eutectic trough.

ACKNOWLEDGEMENTS

I am extremely grateful to Dr. Sam Murphy for overseeing the project, giving professional advice and a great deal of friendly encouragement.

I am also grateful to the Vice Chancellor, Professor Mike Wright, for having sufficient faith when Head of Department, to support an unusual venture and endorse my application for Registration.

Many thanks to two members of the technical support staff, namely, Roger Howell for advice and assistance with the operation of the SEM, and Dave Farmer for first class work in the foundry when preparing the alloys and helping with the ingot cooling and fluidity tests.

Finally, thanks to Dr. John Penny, the Head, and all members of the Department, for allowing me a free run of facilities, even after retirement, and putting up with my overbearing enthusiasm.

CONTENTS

FIGURES

TABLES

1. INTRODUCTION

Zinc base alloys are used mainly in the form of die castings. The important features of such alloys are low cost, excellent castability and the ability to use cheap, carbon steel dies. Zinc metal is weak and brittle, so alloying additions are made to increase strength and toughness without unduly raising the melting point.

A family of die casting alloys, widely used for many years, has various combinations of additions, usually of copper, 0.25-1.25%, aluminium, 3.5-4.5% and small amounts of magnesium. The attractiveness of die casting has been further advanced by the recent development of a series of zinc base alloys with relatively large additions of aluminium, up to 30%. Although initially intended for sand and permanent mould casting, it was found that the alloys could be successfully die cast. Strength, hardness and wear resistance are all improved relative to the conventional alloys referred to earlier, and there is a useful reduction in density. Further benefits are obtained by small additions of copper, silicon, magnesium or manganese. In certain applications, alloys of this type have shown excellent bearing properties and are replacing other established alloys such as brass, bronze and even cast iron, for slow-speed, high-load bearings.

The original alloys developed in the 1920 decade were basically zinc-rich aluminium-zinc binaries, with small additions of other elements. With improvements through minor changes in composition and processing, the market for the alloys was gradually widened over a period of sixty years. In the last fifteen years the new, lighter alloys with higher aluminium content, have broadened the application of zinc-based alloys. Substantial silicon additions are also of interest for several reasons, for example they may give,

* a reduction in the melting point of an alloy
* a possible reduction in the solidification range
* an increase in melt fluidity
* a reduction in density
* a further improvement in bearing properties

In order to encourage wider use of the family of zinc-based alloys, it is essential that the solidification characteristics of individual alloys are precisely understood. It is essential for the development of casting alloys, that for each alloy, the onset of solidification and the solidification range are known. Also, knowledge of any solid state transformations would be invaluable in predicting the final dimensions of a casting on cooling to room temperature. There is a considerable amount of information on the constitution, microstructure, mechanical properties and foundry behaviour of the zinc-rich binary alloys. A study of the Zn-Al-Cu system was published by Koster et al, in 1941. Since then, many publications on the topic have emerged, but there is still little known about the solidification characteristics of the newer alloys of actual or potential commercial value. It is frequently said at conferences that there is still not a full understanding, even of the relevant binary alloys. Thus, there is a need for accurate constitutional information on a range of zinc-based alloys with 30-70% aluminium, and additions of Si, Cu, Mn and Mg.

In order to study fully the constitution and microstructure of an alloy after differing thermal histories, several sophisticated characterisation techniques are required. Thus, the main objective of the project described here was to use differential thermal analysis (DTA) to establish the melting and solidification behaviour of zinc-aluminium binary alloys, zinc-aluminium-silicon ternary alloys, ternary alloys with additions of copper and magnesium, and several ZA commercial alloys. Support information would be obtained mainly from optical and electron microscopy, including semi-quantitative analysis of microstructural phases.

2. LITERATURE REVIEW.

The main objective of the project was to characterise the solidification of selected zinc-base alloys, in order to contribute to the scientific understanding of the behaviour of members of a family of commercial pressure die casting alloys. It was anticipated that the fundamental knowledge gained would be of practical value in the optimisation for industrial use of several of the alloys in the family.

As part of the experimental programme, the phase changes that occur in alloys during the heating of the solid, melting, solidification and cooling of the solid were studied in detail. Thus it was necessary to explore the fundamental aspects of the solid and liquid states, and also of phase changes occurring in those states.

Early theories were based on the initial thought that atomic movement in a solid metal is restricted, but on melting, the atoms move around relatively freely. However, much evidence quickly emerged to show that as melting occurs, there is very little change in the atomic arrangement.

It was considered that there are three features of the liquid state that differentiate it from the solid state and therefore represent the entropy of fusion, namely,

* atom separation distances are greater
* lack of long range order in atomic arrangement
* amplitude of atomic vibration is larger

Although atoms may diffuse more rapidly in the liquid than in the solid state, the measured rates of diffusion in liquid metals indicate that atoms must perform many vibrations in one position, before moving on. In other words, in an instant of time, relatively few atoms are in a state of transience and it is acceptable to assume that a liquid metal consists of a non-ordered array of vibrating atoms.

2.1 The liquid state

The fundamental approach to the study of the behaviour of matter is to consider it as a macroscopic system consisting of a large number of species (atoms or molecules). In order to be able to proceed, it is necessary to study the behaviour of an individual atom or molecule, under a variety of circumstances. This step is feasible for gaseous and solid matter, but not for liquid. The structure of a gas is sufficiently open and diffuse to allow the assumption that an individual specie is not interacting with any others. In a solid, there is both short and long range order, and displacements are similar in magnitude to the size of the atoms. Thus, although the interactions between neighbouring atoms are large, a coordinate transformation exists to allow each atom to be considered independently. In effect, the pictures of the gaseous and solid states are near to "ideal". Any departures from the ideal states are readily accounted for in quantitative models by the introduction of small corrections. Also, since metals are monatomic, the structural models of gaseous and solid states are relatively simple. In a liquid, the atomic structure is not sufficiently irregular to be able to take a gaseous approach, but is too irregular to allow coordinate transformations to be used. Thus a body of liquid must still be viewed as a complex, multi-species, dynamic system.

The structural features and the physical and chemical properties of crystalline solid and gaseous states were well understood a hundred years ago. However, the behaviour of a metal crystal when it melts, and the properties of the resultant liquid, are still something of a mystery. Nineteenth century scientists, having recognised the existence of entropy, readily perceived that changes in entropy were occuring in all natural processes. There was sufficient understanding of thermodynamics to allow the calculation of the changes in entropy that occurred during a wide range of processes. But the acceptance of the concept and the possibility of calculating the absolute entropy of a system, was problematical. Early in the twentieth century, Tetrode (1) used a statistical approach to relate the entropy, S, of a monatomic gas to the multiplicity of states of its atoms, ϖ, in the following way,

$$S = k \log \varpi$$

where k is the Boltzman constant. At the same time, it was realised that using the Debye theory of the heat capacity of solids (2), it was possible to determine the absolute entropy of a crystal from the relationship,

$$S = \int_0^T \frac{C_p}{T} dT$$

In striking contrast, the status of the liquid state in this context, is still not fully resolved.

Some early workers looking at entropy of fusion, became interested in resistivity comparisons. From first principles, it was considered that a pure, crystalline solid metal should be a perfect conductor of electricity. But the existence of "irregularities" in the lattice, due to the thermal motion of atoms, creates resistance. For a given statistical pattern of displacements from lattice rest positions, the resistivity of the metal is proportional to the mean square displacement, which is directly related to temperature. Even with all the atoms stationary, a liquid metal would still offer resistance because of the lattice distortion. Thus it is the additional resistivity, due to thermal motion of atoms, that is directly related to temperature. It was considered possible to estimate the relative amplitude of atom vibration in the two phases, solid and liquid, by studying the change of resistivity with temperature.

In 1934, Mott (3) published the results of resistivity measurements on molten metals, concluding that the entropy of fusion is entirely due to the change in vibrational frequency of the atoms on melting. That is, for one g atom of metal,

$$S_L - S_S = 3R \ln \frac{v_S}{v_L}$$

where, S_L = entropy of liquid
S_S = entropy of solid
v_L = resistivity of liquid
v_S = resistivity of solid
R = gas constant

He implied that the structure of a liquid metal with atoms at rest is so little distorted from that of a solid crystal that there is no appreciable change in resistivity. He also stated that a

liquid metal with no atomic vibrations would have zero entropy and resistivity. In 1939, after further work and thought (4), he accepted that even with no atomic vibrations the lattice distortion in the liquid metal represents entropy, and modified his theory accordingly.

At the same time Fowler and Guggenheim (5), using computational thermodynamics, concluded that the entropy of fusion is due to "randomness" in the location of the atom rest positions within the lattice of the molten metal. In contrast to Mott, they stated that the difference in vibrational frequencies of atoms in the solid and liquid states is very small, and makes only a minor contribution to the entropy.

A few years later, Gamertsfelder (6) used X-ray diffraction to study several low melting point pure metals and observed that the number of nearest neighbours of an atom in the molten metal ranged from 8.4 to 10.8. This confirmed the view already expressed that the atomic structure of a melt was little different from that of the solid. It also tied in with the known fact that when a metal melts, it expands only by about ten percent. Having studied the published information, Lumsden (7) opted for a compromise and suggested that vibrational frequency and lattice distortion make equal contributions to the entropy of fusion.

Important phase changes in materials are solid-to-liquid and liquid-to-vapour. Energy is required to effect those phase changes, manifested by the respective latent heats. The differences between liquid and vapour states are large and clear. The latent heat of vaporisation is much greater than the latent heat of fusion. This is strong evidence that when a solid crystal melts, the immediately formed liquid is physically similar to the solid.

Although there is considerable evidence to show that the structural differences between solid and liquid states are relatively small, it is clear that the mechanisms and thermodynamics involved in the transformation of a solid into a liquid are quite different from those involved in the reverse transformation.

2.2 The solid state

The metallic solid state has been extensively researched and is well understood. Metallic solids are crystalline, consisting of a regular array of atoms exhibiting long range order, having a characteristic structure determined by the lowest energy configuration of the system. Most metals are polycrystalline, having a large number of mosaic blocks or grains. Each grain has a crystalline form and is normally randomly orientated with respect to neighbouring grains. Grain boundaries, being irregularities in the crystal structure, strongly influence the physical and chemical behaviour of the solid mass. The crystalline structure within grains is not perfect, and other forms of irregularity also strongly influence physical and chemical properties. The crystal imperfections may be itemised as ,

* point defects - interstitial and substitutional atoms as impurities or alloying elements, vacant sites

* linear defects - edge and screw dislocations

* boundaries - external surfaces, interphase boundaries, intergrain boundaries, stacking faults

2.3 Solidification and melting

The characteristics of the melting of an alloy and its subsequent solidification to form an ingot or a component are of prime importance to a foundry technologist. Those characteristics are also important to the applied scientist performing thermal analysis experiments in order to gain an understanding of phase relationships in an alloy.

Solidification

When a cooling liquid metal reaches the solidification temperature, it will not solidify. Some degree of undercooling is invariably necessary to provide a sufficient driving force for solid to form, and the process of solidification to proceed. In addition the solid state must be nucleated, an event which is also not instantaneous at the solidification temperature. Often in practice, a considerable amount (tens of degrees K) of undercooling may occur prior to the onset of the solidification process. The degree of undercooling is directly related to the rate of cooling of the liquid. Thus, when studying the solidification characteristics of alloys by thermal analysis, very slow rates of cooling are used to minimise the degree of undercooling experienced. Even accepting these observations, the convention is to use the symbol, T_m, to represent both the melting and solidification temperatures.

In a given system during cooling, the Gibbs free energy of the solid phase is lower than that of the liquid phase, when T_m is reached, which provides a driving force for solidification. However, it is the nucleation of the solid phase that determines the instant and therefore the temperature, when solidification starts. In theory, as the temperature of the liquid falls towards T_m, transient groups of atoms form, with greater cohesion and coordination than the atoms in the bulk liquid. At T_m the groups stabilise to become nuclei, and then grow as solid deposits on them. In practice, if the liquid is pure and free from "foreign" particles, nucleation will not occur in the manner described above. Considerable undercooling will be necessary to allow homogeneous nucleation of the solid to occur. However, in most real situations, the solid nucleation mechanism is heterogeneous, with a minimum of undercooling. If, at the time when solidification should start, there are solid surfaces available which are wetted by the liquid, conditions are favourable for stable nuclei to form on those surfaces. The surface nucleation sites may be on inclusions present in the liquid, or more commonly on the walls of the container holding the liquid. At a slow rate of cooling with heterogeneous nucleation, solidification will occur at T_m.

Melting.

In a recent book, Porter and Easterling (8) suggested that Professor Robert Cahn, in a letter to Nature in 1978 (9), summarised succinctly the state of scientific knowledge, after briefly discussing the more popular theories of melting. In the "dislocation theory", Mackenzie and Mott in 1952 (10), proposed that at the melting temperature a catastrophic

increase in dislocation density disrupts the solid crystal and converts it to liquid. Cotterill, Kristensen and Jenson (11,12), used computer simulation to support the theory that an explosive increase in the population of expanding dislocation loops, "cut the crystal structure to pieces" at the melting point. The creation of large numbers of vacant sites where the dislocations intersect, adds to the opening up of the structure and thus enlarges the state of disorder and increases entropy.

A vacancy model of melting was offered by Frenkel in 1930 (13). He proposed that heating a solid crystal increases the vacancy concentration and when a critical value of 0.37% is reached, there is an instantaneous creation of "holes", (Frenkel's term), representing the passage from solid to liquid. The energy required to form the additional vacancies, or holes, is manifested by the latent heat of fusion. The model explains the frequently observed increase in specific heat at constant pressure, which relates to an increase in the coefficient of thermal expansion. It follows that the specific heat at constant volume may decrease slightly on melting.

A Polish scientist, Gorecki, published several papers (14,15,16) giving strong support to the Frenkel model. For example, by using gamma radiation treatment on several metals, he demonstrated that the melting point was lowered by an amount directly proportional to the dose of radiation, that is, the number of extra vacancies created. However, as Cahn pointed out, the mechanisms involved in the increase in vacancy concentration from the critical level of 0.37% in the solid, to about 10% in the liquid, are not explained. The dislocation model does offer a mechanism for the volume change, but there is still the problem of explaining the observation that all metals melt at about the same vacancy concentration.

Cahn referred to the experiments of Fukushima and Ookawa (17) who used a soap bubble raft to simulate the atomic arrangement in a metal. The experiments supported the view that vacancies in the solid become more diffuse as temperature increases, rather than increasing in number. Groups of vacancies merge to become an area of reduced atomic density. Increase in temperature was simulated by increasing the amplitude of vibration of the bubbles. Eventually, at high vibration levels, the raft "melted". It was noticed that within the raft, as the melting temperature was approached, there existed regions of anomalously high vibrational amplitude, which could have triggered the destruction of the lattice. This observation countered the objection to the vacancy model, that an overall vacancy concentration of 0.37% is too low to affect the stability of the crystal lattice. Finally, Cahn referred to a theoretical study (18) of the size and concentration of holes in metallic glasses. He suggested that there is a parallel between the glass transition and melting in the context of a vacancy model. At the same time he pointed to a possible weakness in the Frenkel/Gorecki model, namely, the assumption that the holes in the molten metal are the same size as those in the solid. Even as an approximation, that assumption would seem to be invalid. In the opinion of the writer, Frenkel does imply a size difference by referring to "gaps" in the solid lattice, and (much larger) "holes" in the liquid.

Following from the comments made above and those made in the previous section, the question is, when a solid metal melts, will it normally occur at T_m, or will overheating

be necessary to initiate the melting process? We know that latent heat of fusion must be supplied to allow the phase change from solid to liquid. However, this does not necessarily imply a rise in temperature above T_m. Since nucleation of the solid phase is so important in solidification, it would be expected that nucleation of the liquid phase is a significant factor in melting. Consider a mass of solid which is being uniformly heated, at constant pressure. When T_m is reached, the first liquid to form should be on an outer surface, if only to accommodate the volume increase. This event is also predicted by thermodynamic considerations. Below T_m, the solid phase exists in equilibrium with the vapour phase, with an interfacial energy of γ_{SV}. When liquid is formed, further interfacial energies arise, namely, γ_{SL} and γ_{LV}. It is known that ,

$$\gamma_{SL} + \gamma_{LV} < \gamma_{SV}$$

with a wetting angle $\theta = 0$. A zero wetting angle reflects the close constitutional similarity of the liquid and solid phases at T_m.

Thus, as pointed out by Porter and Easterling (8), there is always a driving force for the formation of liquid phase on the surface of a solid, even before T_m is reached. Nucleation is not a problem. Thus, the melting of a solid metal invariably occurs at the equilibrium melting temperature T_m, even at relatively fast heating rates. This is useful information when planning thermal analysis experiments, and implies that the solidus of an alloy obtained from a heating curve will be preferable to that obtained from a cooling curve.

The solid/liquid interface.

Most solid/vapour interfaces tend to be atomically close packed, flat and relatively smooth, representing the boundary between a high density solid phase and a low density gas phase. A solid/liquid interface may be similar in structure to the solid/vapour interface, with a narrow (say one or two atoms thick) transition zone between the solid phase and the liquid phase. However, there are solid/liquid interfaces that have a broad, atomically diffuse transition zone.

In thermodynamic terms, instead of a sharp change at the interface, both enthalpy and entropy change gradually over many interatomic distances. Topographically, that type of interface is deeply stepped. At T_m, the higher enthalpy of the liquid phase is balanced by the increase in entropy, so that solid and liquid phases have the same free energy and can exist together. At the interface, the balance is disturbed, giving rise to an excess free energy, designated γ_{SL}. The type of interface formed in a given system will be the one with the lowest free energy. According to Jackson (19), the optimum interface depends on the relationship between T_m and L_f, the latent heat of fusion. For most metals, the liquid/solid interface is diffuse and the ratio of L_f to T_m is constant, designated R by Jackson. Some metals deviate from constancy, with higher L_f to T_m ratios, and above 4R, have flat interfaces. Non metals and semi metals have particularly high values of R and flat interfaces. The model may be applied to the liquid/vapour interface by using L_S, the heat of sublimation. A high value of the ratio, R, is obtained for most materials, correlating with the observed prevalence of flat interfaces. Finally, providing further evidence of the strong driving force for the formation of liquid phase when a solid metal

is heated, it has been shown experimentally (20) that the following approximate relationship applies,

$$\gamma_{SL} = 0.45\gamma_b = 0.15\gamma_{SV}$$

where γ_b is the grain boundary free energy.

Heat capacity and heat content.

The molar heat capacity, C, of a substance is the amount of heat required to raise the temperature of one mole, one degree Kelvin. The heat capacity increases with rising temperature, starting with zero at zero Kelvin. Thus it is necessary to define an incremental heat capacity as,

$$C = \frac{dQ}{dT}$$

where Q = quantity of heat energy, and
T = temperature in degrees Kelvin.

The heat capacity per unit of mass (one kilogramme), known as the specific heat, c, is similarly defined.

The actual quantity of heat involved in a change in the state of a system, brought about by a change in temperature, will also depend on changes in other variables such as pressure and volume. In other words, heat capacity is an extensive variable. Experimentally, the heat capacity of a substance, be it gas liquid or solid, is most readily determined at constant pressure. The symbols used are C_P and c_P. The relationship between the heat capacities at constant pressure and constant volume, C_p and C_v, is,

$$C_p - C_v = VT \frac{a^2}{b}$$

where a = coefficient of cubical expansion,
b = coefficient of compressibility,
T = temperature K, and
V = volume.

A rule presented by Dulong and Petit (21), demonstrates the expected fundamental basis of heat capacity. The rule states that the atomic heat of an element, being the product of specific heat and atomic weight, at room temperature is about 6.2 cal (26 joule)/°C. As noted earlier, the value increases with rising temperature and with metals is always about 7.5 cal (31 joule)/°C at the first phase change. Again, it is useful to know that the heat capacity of an alloy may be reliably estimated using the values for the constituents, and applying the rule of mixtures (22).

Thus, for constituent metals 1 and 2,

$$C_{alloy} = f_1C_1 + f_2C_2$$

where f_1 and f_2 are the atomic fractions of the constituents.

The total heat content, or enthalpy, H, of a substance is defined by the equation,

$$H = E + PV$$

where E = internal energy,

P = pressure, and

V = volume.

Like heat capacity, enthalpy is an extensive variable. It is only possible to measure changes in enthalpy, not absolute values. Therefore any set values of enthalpy must have an arbitrary zero at a selected temperature. Conventionally H is zero for a pure element in its most stable state at 298K (25°C). The relationship between heat capacity and enthalpy is given by,

$$C_P = \left[\frac{dH}{dT}\right]_P$$

Thus, enthalpy values may be obtained from graphical or numerical integration of the variation of heat capacity with temperature, provided there is no other thermal event involved, such as latent heat of a transformation. The problem is unlikely to arise since it is very difficult to determine heat capacity experimentally near to an invariant transformation point. Thus,

$$H = S^T C_P dT$$

also,

$$\frac{C_p}{T} = \left[\frac{dS}{dT}\right]_p$$

Taking entropy as zero at zero K,

$$S = \frac{S^T}{T}\frac{C_p}{dT}$$

Combining equations, it follows that,

$$dG = - S\,dT + V\,dP$$

but at constant pressure, dP = 0, so,

$$\frac{dG}{dT} = - S$$

This means that G decreases with increasing temperature at a rate given by - S.

Considering the solid and liquid states of a metal, illustrated graphically in Figure 1, the solid state will have a lower enthalpy than the liquid at low temperatures, due to stronger atomic binding. However, at high temperatures the higher entropy of the liquid dominates, mainly due to greater freedom of atomic movement. On balance, as temperature increases, the Gibb's free energy of the liquid falls at a faster rate than that of the solid. At the melting point, both phases have the same value of Gibb's free energy, and can exist together, in equilibrium at constant temperature.

As discussed later, the change in heat capacity following a transformation, such as solid to liquid, is of interest when using thermal analysis techniques to establish phase relationships in an alloy.

2.4 Thermodynamics and phase transition

Prime objectives of the research being presented, were to assess the accuracy of published data relating to the melting and solidification of alloys in the zinc-aluminium

binary system and to explore regions of the silicon containing ternary system. To achieve those objectives it is essential to understand the fundamental aspects of phase equilibria and transformations occurring in the alloys. Thermodynamics is a powerful tool for the study of the relationships between phases and the attainment of equilibrium.

Gibb's Phase Rule

The Rule states that, in a system at equilibrium,

$$F = C - P + 2$$

where F = number of degrees of freedom,

C = number of components, and

P = number of phases

If the pressure remains constant, the Rule becomes,

$$F = C - P + 1$$

The Gibbs Phase Rule, put forward over a hundred years ago, is an essential tool for researchers. When in doubt about the status of a system in equilibrium, applying the phase rule will usually resolve the problem.

Equilibrium

When the variables of a system are changed, phase changes may result. In an alloy (a system), a particular phase may change to become a new phase or a mixture of phases. Alternatively, several phases may combine to form a single phase. The driving force for any phase change is the attainment of a more stable system, or in other words, a reduction in the internal energy of the system. For transformations that occur at constant temperature and pressure, the stability of a system is determined by its Gibb's Free Energy G and,

$$G = H - TS$$

where H = enthalpy and

S = entropy

as previously explained,

$$H = E + PV$$

When dealing with condensed phases, such as liquid and solid metal, the term PV is very small relative to the size of E, and may be ignored. This is a useful approximation as will be seen later. A system is said to be in equilibrium when it is in its most stable state, that is, there is no impetus for change, even over a very long period of time. In a closed system, that is fixed in composition and mass, at constant temperature and pressure, the most stable state is defined as having the lowest possible Gibb's Free Energy, or in mathematical terms, $dG = 0$.

In a given system, as the variables change, the atomic arrangement changes and G fluctuates, usually showing several minima. The lowest value of G represents the stable state of the system, and the other energy minima are metastable states. The intermediate states are unstable. When studying an alloy system, unstable states remain for such short time intervals that they are rarely observed experimentally. Metastable states normally exist for a sufficient length of time to be characterised experimentally, and are frequently

as significant as stable states when seeking an understanding of the behaviour of a system. Any transformation is possible if it results in a reduction of G, in other words, the change in G, dG, is negative. The transformation need not be direct, but can pass through one or even a series of metastable states. It is also possible for a metastable state to exist for such a long time that for all practical purposes it is classed as stable.

Thermodynamics is concerned with the likelihood of a change taking place in a system. The rate at which any change proceeds must be assessed using kinetics. Understandably, temperature is an important variable in kinetic studies.

Single component systems

For a proper understanding it is essential to start at the beginning and examine a single component system subject to varying temperature at constant pressure. Consideration will be given to the heating of a pure solid metal to above the melting temperature and the subsequent cooling through solidification, down to ambient temperature.

As discussed earlier, if a pure metal is heated from absolute zero temperature the enthalpy will increase at a rate determined by its heat capacity, and free energy will decrease at a rate determined by the entropy. By considering the behaviour of both solid and liquid states as the temperature changes, it is possible to define the equilibrium melting point of the metal, as shown graphically in Figure 1. At T_m, heat supplied to the system does not raise the temperature, but satisfies the need for latent heat of fusion.

The basic principles discussed above may be applied to the more complex interactions arising in alloy systems.

2.5 The zinc base alloys

Alloy development

When reviewing the development of the zinc base alloys, a particularly useful source of information was the publication by the International Lead Zinc Research Organisation Inc. (23).

A range of zinc base, pressure die casting alloys, designated by the trade name Zamak, was introduced towards the end of the 1920 decade. The attractions of the alloys to the foundryman were,

* low melting point
* good fluidity
* low energy consumption
* no adverse effect on the steel dies
* suitable for the hot chamber process, allowing high production rates,

and to the product designer,

* low cost, particularly for thin walled castings
* good dimensional control in small castings
* low draft angles
* excellent surface finish on castings
* good machinability.

The negative aspects related to the marketing of these alloys were high density, a

resistance to use on the expectation of very poor mechanical properties and problems with atmospheric corrosion. The most popular alloys in the range offered were (and still are), Zamak 3 and Zamak 5. As can be seen in Table 1, the alloying additions are aluminium, copper and magnesium. Initial applications were "non-engineering", indeed the alloys were mainly used for making decorative articles, such as cheap jewellery. However, once the excellent mechanical properties were properly publicised, applications broadened considerably to include the lower levels of structural engineering components, such as gears for kitchen appliances.

The next major development did not occur until the end of the 1970 decade, with the introduction of a range of alloys, designated ZA, with additions of up to 27% aluminium. The compositions of the most widely used alloys, ZA 8, ZA 12 and ZA 27, are given in Table 1. The benefits over the established zinc base alloys may be summarised as,

* suitable for the whole range of casting processes
* feasibility of using forging and extrusion processes
* lower density
* better atmospheric corrosion resistance
* even better machinability
* improvements in most of the mechanical properties
* suitability for non - sparking applications (with alloys of < 11% aluminium)
* excellent bearing properties.

On the last mentioned point, the ZA alloys proved to have better wear and bearing properties than the current industry standard SAE 660, lead-tin bronze. The natural lubricity and relatively high hardness of ZA alloys eliminated the need for bushings and wear inserts in small components. Thus secondary fabrication operations were often not needed, giving considerable cost savings

In the new alloy range, addition of copper and magnesium was retained on the basis of the already proven benefits. A significant feature of the development and launch of the ZA range of alloys was the accompanying large increase in the interest of research metallurgists in the topic of zinc base alloys. The growth in research interest has been maintained in subsequent years. Prior to the birth of the ZA range of alloys, there was very little interest in the scientific aspects of zinc base alloys, but over the last ten years, research groups have emerged all over the world, in particular in Birmingham, England.

The logical next step in development was taken about ten years ago, when a new range of alloys, designated COSMAL, was launched. In those alloys, the aluminium content was much increased, and ranged from 40% to 60%, and substantial levels of silicon were added. The alloys were developed specifically for pressure die casting, with bearings as the intended, primary application. Apart from the obvious lower density, there was also claimed to be improved strength, higher hardness, better creep resistance and enhanced damping capacity compared with existing alloys.

Metallurgical structures

Of prime importance when researching and developing alloys for commercial applications

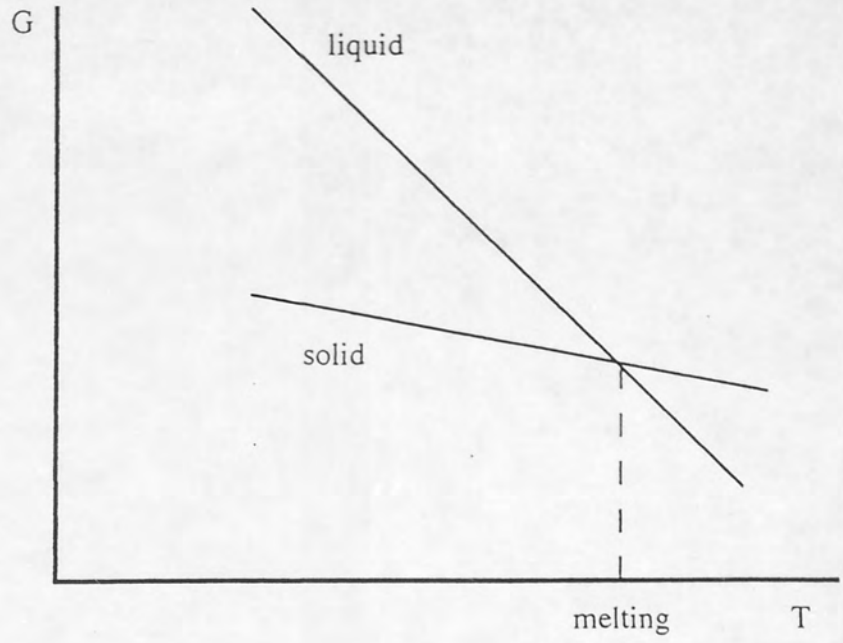

Figure 1 Changes in molar free energy G, with temperature T.

Alloy designation	Additions %			
	Al	Cu	Mg	Others
Zamak 3	4	0.25	0.03	-
Zamak 5	4	1	0.05	-
ZA 8	8	1	0.03	-
ZA 12	12	1	0.03	-
ZA 27	27	2	0.02	-
Cosmal	40	1	-	3 Si, 0.3 Mn
Super Cosmal	60	1	-	6 Si, 0.3 Mn

Table 1 Nominal compositions of commercial zinc base alloys

are the microstructures developed at intermediate stages of processing and in the finished state. Understandably, microstructural aspects were a significant part of the study to be described later.

The current consensus of opinion is that in the zinc-aluminium binary system, a eutectic reaction occurs at 5% aluminium and 380°C, and a peritectic reaction at 28.5% aluminium and 443°C, as shown in Figure 2. Thus, the microstructure of the Zamak alloys consists of primary dendrites of the zinc rich, η phase, with an interdendritic eutectic of $\beta + \eta$, the β of which decomposes eutectoidally to form aluminium rich α with η on cooling. Slow cooling will create a coarse structure, leading to very poor mechanical properties, but the rapid rate of cooling during die casting gives a fine structure and often, surprisingly good mechanical properties. Indeed, pressure die cast small components have a particularly fine structure and excellent mechanical properties. This partly explains the wide use of that process. Sometimes, graphite chills are inserted into dies to further increase cooling rates in particular regions of a casting. Due to the presence of copper, there are also small amounts of ε phase, the intermetallic compound, $CuZn_4$ in the microstructure. Also, due to changes in solid solubility, precipitation of zinc from the aluminium rich α phase may occur at room temperature. Thus the alloys offer the propensity to age harden. Relatively small additions of magnesium were found to give a considerable increase in strength, but with an accompanying decrease in ductility. Numerous attempts have been made by researchers to establish the hardening mechanism, so far with no success. Some workers claim that the presence of magnesium protects an alloy from the various forms of brittle failure, such as stress corrosion.

Alloys ZA8 and ZA12 solidify with primary dendrites of β phase, which decompose on cooling to $\alpha + \eta$. The interdendritic regions are occupied by the eutectic. Observations made earlier regarding the effects of cooling rates apply also to these alloys. Comments made about the presence of copper and magnesium, and changes in solid solubility, also apply.

The COSMAL alloys are very new and information on them is limited. The results obtained by the writer, to be presented and discussed later, are relevant. A particular feature of the solidification of this type of alloy is the severe coring which occurs, even during relatively slow cooling. Thus, experiments have shown that the last liquid to solidify in a 40% aluminium alloy is likely to have a composition in the region of the peritectic reaction, certainly not expected from a study of the equilibrium phase diagram.

An impurity common to all of the alloys, is iron. Thus needles of the intermetallic compound, $FeAl_3$ may be seen in microstructures.

Alloy phase diagrams

The components.

The research was focussed mainly on a portion of the zinc-aluminium-silicon system. Those elements differ considerably in physico-chemical properties. Thus, before discussing the systems, it is necessary to examine in detail, the components. Table 2 presents the relevant properties of the component elements.

Property	Zinc	Aluminium	Silicon
Atomic number	30	13	14
Atomic weight	65.4	27.0	28.1
Periodic group	2b	3b	4b
Crystal system	CPH	FCC	DIAM
Melting point, K	693	933	1683
Enthalpy of fusion, J g^{-1}	113	395	1653
Density, solid, Mg m^{-3}	7.14	2.70	2.32
Density, molten, Mg m^{-3}	6.70	2.40	-
Atomic radius, nm	0.133	0.143	0.118
Valence	2	3	4
Electronic structure	Ar $3d^{10}4s^2$	Ne $3s^2 3p^1$	Ne $3s^2 3p^2$
Linear expansivity, 10^{-6} K^{-1}	29.7	23.0	2.6
Specific heat, J g^{-1} K^{-1}	0.4	0.9	0.7
Thermal conductivity, W cm^{-1} K^{-1}	1.13	2.38	1.48
Lattice parameter, nm	0.494	0.405	0.543
Surface tension, mJ m^{-2}	750	850	1560
Viscosity, centipoise	3.17	2.89	-

Table 2 Properties of the elements

Binary zinc-aluminium

Published information about solidification characteristics and equilibrium phase relationships of zinc-aluminium alloys first appeared eighty years ago (24, 25). As more papers were published, there was good agreement on the liquidus line, and the general size and shape of the phase fields in the binary phase diagram. Several of the early workers also agreed on the presence of a peritectic reaction at a temperature of 443°C, and 72% zinc (24 - 28). Later workers began to doubt the existence of the peritectic. In 1935, Owen and Pickup (29) used a high temperature X-ray technique to study the lattice parameter changes of phases, and concluded that the peritectic reaction did not occur. One year later, Fink and Willey (30) described experiments using resistivity measurements and optical metallography, again concluding that the peritectic did not exist. Two years later, Gayler and Sutherland (31) used a range of experimental techniques to confirm the absence of a peritectic, although a thermal arrest in cooling curves was observed at 443°C. However, Professor Hume-Rothery took an interest in the topic and made a contribution to the discussion of the paper. He re-analysed the data presented and pointed out that, when based on cooling curves only, there was an inflection in the liquidus at 443°C, and a two phase field might exist between 67 and 68% zinc.

Probably the most accurate representation of the binary diagram was obtained by combining the work of Elwood (32,33), and Presnyakov et al (34) who used X-ray diffraction to measure the lattice parameters of phases present in selected powder samples, and Goldak and Parr (35), who used a similar experimental technique, with high purity solid samples. Each worker concluded that a peritectic reaction did occur, and there was good agreement on the phase boundaries. As mentioned earlier, the rest of the diagram was already well established. The resulting diagram, shown in Figure 2, was incorporated into phase diagram texts, such as the one by Elliott (36). Strangely, although it would appear that the existence of the peritectic reaction was well proven, several subsequent publications by both researchers and reviewers, contain the non-peritectic diagram. Recent examples are a research paper from China (37), and the ASM Handbook (38)

An interesting feature of the alloy system is the occurrence of solid state immiscibility in alloys with between 50 and 70% zinc, at around 350°C. Looking at the characteristics of the pure metals, presented earlier, it is not surprising that a "lack of attraction" occurs near the centre of the diagram. The monotectoid region is relatively small, and some researchers have observed that the difference in lattice parameter between the α' and β phases is small, and suggest ignoring the presence of the miscibility gap.

Finally, depicted at either side of the diagram, there is a reduction in the solid solubility of both zinc in aluminium and aluminium in zinc as the temperature falls to ambient. In the case of the aluminium rich alloys, the solubility line is not clearly defined. Indeed, the writer attempted to locate that phase change in the aluminium rich alloys tested, with no success. As mentioned in the review of commercial alloys, the decrease in solid solubility with temperature provides the commercially exploited age hardening capability in zinc rich alloys.

Recently, Zahra et al (39), published a "contribution" to the Zn-Al phase diagram.

The apparent motivation for the work was the existence of "two types of diagram". The authors used differential scanning calorimetry, DSC, to study an aluminium-60% zinc alloy. The conclusions were that an α'' phase (peritectic β phase in the Elliott diagram), does not arise, and the eutectoid reaction at 340°C does not occur. Referring to the work of Goldak and Parr (35), they note the very small, (0.001×10^{-10}m), difference in lattice parameters between the α' and α'' phases, implying that, even if the reaction does occur, it is undetectable and of little consequence.

Binary aluminium-silicon

The equilibrium phase diagram shows a simple eutectic, with small amounts of solid solubility at each end. The diagram was established many years ago, and there has been little dissension over the years. In some recent work by Mey and Hack (40), phase boundaries obtained by computational thermodynamics were compared with experimentally determined diagrams. For aluminium-silicon, good agreement was found. The generally accepted diagram, due to Philips in 1959 (41), is shown in Figure 3.

Binary zinc-silicon

Looking at the characteristics of the pure elements, one would not expect much mutual solubility, or indeed interaction. Even so, alloying investigations were made as far back as 1857 (42, 43, 44). The general consensus was that with substantial superheat, some silicon did dissolve in molten zinc, but it precipitated out completely on slow cooling to room temperature. Vigouroux (45) used an electric furnace for experimentation, with very limited success due mainly to the vaporisation of zinc. For interest, the writer experimented in the foundry with a "plunge" technique to introduce a zinc-silicon powder compact into superheated molten zinc. The only noticeable result was the vast quantity of zinc oxide. There was no apparent metallurgical interaction and after two attempts, the project was abandoned. In 1904, Moissan and Siemens (46) prepared melts of zinc saturated with silicon at temperatures between 600 and 850°C. Each melt was quenched from the test temperature and a chemical analysis made of the silicon content of the zinc. The results ranged from 0.06% at 600°C to 1.62% at 850°C. Thirty years later, Jette and Gebert (47) attempted to make alloys and used X-ray diffraction to measure the lattice parameters of phases in samples taken from the melts. They concluded that there was no mutual solubility in the alloy system. In 1960, Thurmond and Kowalchik (48) held a known weight of molten zinc at a particular temperature in contact with an ingot of silicon, also of known weight. The loss in weight of the silicon was taken as the amount dissolved in the zinc at the test temperature. The workers claimed that their results indicated the presence of a eutectic reaction at 0.04% silicon and a temperature of 0.2°C below the melting point of pure zinc. The claim demonstrates commendable confidence in the capability of the experimental equipment, but is difficult to accept. Trumbore (49), studied published information, selected the best value of the various distribution coefficients and calculated the solubility of zinc in silicon as ranging from 6×10^{-6} at % at 1000°C to 1.8×10^{-5} at % at 1400°C.

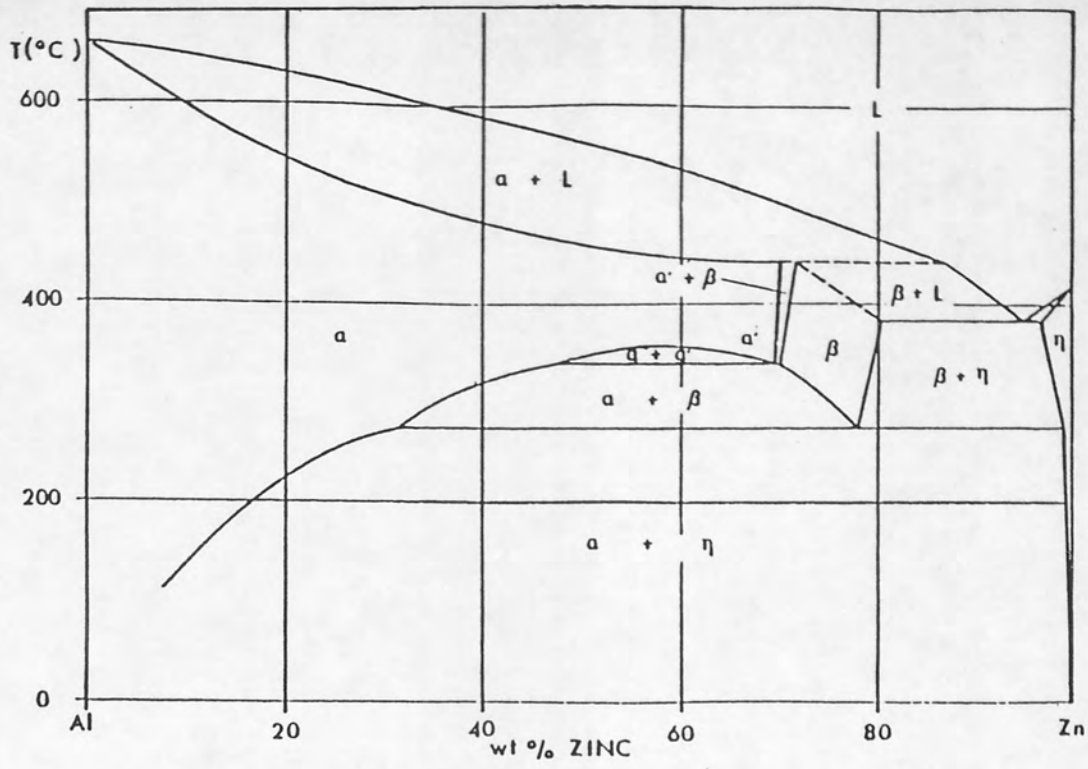

Figure 2. The zinc-aluminium phase diagram

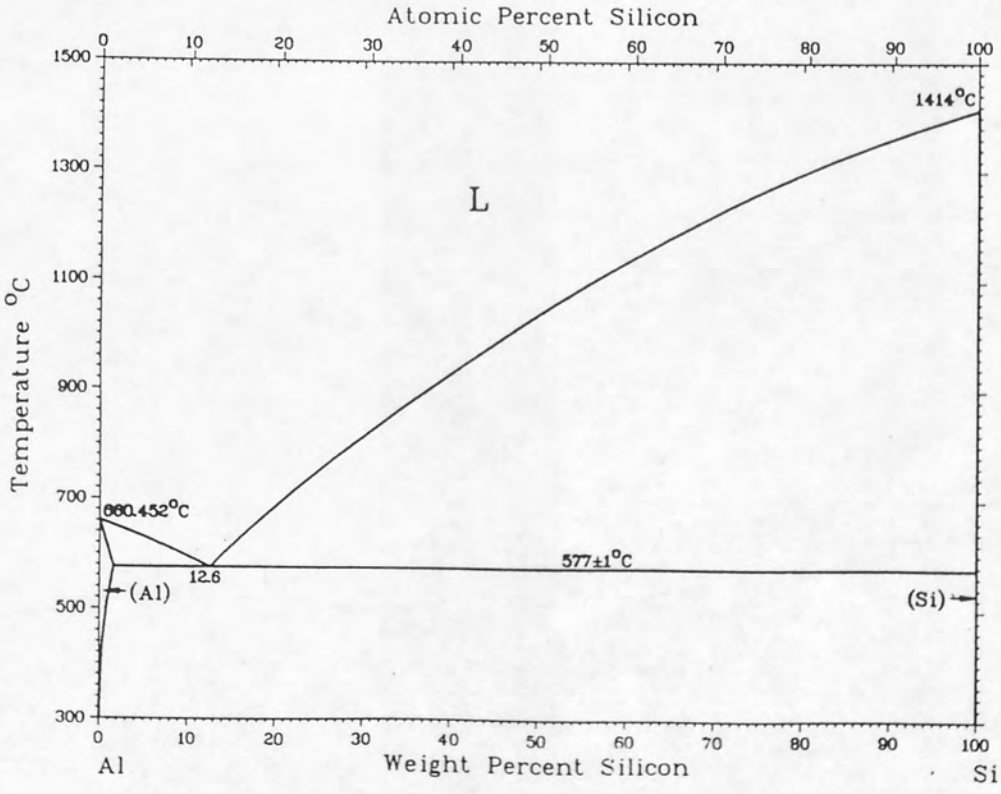

Figure 3 The aluminium-silicon phase diagram

Based on the observations above, it is generally accepted that the system is treated as having no mutual solubility of the component elements.

Ternary Zn-Al-Si

The computational work of Mey and Hack (40), referred to earlier, included an analysis of available experimental data for the ternary Zn-Al-Si system. They demonstrated good agreement between calculated and experimental data and claimed minor improvements to the accuracy of some of the phase boundaries. Of particular interest, they presented a liquidus surface diagram, Figure 4, detail of the liquidus surface near to the ternary eutectic, Figure 5, and isothermal sections at various temperatures, Figure 6.

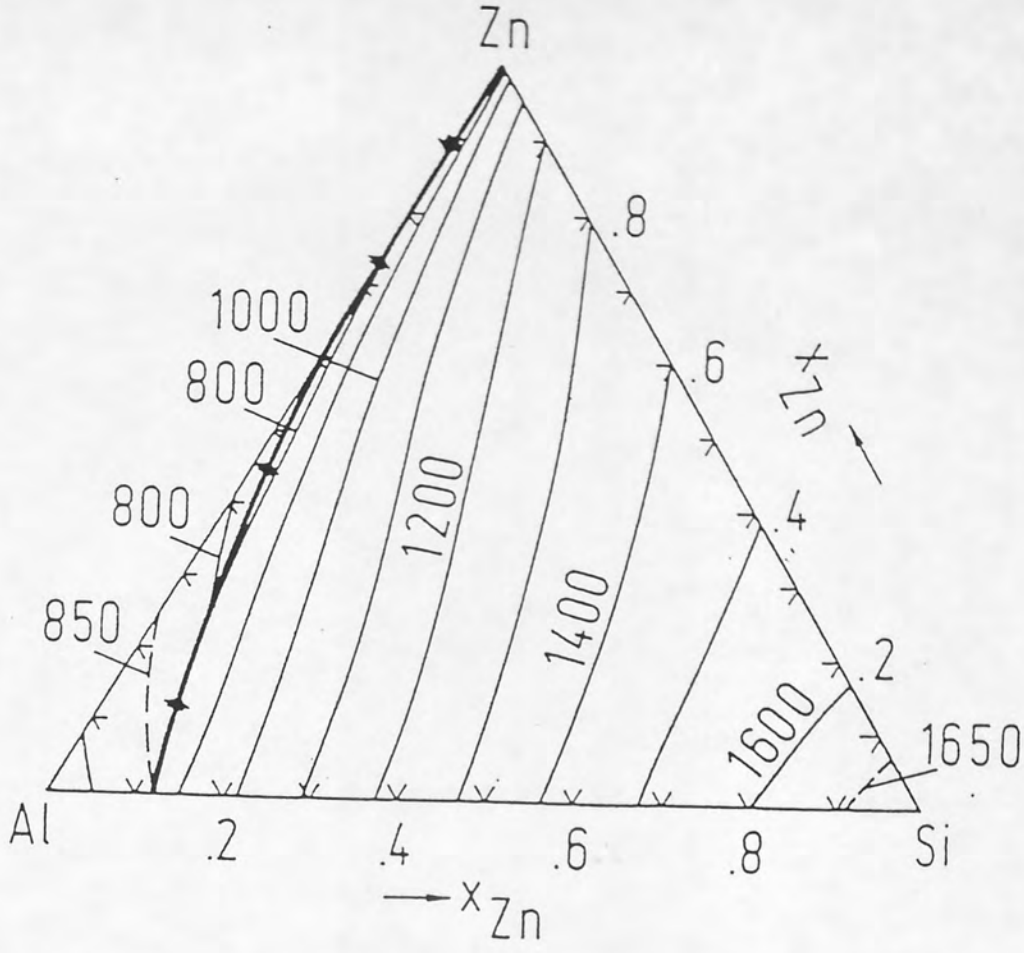

Figure 4 Liquidus surface of the zinc-aluminium silicon system

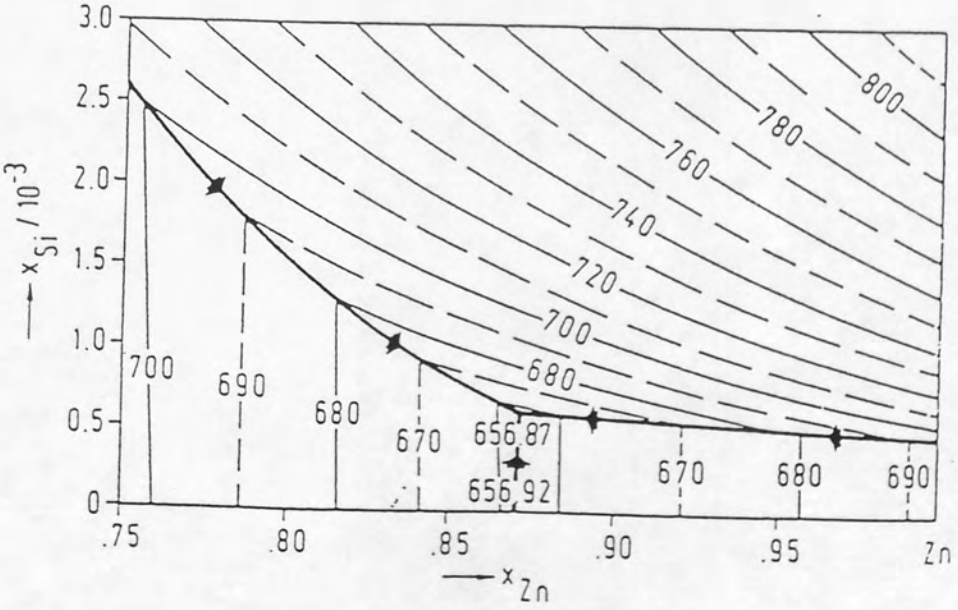

Figure 5 Section of the liquidus surface, zinc rich corner of the Zn-Al-Si system

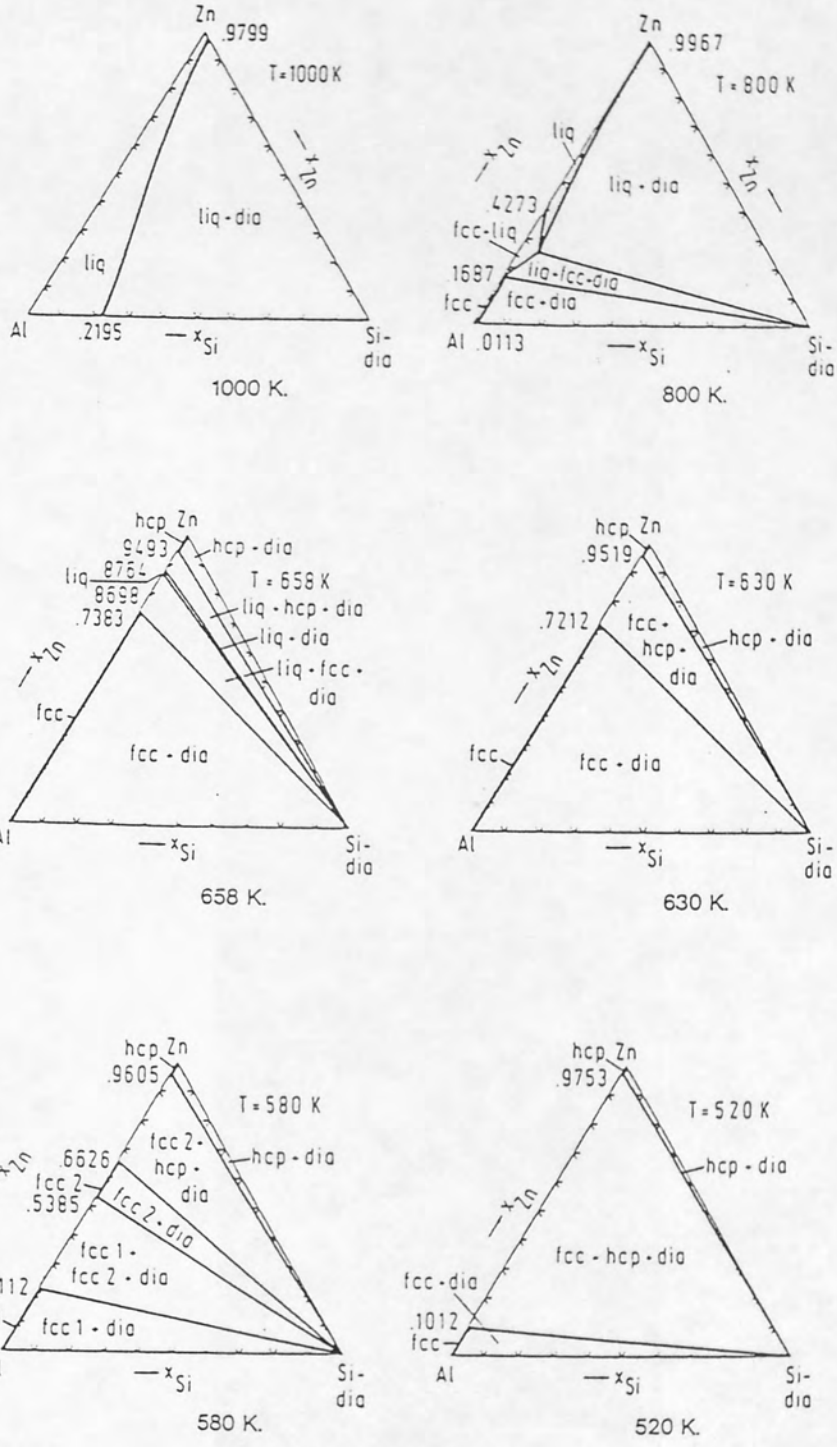

Figure 6 Isothermal sections of the Zn-Al-Si system at various temperatures

3. THERMAL ANALYSIS

In the first chapter of a recently published book (50), Warne expressed the need to recognise a distinction between the two different ways of applying thermal analysis. His view is that a "method" is used to determine a single parameter, such as changes in weight with temperature, ie thermogravimetric (TG). A "technique" is the result of developments and modifications to a method. Thus, simultaneous thermal analysis (STA), is a technique where TG can be performed at the same time as differential thermal analysis (DTA). Thermal analysis methods were used regularly by research metallurgists as long as sixty years ago, but full recognition of the value of thermal analysis has occurred only during the past twenty years. Indeed, in the last five years, there has been a rapid increase in use, and a considerable broadening of applications. The introductory chapter of the book referred to earlier (50), lists twenty four methods of thermal analysis in regular use. Some reasons for the recent expansion may be itemised as,

* the establishment of sets of fully certified reference materials
* the introduction of new, sophisticated methods and techniques
* the introduction of microprocessors for equipment control, data collection and data manipulation
* the publication of detailed, specialised books
* the recognition by industry of the value of thermal analysis

On the last point, the writer has tested alloys for a jewellery maker, assisted with research into the deterioration of concrete in motorway bridges and considered the use of STA for the development of solid wire-drawing lubricants.

At the end of his introduction to thermal analysis, Warne commented that, "the use of cooling curves, although well documented, does not seem to be nearly as widely used as would be expected". Endorsing that view, Sale and Taylor, in another chapter of the same book, entitled "Applications in Metallurgy and Material Science", did not even mention cooling curves. In addition, when commenting on the study of metals and alloys, they only covered the solid state, and made no reference to melting and solidification. It is true, however, that the recent publications describing studies of alloy constitution, referred to in Chapter 2, reported the use of a wide variety of experimental techniques, other than cooling curves. These observations supported the use in this research programme, of sharply defined and extremely accurate heating and cooling curves for the investigation of transformations in zinc base alloys.

When preparing a review of thermal analysis, of the numerous texts available, the writer found three of particular value. The editors of the book referred to earlier (50), have been operating a thermal analysis consultancy service for a number of years. The book provides detailed analyses, by respected specialists, of the most commonly used techniques in a variety of fields of application. A chapter on "Thermal analysis" by Woodhead, in the well known book edited by Chalmers and Quarrell (51), analyses the fundamental scientific and mathematical bases of examples taken from a wide range of techniques. The third book by Todor (52), gives descriptive but very practical, detailed appraisals of selected techniques.

3.1 Cooling curves.

When a transformation takes place in a metal at constant temperature, there will be an evolution or absorption of latent heat of transformation, and/or a change in specific heat. Thus, if a sample of metal is heated or cooled under controlled conditions and a record made in the form of a curve of time lapsed and temperature, phase changes will be revealed either by inline discontinuities or changes in the shape of the curve. The determination and interpretation of such curves is one of the experimental methods encompassed by the term Thermal Analysis.

The simplest approach is to place a sample carrying a thermocouple in a heating environment, such as a furnace, subject the sample to a thermal cycle, and record the temperatures of sample and furnace at appropriate intervals of time. Simple precautions would be, to ensure a uniform temperature distribution in the sample ($< 0.1°C$ variation) and a slow rate of change of temperature (1-2°C/min).

It was soon established by early experimenters that inverse rate cooling curves were more informative, with more sharply defined thermal events, than direct cooling curves. However, the method suffered from lack of accuracy because readings were taken at finite temperature intervals, say every 2°C, rather than continuously as with a direct curve. If undercooling occured, which was often the case, the inverse rate method was unsatisfactory. Due to recent development work, when using good quality modern equipment, direct recording of temperature vs time is sufficiently accurate and sensitive.

Sensitivity to thermal events is considerably improved by using a differential technique. Here, the temperature of the sample is regularly compared with that of a standard, which undergoes no phase change during the experimental thermal cycle. The best arrangement for such a comparison is a cylindrical standard, surrounding but not touching the sample. DTA, used in conjunction with direct cooling curves, is particularly good for solid state transformations. Interpretation of curves for alloys is often difficult, so there is good reason to spend some time working with pure metals to establish their basic characteristics.

The experimental set-up for DTA is shown in Figure 7. It is necessary that the heat supply to each sample is the same. Thus, if no phase change occurred in the test sample, the temperature difference, ΔT, would be zero at all source temperatures and after each interval of time. Further, if a test run was made under those conditions, measuring the temperature difference at regular intervals of time, an event free "base line" would be determined. The same observations will apply to a cooling situation, with the heat extraction from each sample being equal. Clearly, if a change occurs in the test sample which is either exothermic or endothermic, the event will be indicated by a positive or negative record of ΔT. An idealised DTA heating curve, is shown in Figure 8. Understandably, the type of equipment, the experimental procedure and the physical and chemical properties of the two samples will affect the shape of the curve .

3.2 Effect of test procedure.

The important experimental factors are,

* sample size and shape

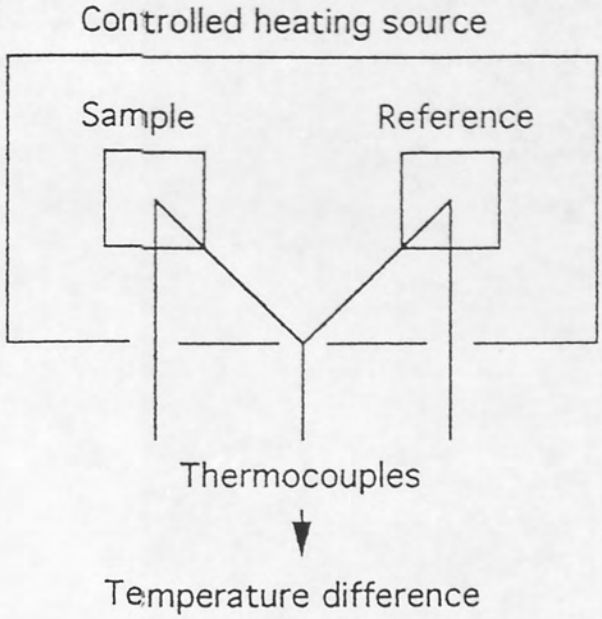

Figure 7 Basic set-up for DTA

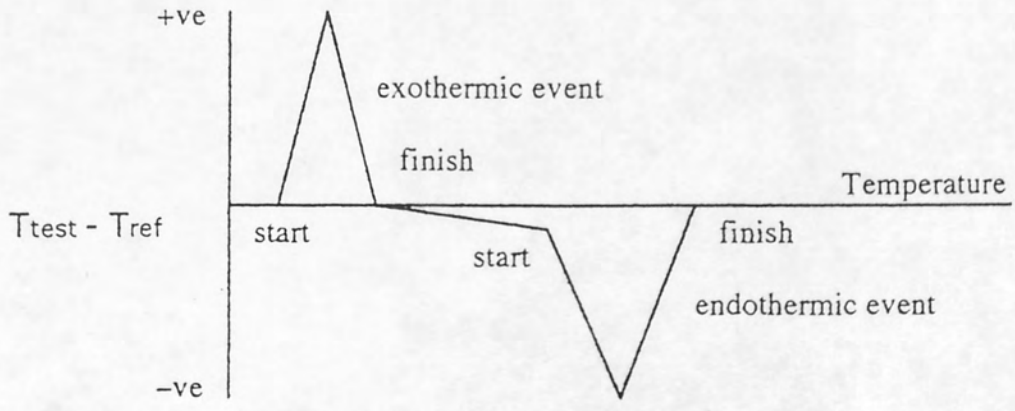

Figure 8 Ideal DTA heating curve

* sample condition,
* how sample is held in position,
* rate of heating or cooling,
* position of thermocouples,
* atmospheric environment of sample,
* type of thermocouple and
* type of thermal event occurring.

Each factor is now considered in turn.

Sample size and shape

This is a very important factor and it must be given early consideration in order to avoid experimental failure. Based on shared experiences of early experimenters, the established approach was to use the smallest sample possible. The arguments leading to that decision are presented below.

The amount of sample tested must be related to the intensity of the expected thermal changes and the sensitivity of the measuring equipment. A further consideration is the control of the experimental conditions. Very sensitive measuring devices may allow the convenience of a small sample size, but experimental control will become more critical.

The size and shape of the sample must be related to the specifications of the thermocouple. Ideally, the sample will be spherical, symmetrically enclosing the thermocouple bead. This arrangement is rarely feasible and the frequently chosen shape for a solid sample is cylindrical, with the thermocouple sited at the geometric centre, through a hole drilled in a flat face. However, samples are commonly in powdered form, and for metals, may be liquid at some stage of the test. The ensuing problems will be discussed later.

It is fortunate for the research metallurgist that the size of the sample is far less important when studying physical changes than when investigating chemical reactions. A common circumstance is that a sample for DTA is taken from a relatively large mass of material, and must be representative. Fortunately, the methods of obtaining a representative sample of a body of material have been extensively analysed, discussed and standardised. Even so, there are still new ideas emerging, as revealed later. Knowing the types of equipment and measuring devices involved, one would expect test samples to weigh grams rather than kilograms. Indeed, in recently introduced techniques, the recommended sample weight is likely to be in milligrams. Since both micro- and macro-inhomogeneity are common in metal masses, samples for thermal analysis have traditionally been relatively large, usually, hundreds of grams. It is only recently, with the introduction of sophisticated and versatile equipment, that the use of small metallurgical samples has become a possibility. Other aspects of the issue of sample size will be more specifically discussed in the next Chapter.

Mackenzie and Farquharson (53), put forward a scheme for standardising DTA, with a major interest in powdered, crystalline samples. They tested samples ranging from 0.2 to 1.0g in size and found acceptable correlation between the results of DTA, irrespective of sample size.

Sample condition.

A commonly occurring situation is that the material to be sampled is a crystalline solid, for example, chemical compounds, minerals, metals and ceramics. Further, the material is likely to be polycrystalline. If the material is brittle, a portion is selected, crushed to a powder and a representative test sample taken. The problem is, how fine should the powder be ground. There are two main considerations, namely, the particle size of the powder in relation to the grain size of the source material and how the particle size affects the physical and chemical behaviour of the the sample during the test. Initial thoughts about obtaining a representative sample would suggest that the particle size of the ground powder must be similar to, or finer than the grain size of the source material. Todor (52), working with the mineral siderite, concluded that a sample powder particle size of 10-20μm, gave accurate and consistent results. Unfortunately, he did not mention the grain size of the siderite, but it it was likely to be larger than 20μm. Todor implied that for physical changes and chemical reactions, except oxidation, the finer the powder, the better the results. Testing a "loose" powder may create unacceptable base-line drift. However, in the writer's experience with cements, compaction of a 50mg powder sample in a crucible by hand pressure, was sufficient to give satisfactory results. Generally, metals are not brittle, so crushing and grinding operations are rarely feasible. However, milling or filing, as a means of obtaining powder samples, are often used with success. Again, for convenience, a metal powder may be readily compacted to a cylindrical shape using simple press tools. Even "as compacted" particle bonding is sufficient to allow the handling of the cylinder in preparation for testing.

A solid sample may experience collapse at some stage during a test run, for example, due to the formation of liquid. Thus, when studying the melting and solidification characteristics of metals and alloys, the sample needs to be in a container. The immediate problem is where to site the thermocouple bead. Certainly it is very difficult to arrange for the bead to be positioned within the sample for the duration of a test run. Fortunately, bearing in mind the recognised requirement of temperature uniformity and slow heating or cooling rates, fixing the bead to a support on which the base of the sample container rests, has proved to be acceptable. Endorsement of this observation is given later in the Thesis. With the sample in a container, a very important consideration is whether it should be covered. If gas or vapour is evolved from the sample during the test, the presence of a cover will invariably give results different to those obtained with the container open to ambient atmosphere. Again, a reaction between the sample and the atmosphere, such as oxidation, will be strongly affected by the presence of a cover. Most pieces of thermal analysis equipment have the provision for controlling the atmosphere surrounding the sample, thus providing greater flexibility. As discussed later, by combining the use of a loose container cover and a slow flow of inert gas, the rate of oxidation of a metal sample may be controlled to considerable experimental advantage.

Sample positioning.

Ideally, the sample would be "suspended" within the heating chamber, the only contact

being with a thermocouple bead. This can be achieved by electromagnetic levitation, but the writer is not aware of a practical example. Solid samples may be held in position with minimum contact in a variety of easily visualised ways. When a container is used, support is necessary, but as mentioned in the previous section, the provision of a lightweight platform to which the thermocouple is attached, is a perfectly acceptable method of measuring the sample temperature.

Rate of change of temperature.

Heating and cooling rates are, understandably, crucial to the validity of the test results. Consider an event in the sample, such as a phase change, which may be either endo- or exothermic. At an ideal heating (or cooling) rate during DTA, the event would be recorded on the trace as inflections, with sharply defined start and finish points, giving temperatures for the event, and a measurable energy involved, from the "area under the curve". A considerably slower rate of temperature change than the ideal, would blur the start and finish points and exaggerate and distort the energy area. With too fast a rate of temperature change, the start and finish points would be shifted from the true positions and would move closer together on the trace, to give a narrow energy area, reducing reliability. At fast rates of heating and cooling, it is possible that an event could be missed by giving no indication on the trace. In current practice, DTA on minerals and ceramics is commonly conducted at rates of between 10 and 20°C per minute. With metals, it was quickly realised by the first experimenters, that rates as slow as 0.5 or 1°C per minute were necessary for success. However, with modern equipment, it is possible to use rates of 2 or even 5°C per minute with confidence, as explained later.

If there are two events close together or even overlapping, which often occurs with minerals, additional consideration must be given to heating rates. Todor (52), illustrated the issue very well by referring to the use of DTA heating curves to define the dehydration of gypsum. He showed that at 5°C per minute, three stages of dehydration are clearly defined. At 10°C per minute, only two stages appear on the trace and at 20°C per minute, the two intermediate stages are barely discernible.

It is interesting that, at the 1952 International Geology Congress, Mackenzie and Farquharson (53), proposed that a heating rate of 10°C per minute should be adopted as a standard for DTA. According to Todor (52), the proposal was immediately widely adopted, although he points out the obvious reservation "it depends on what you are after". In some recent work undertaken by the writer, the specified heating rate was 10°C per minute for cements and other similar building materials, but for some purposes, 20°C per minute was acceptable.

Positions of the thermocouples

The main purpose of thermal analysis is to determine accurately the temperatures at which thermally activated changes occur in a test sample. Thus, a thermocouple needs to be positioned in, on or near to the sample in order to precisely monitor its temperature. As mentioned in a previous section, because thermal analysis is performed at a slow rate and experimental conditions are designed to minimise thermal gradients, a thermocouple sited

in close proximity to the sample may well be effective. In DTA, all these observations apply equally to the inert reference sample.

A third thermocouple may be positioned to measure the temperature of the furnace, and used for control purposes. In use, the furnace is put through a thermal cycle which reflects that required to be experienced by the test sample. When the experimental procedure is being planned, it is necessary to know the temperature difference, under steady state conditions, between the furnace and the test sample, and also the extent of the temperature lag.

Ambient atmosphere.

The atmosphere around the test sample is an important issue. A very common reason for thermal analysis is to gain data on thermal decomposition processes which occur in the test sample. If gases are evolved during decomposition, the recorded data will depend on factors such as,

* the composition of the atmosphere at the start of the test
* the variation of the atmosphere composition during the test
* the decomposition pressure
* the variation of the partial pressure of the gas evolved during the test
* the variation of the pressure of the atmosphere during the test

Thus, it is common that thermal analysis equipment has provision for the control of the atmosphere around the test sample.

When testing metals and alloys, the main concerns will be oxidation in the ambient atmosphere and to a lesser extent, vaporisation of a constituent of the test sample. Although the initial reaction would be to prevent oxidation unless, of course, that is the topic being studied, the writer discovered an unpredictable benefit from allowing slight oxidation of the zinc alloy samples, as explained later.

Type of thermocouple.

The main considerations in selecting the type of thermocouple to be used, are the operating temperature range and sensitivity, although recent advances in electronic measuring equipment allows an ever widening choice. Other considerations are chemical and physical stability of the components of the thermocouple over the temperature range envisaged and in the environment existing during testing.

Useful developments of recent years are automatic cold junction compensation, computerised linearisation of the output, and mineral insulation.

It is possible to incorporate a popular, well-documented thermocouple system, such as platinum-platinum/rhodium, into a piece of equipment which will offer a very wide range of applications. A good example of this is the STA 1500, to be described later.

Type of thermal event.

Frequently, when testing minerals or chemical compounds, several thermal events occur due to chemical and physical reactions. During the thermal cycle, there may be secondary reactions, following the "main events", which in turn may cause either diminishing or

enhancement or even annihilation. The specific temperatures at which events occur may be faithfully recorded, but the shape of the experimental trace may be adversely affected, causing problems of interpretation.

Fortunately, the situation with metals and alloys is relatively straight forward. With melting and solidification, the thermal events are generally well defined on the experimental traces. Thermal events in the solid state may cause problems due to factors such as slow diffusion rates, metastability, and miscibility.

Thus, when choosing equipment and planning an experimental procedure, careful consideration must be given to the known characteristics of the thermal events to be studied.

3.3 Interpretation of DTA results.

A fully quantitative interpretation of a DTA trace is almost impossible to achieve, because the "thermal balance" of the test environment inevitably changes during the run. For example, a phase change in the sample will usually result in a physical property change, which in turn affects the thermal response. Again, the balance between the various modes of heat transfer operating within the chamber, may change during a test. In a perfectly balanced set-up, the resulting base line plot will be straight (and probably horizontal). That response is rarely seen, but with skilled manipulation of a well designed piece of equipment and a competent calibration procedure, a close approach to the ideal is possible.

Fortunately, the requirement may not be for a fully quantitative interpretation, but a combination of quantitative, semi-quantitative and qualitative. For example, in the metallurgical study described later, the requirements were, the exact start temperature of a phase change, a reasonable estimate of the finish temperature, coupled with a qualitative analysis of the shape of the trace. Achieving those mixed objectives was not too difficult.

The important features of the ideal heating trace shown in Figure 8 are,

* the start temperature of the event
* the steady state temperature
* the peak height,
* the area under the curve between start and finish
* the finish temperature

An ideal cooling trace will be similar in shape.

Published experimental curves rarely show sharply defined start and finish points and straight line steady states, so interpretation is required. Conveniently, the traces obtained with the STA1500 almost invariably showed sharply defined start temperatures.

It is important to consider experimental relationships in a quantitative manner, if only to feel safer in making assumptions. It is also important to examine the simplest situation first, in order to establish a firm basis for further, more extensive deliberations. Of the many theoretical treatments of the topic, the writer found the approach taken by Woodhead, in a chapter of a book on thermal analysis (51), to be the most analytical and informative. His arguments are summarised below.

Consider a sample suspended in a furnace, subjected to a steady rate of heating and

assume that no transformation occurs in the sample. The heating of the sample may be represented by,

$$\frac{dQ}{dt} = mc\frac{dT}{dt} \qquad 3.1$$

where Q = quantity of heat supplied to the sample,
t = time,
m = mass of sample,
c = specific heat of sample and
T = temperature of sample, K

The heat supplied by the furnace is mainly by radiation, so,

$$\frac{dQ}{dt} = k\,(T_F^4 - T^4) \qquad 3.2$$

where k = a constant incorporating emissivity and area effects and
T_F = temperature of the furnace, K.

combining the two equations,

$$\frac{dT}{dt} = \frac{k}{mc}(T_F^4 - T^4) \qquad 3.3$$

It was proposed by Woodhead that this relationship is fundamental to the understanding of thermal analysis, and it covers all eventualities. However, attempts to apply the relationship result in the generation of complex equations, which until recently were almost impossible to manipulate, let alone satisfactorily solve. The availability of powerful computers within the last decade, would allow problems to be solved, given a suitable programme. The writer is not aware of any specific instance, but in a similar situation involving complex heat flow considerations in fusion welding, the long standing stalemate caused by unsolveable equations was eventually broken by the development and execution of computer programs. In order to make progress, the approach adopted by the early researchers was to accept the importance of the relationship, but use it in a semi-quantitative manner, to validate (or otherwise) the results of DTA. It is still valuable for that purpose.

Going on to consider the basic situation where the furnace temperature is a linear function of time,

$$T_F = T_0 + Rt$$

where T_0 = start temperature of the furnace, and

$$R = \frac{dT_F}{dt}$$

Substituting in the basic equation, gives,

$$\frac{dT}{dt} = \frac{k}{mc}[\,(T_0 + Rt)^4 - T^4\,] \qquad 3.4$$

A graphical representation of the heating curve is shown in Figure 9. Understandably, in the initial stages, the increase in the sample temperature lags that of the furnace, but eventually, the sample curve becomes virtually parallel to the furnace curve, although strictly, it is an asymptote. A similar relationship exists on cooling, Figure 9, with the

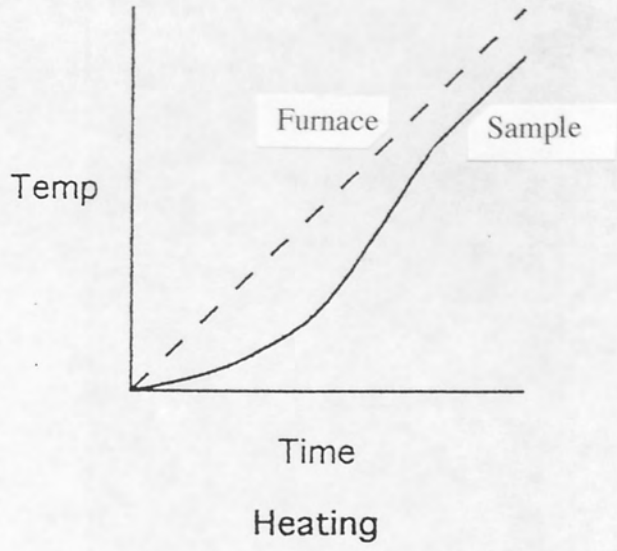

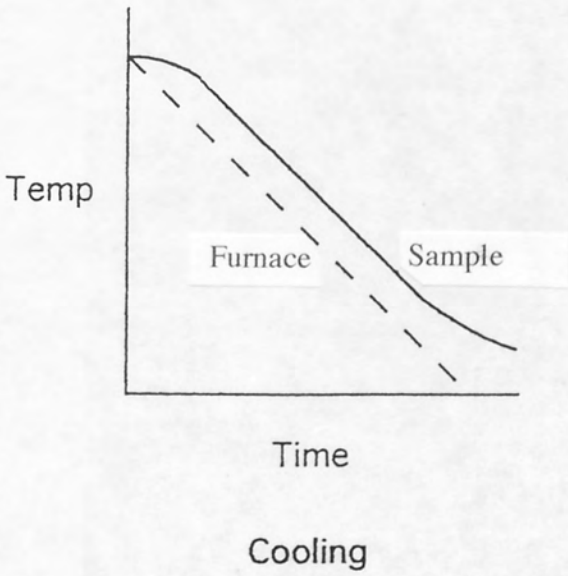

Figure 9 Heating and cooling curves, no transformations

important difference that the curves diverge at lower temperatures. In a well designed and executed experiment, the near parallel regions of the curves extend over the whole of the relevant thermal cycle. Then, assuming that Newton's Law applies to the operating mode of heat transfer, Russell (54) observed that a simpler equation may be used, namely,

$$\frac{dQ}{dt} = \alpha (T_F - T) \qquad 3.5$$

where α is a constant, and using equation 3.1,

$$\frac{dT}{dt} = \frac{\alpha}{mc} (T_F - T) \qquad 3.6$$

In DTA, there are two samples being heated in the furnace, namely, the test sample and a standard sample. Ideally, both the heating curves and the cooling curves will be coincident. In practice, with well designed equipment, good experimental procedure and careful calibration, that circumstance is achievable.

In attempting to understand the significance of Russell's approximation, consider ΔT, the temperature difference between furnace and sample, ie $(T_F - T)$, then,

$$T_F^4 - T^4 = 4T^3\Delta T \left[1 + \frac{3}{2}\left(\frac{\Delta T}{T} \right) + \left(\frac{\Delta T}{T} \right)^2 + \frac{1}{4}\left(\frac{\Delta T}{T} \right)^3 \right]$$

Since ΔT will be small compared with T, terms in ΔT may be neglected, giving,

$$T_F^4 - T^4 \approx 4T^3 \Delta T \approx 4T^3 (T_F - T) \qquad 3.7$$

similarly,

$$T_F^4 - T^4 \approx 4T_F^3 (T_F - T) \qquad 3.8$$

There will be a temperature T_x between T and T_F for which it will be strictly correct to write,

$$T_F^4 - T^4 = 4T_x^3 (T_F - T) \qquad 3.9$$

Thus, Russell's approximation involves the neglect of the T^3 term, a quantity that varies rapidly with T. It is apparent that the approximation is not good, and numerical results derived from it are likely to be in error. However, Handford (55) pointed out in a discussion of Russell's paper, that none of his general conclusions are invalidated by using the approximation.

It is worth showing how the approximate equation leads to the conclusion that the $\frac{T}{t}$ curve is linear if $\frac{dT_F}{dt}$ is constant. So, let the enclosure temperature be given by,

$$T_F = T_0 + Rt$$

then, from equation 3.6,

$$\frac{dT}{dt} = \frac{\alpha}{mc} [(T_0 + Rt) - T]$$

rearranging,

$$\frac{dT}{dt} + \frac{\alpha}{mc} T = \frac{\alpha}{mc} (T_0 - Rt)$$

Integrating for boundary conditions $T = T_0$ when $t = 0$

$$T = T_0 + Rt - \frac{Rmc}{\alpha} (1 - \exp \frac{-\alpha t}{mc}) = T_F - \frac{Rmc}{\alpha} (1 - \exp \frac{-\alpha t}{mc}) \qquad 3.10$$

as t becomes large, the exponential term approaches zero, so that,

$$T = T_F - \frac{Rmc}{\alpha} \qquad 3.11$$

The relationship above is for heating. For cooling, the equation is similar, but with R negative.

Sample undergoes a transformation at constant temperature.

On heating , the transformation will be either endo- or exo-thermic. On cooling, the reverse will apply. Thus, it is not difficult to envisage the effect of a transformation on DTA heating or cooling curves, as shown in Figure 10. Some comments about the shape of the curves are in order and will follow.

During the transformation, ΔT is constantly increasing, thus, rewriting equation 3.3 in terms of ΔT, gives,

$$\frac{dT}{dt} = \frac{4k}{mc} T_x^3 \Delta T \qquad 3.12$$

At the end of the reaction, ΔT is much greater than at any other time, while the value of the other terms will have changed very little. Consequently, the value of dT/dt is large when the temperature starts to change again. This causes the value of ΔT to decrease, and the curve will tend to become parallel to the furnace curve.

It has frequently been stated that the amount of heat evolved (or absorbed) during a constant temperature transformation is proportional to the time taken for the reaction to be completed. This cannot be true, since Russell (54) has shown that, putting L for the heat transfer,

$$L = R (\frac{\alpha t^2}{2} + mct) \qquad 3.13$$

As shown in Figure 11, the demarcation of the beginning and end of a reaction are rarely sharply defined, the former is rounded and the latter gradually merges with the baseline. These effects are caused by a combination of several factors, such as,

* temperature lag between thermocouple and sample,
* thermal gradients in the sample and
* mode of nucleation of the phase change.

However, with well designed and manufactured equipment and a carefully prepared and executed experiment, using slow rates of heating and cooling, the problems mentioned above may be minimised sufficiently to provide acceptable results.

When discussing the use of cooling curves to locate the liquidus of an alloy, it is inevitable that undercooling is raised as an issue. However, it is possible to virtually eliminate undercooling with good experimental technique and modern equipment, as will be explained later. In any case, if the effects of undercooling show on the cooling curve,

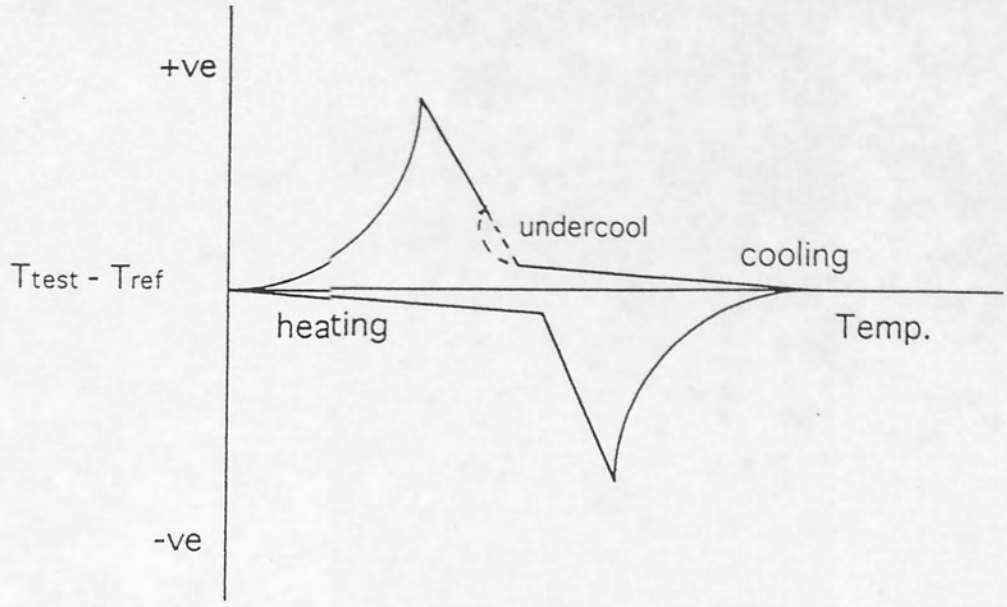

Figure 10 Ideal DTA heating and cooling curves, with a transformation in sample

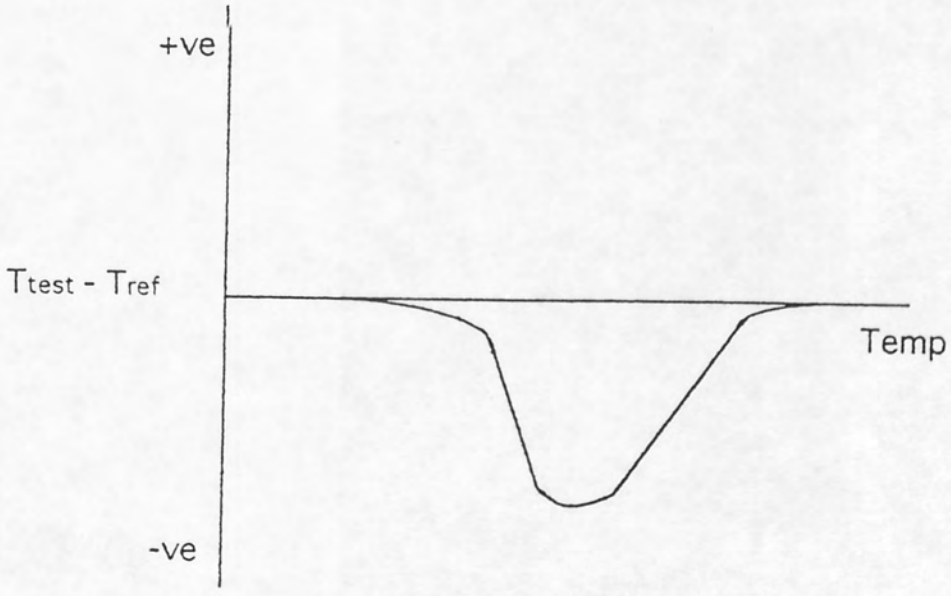

Figure 11 Experimental DTA heating curve

a simple extrapolation will give the temperature of first solid formation, as illustrated in Figure 10. The key factors are rate of cooling and nucleation of the solid state. With a very slow cooling rate and the availability of heterogeneous nucleation sites, undercooling will not occur.

The initiation of a phase transformation, is affected by,

* rates of diffusion of the participating species,
* nucleation and
* composition gradients.

Each of these factors tends to produce a temperature lag.Thus, even at very slow rates of temperature change, it is usual for experimentally determined transformation temperatures to be higher than the true equilibrium temperature on heating, and lower on cooling. But, once again, with good equipment and good technique, the temperature "shifts" may be small enough, say less than 0.5°C, to be ignored.

Transformation over a range of temperature

The shape of the T/t curve for a sample undergoing a transformation over a range of temperature is not easy to visualise, and various conflicting views have been expressed over the years. Woodhead (51) states that the situation is resolved by a simple analytical approach, which centres on the consideration of the "effective" specific heat of the sample during transformation.

Consider a sample with phase 1 changing to phase 2, the suffixes indicate the phase, the heat absorbed is given by,

$$dQ = (m_1 c_1 + m_2 c_2 + \Delta H^{1\rightarrow 2} \frac{dm}{dT}) dT \qquad 3.14$$

where H is the heat of transformation from phase 1 to phase 2 at the temperature under consideration. Also, dm is the mass of phase 2, produced in the temperature interval dT. The apparent specific heat, c, of the alloy at that temperature is then given by,

$$c = \frac{\frac{dQ}{dT}}{m_1 + m_2} = \frac{m_1 c_1 + m_2 c_2 + \Delta H^{1\rightarrow 2}}{m_1 + m_2} \cdot \frac{dm}{dT} \qquad 3.15$$

The change in specific heat is gradual and often c_1 and c_2 do not differ by very much, so there is no discontinuity in the T/t curve. Thus, the equation may be simplified to,

$$c = c' + \frac{\Delta H^{1\rightarrow 2}}{m} \cdot \frac{dm}{dT} \qquad 3.16$$

where c' is the average value of c_1 and c_2 and $m = m_1 + m_2$.

Substituting in equation 3.3,

$$\frac{dT}{dt} = \frac{k}{m\left(c' + \frac{\Delta H^{1-2}}{m}\frac{dm}{dT}\right)} \cdot \left(T_F^4 - T^4\right) \qquad 3.17$$

It is now apparent that the shape of the T/t curve will be profoundly affected by the value of dm/dT.

Masing (56), offered a general solution to the problem, as follows. In an equilibrium diagram of the type shown in Figure 12, he considered the cooling of an alloy of composition x_0. At a temperature T the composition of the liquid is x_L and the solid x_S , then,

$$\frac{dm}{dT} = \frac{(x_S - x_0)\frac{dx_L}{dT} + (x_0 - x_L)\frac{dx_S}{dT}}{(x_S - x_L)^2} \qquad 3.18$$

At the liquidus, $x_0 = x_L$, and

$$\left[\frac{dm}{dT}\right]_L = \frac{\frac{dx_L}{dT}}{(x_S - x_0)} \qquad 3.19$$

Similarly at the solidus,

$$\left[\frac{dm}{dT}\right]_S = \frac{\frac{dx_S}{dT}}{(x_0 - x_L)} \qquad 3.20$$

The way that dm/dT varies over the solidification range can now be visualised, for example, by taking the three cases shown in Figure 13,

in case (a) $\left|\frac{dx_L}{dT}\right| > \left|\frac{dx_S}{dT}\right|$ and $|x_S - x_0| < |x_0 - x_L|$

so $\left[\frac{dm}{dT}\right]_L > \left[\frac{dm}{dT}\right]_S$

similarly in case (b) $\left[\frac{dm}{dT}\right]_L = \left[\frac{dm}{dT}\right]_S$

and in case (c) $\left[\frac{dm}{dT}\right]_L < \left[\frac{dm}{dT}\right]_S$

The way dm/dT varies is illustrated graphically in Figure 14 .

It is clear that the actual difference between $[dm/dT]_L$ and $[dm/dT]_S$ in cases (a) and

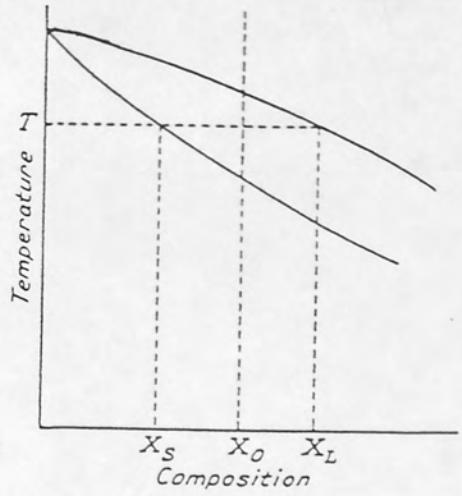

Figure 12 Alloys transform over a range of temperatures

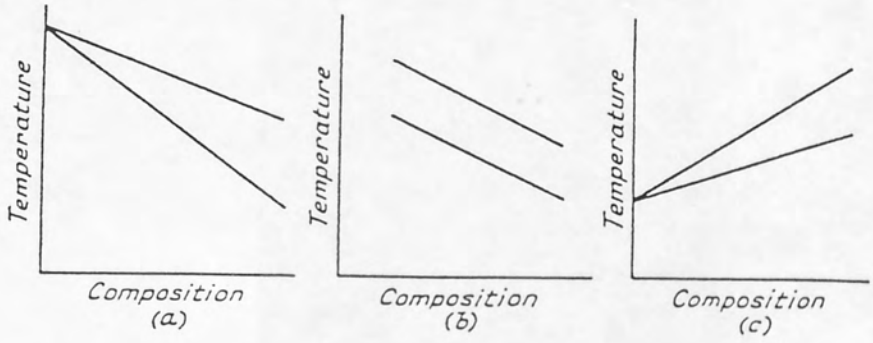

Figure 13 Dispositions of liquidus and solidus considered in text

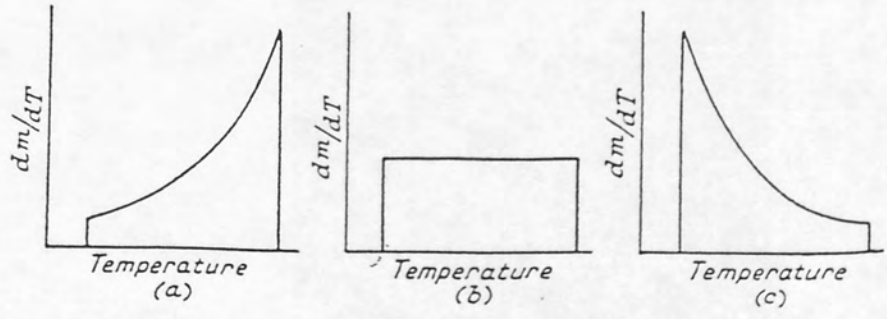

Figure 14 Variations of dm/dT relative to Figure 13 (a), (b) and (c)

(c) will depend on the difference in the slopes of the liquidus and solidus, in other words, the solidification range.

From a consideration of Figure 14 and equation 3.17, it is possible to sketch the heating and cooling curves to be expected for cases (a) and (c). It must be remembered that any decrease in dT/dt causes an increase in $[T_F^4 - T^4]$, which tends to minimise the effects of changing dm/dT. The ideal curves are shown in Figures 15, 16, 17 and 18. The curve for case (b) would be intermediate between (a) and (c).

As mentioned earlier, the experimental curves will have less well defined transformation start and finish points. Woodhead (51) observes that it would be difficult to detect accurately the solidus on a cooling curve of an alloy of type (a), or the liquidus on a heating curve of an alloy of type (c). These interesting observations endorse both the views of Porter and Easterling (8), and the writer's experimental findings. Any departures from equilibrium will also influence the curves. Undercooling results in emphasised discontinuities at the liquidus and if the reaction is not completed until the temperature has fallen below the solidus temperature, then the discontinuity at the solidus is reduced. The effect on heating curves is to emphasise the solidus and diminish the liquidus discontinuities. In the case of heating curves, such effects are only likely to be serious for transformations from one solid phase to another.

It is particularly important to realise that heating and cooling curves for transformations taking place over a range of temperature are quite different in shape and that the exact forms of all curves depend essentially on the relationship between apparent specific heat and temperature for the particular alloy

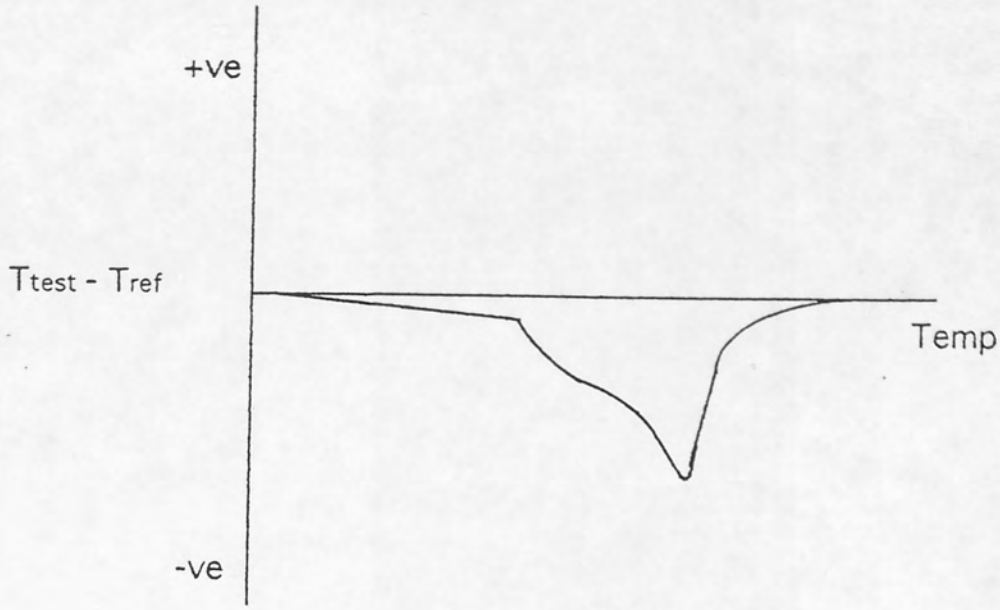

Figure 15 DTA heating curve for sample illustrated by Figs. 13 (a) and 14 (a)

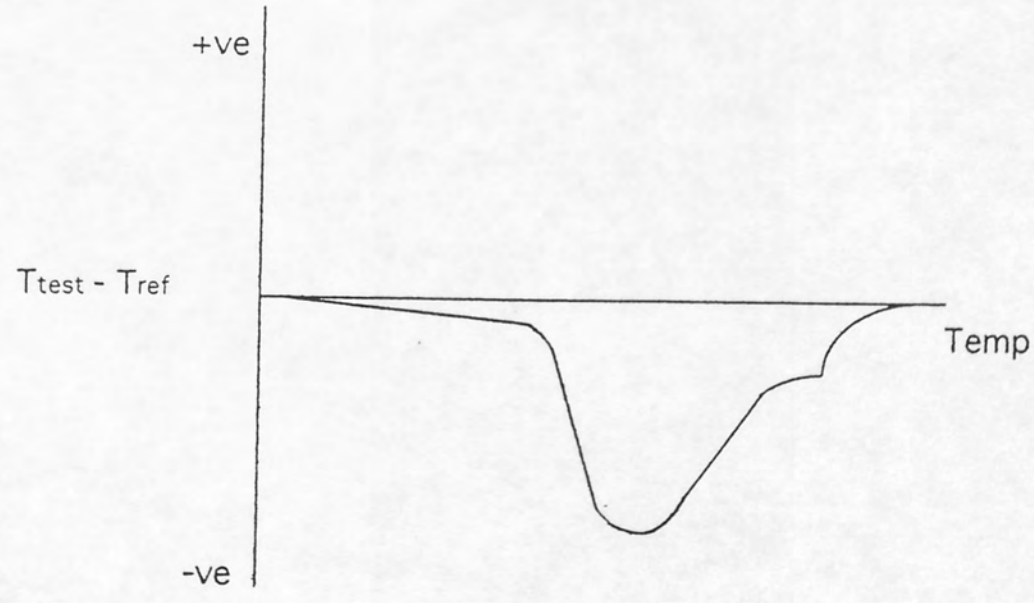

Figure 16 DTA heating curve for sample illustrated by Figs. 13 (c) and 14 (c)

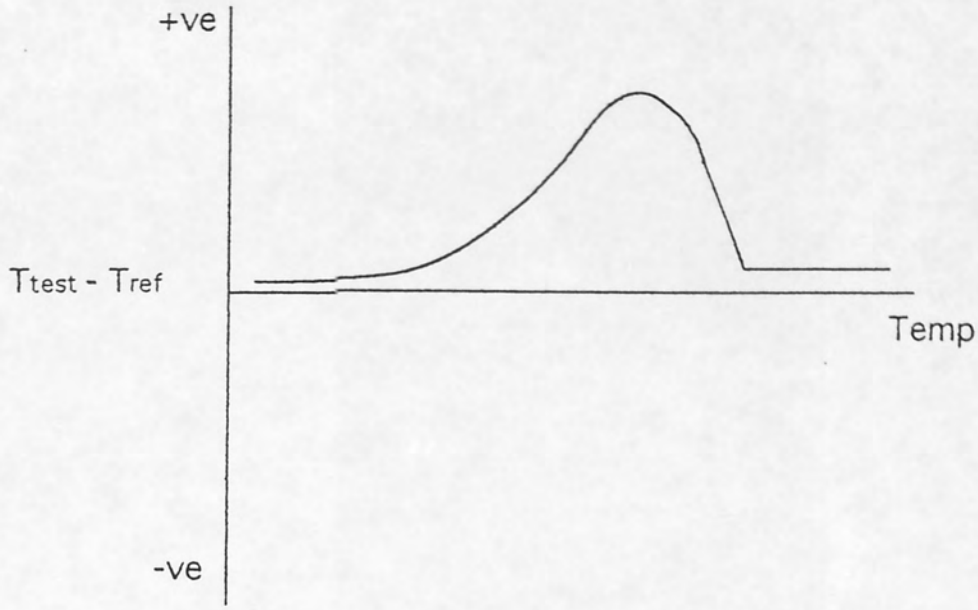

Figure 17 Cooling curve for sample illustrated by Figs. 13 (a) and 14 (a)

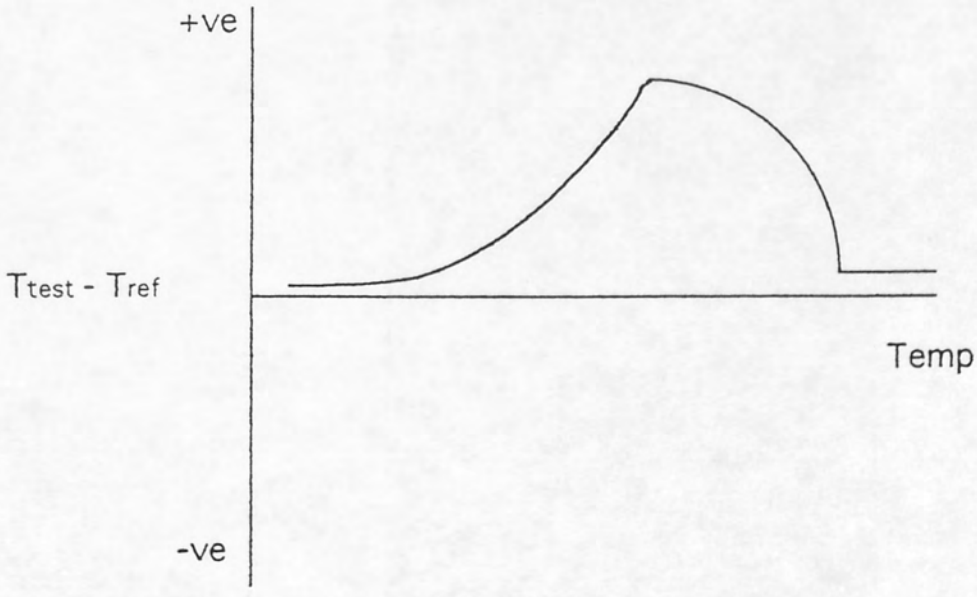

Figure 18 Cooling curve for sample illustrated by Figs. 13 (c) and 14 (c)

4. EXPERIMENTAL METHODS

4.1 Thermal analysis

Equipment

In 1989, Stanton Redcroft Ltd., a company with a reputation for high quality instruments based on microbalances, became part of Polymer Laboratories Inc. and has since traded under the name of PL Thermal Sciences Ltd. At the same time, an integrated range of thermal analysis instruments including some new products, was launched. One of the instruments, known as a Simultaneous Thermal Analyser (STA), is capable of performing Differential Thermal Analysis, Thermogravimetry and Derivative Thermogravimetry, at temperatures between ambient and 1500°C. A particular feature of the range of thermal analysis instruments is the availability of a PC based data acquisition and manipulation software support system, known as TRACE.

In 1990, an STA 1500 with TRACE 2 support system was installed in a laboratory in the Department of Mechanical and Electrical Engineering at Aston University.

The STA 1500 is capable of detecting and recording weight changes and thermal events occurring in a suitable sample of up to 200mg weight. A general view of the equipment is shown in Figure 19 and a schematic diagram in Figure 20. The main module houses an electronic microbalance. The TG-DTA hangdown carries sample and reference crucibles, side by side, on a platform. The Pt-Rh wound furnace has controlled up and down movements. With the furnace down, the crucibles are accessible. When the furnace is raised, the crucibles are positioned in a "micro-environment cup" which is supported by a hollow stem, attached to the base of the furnace. A gas may be passed up the stem, to surround the sample during a test.

The balance control unit (BCU), controls the microbalance system, gives a digital display of the sample weight and provides an analogue signal output, proportional to the weight. The BCU also provides an analogue output signal proportional to the rate at which the weight is changing. The differential temperature signal from the thermocouples on the crucible holder, passes to the DC amplifier, the analogue signal then goes through the preamplifier before reaching the data acquisition system interface.

When using the TRACE system, a detailed thermal cycle is keyed into the computer, which then programmes the microprocessor temperature controller, in readiness for the experimental run.

While an experiment is in progress, the PC monitor displays a real time graph of either the differential thermocouple output in micro-volts, or the weight change in milligrams or both together, against temperature.

More details of the Main Module are shown in Figure 21 and of the DTA head in Figure 22.

Establishing a procedure

The major part of the experimental work was to be thermal analysis. It was, therefore, important to establish an experimental technique which gave reliable and reproducible results. The STA1500 is a new instrument, so there was no previous experience at Aston,

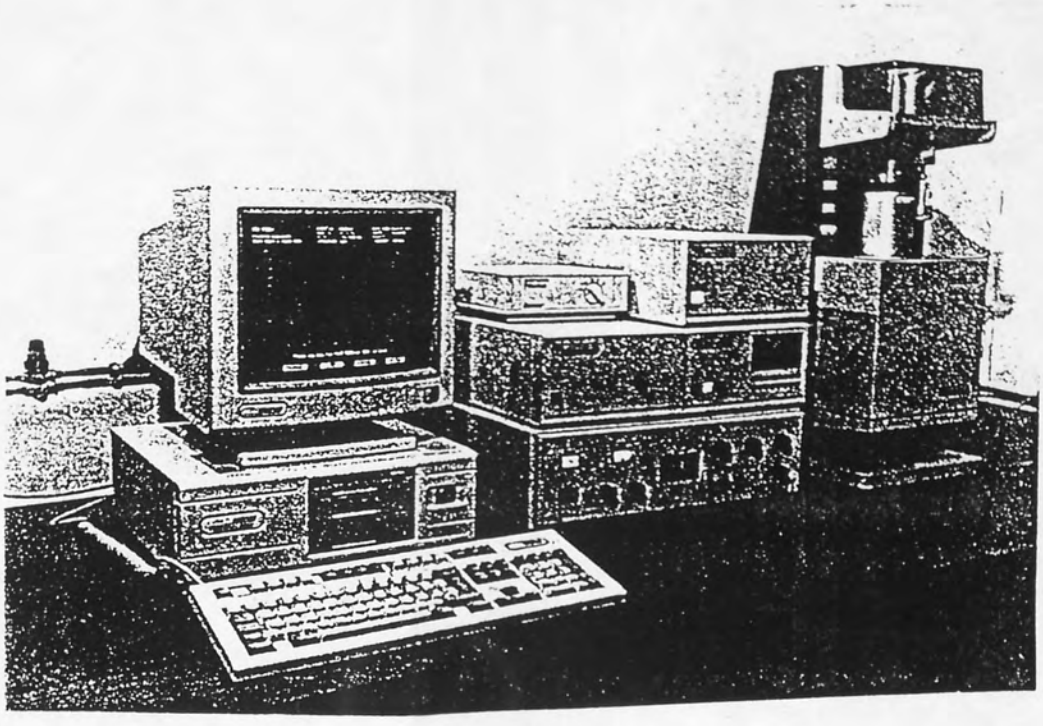

Figure 19 The STA 1500.

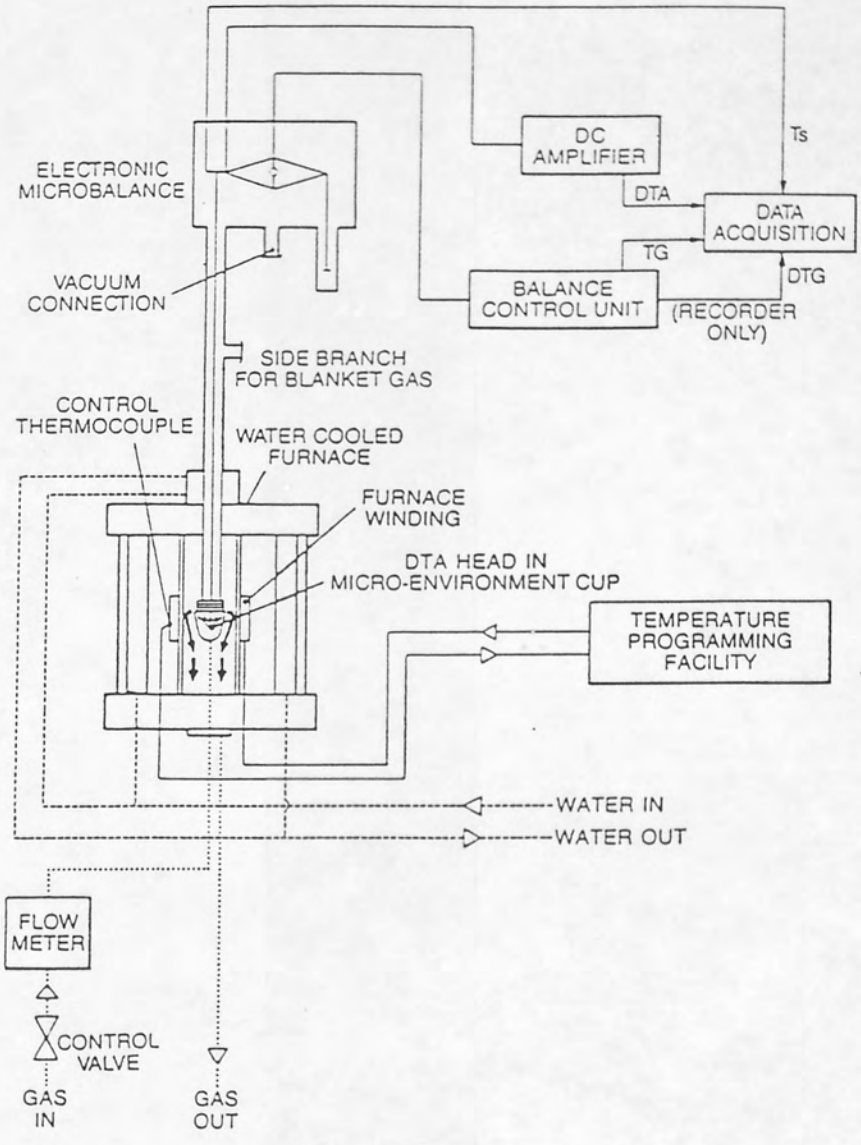

Figure 20 Schematic of the STA 1500.

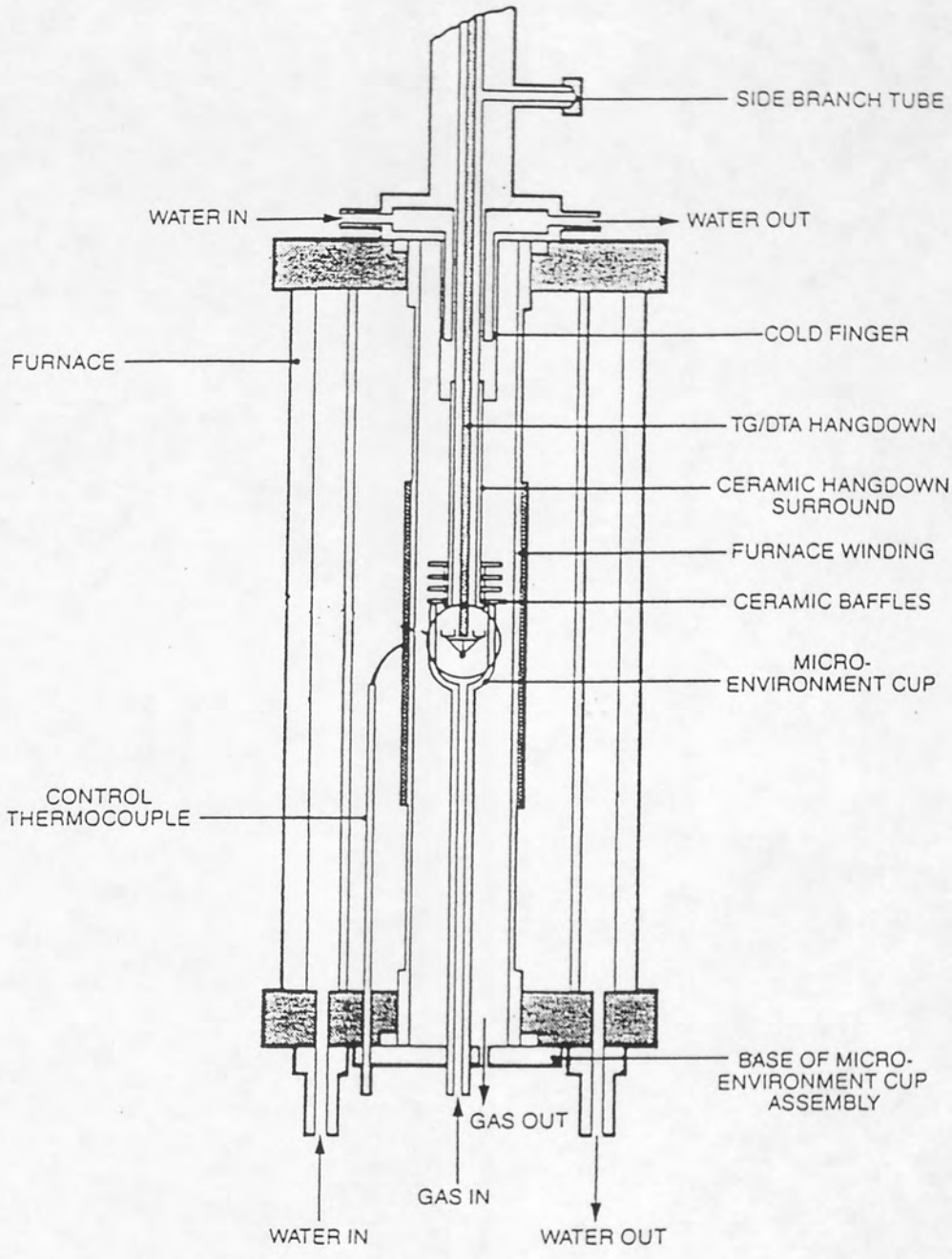

Figure 21 Cross section of the furnace in use.

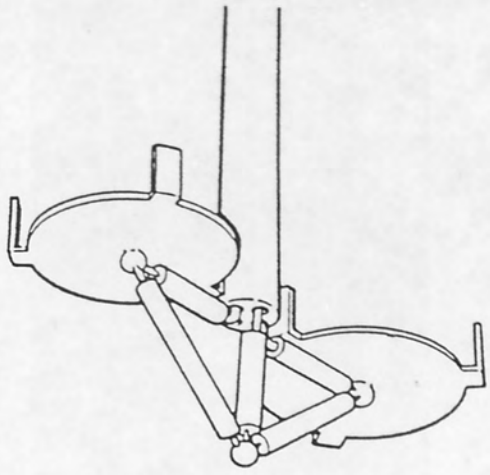

Figure 22 The DTA head.

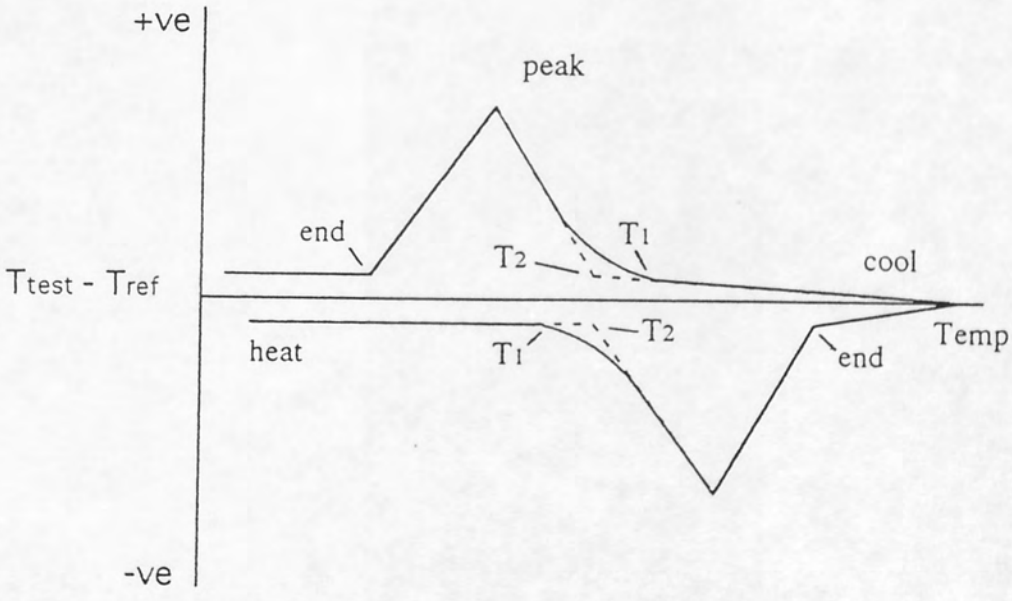

Figure 23 DTA trace for pure zinc

nor, to the writer's knowledge, anywhere else within access.

When the equipment was installed by the makers, the standard procedure was followed, involving the fitting of alumina crucibles, with alumina powder in one of them as the standard. During calibration, several pure metals such as zinc, tin and indium, were melted and cooled so that the melting/solidification points could be used as set temperatures. The installation technician made the useful practical observation that, after a melting and solidification run, the sample of metal was readily removed from an alumina crucible intact. It was remarked that a platinum crucible would tend to bond to the crucible platform unless precautions were taken such as placing an alumina disc in between, and metal samples may bond to the inside of a platinum crucible. Thus, it seemed sensible to go ahead with characterisation for use with metals and alloys, with the equipment in the "as installed" condition, that is, using alumina crucibles.

The instrument makers suggested using samples of five to ten milligrams in weight. Indeed the calibration runs performed by the installing engineer included one with a five milligram sample of zinc. Thus, familiarisation runs were made using 10mg samples of the pure zinc and aluminium which were to be used to make up experimental alloys, and Analar lead. The approach was to heat the sample at 20°C/min. to within 20°C of the expected melting point, hold for a few minutes, heat at 5°C/min. to 50°C beyond the melting point, hold for a few minutes, then cool at similar rates. It became clear that the instrument was very sensitive, and well defined arrests were seen. Also, there was only a few degrees difference between the heating arrest and the cooling arrest. Reproducibility proved to be excellent, with duplicate runs giving results within +/- 0.2°C. Another observation of significance related to the physical behaviour of the sample during the thermal cycle. Samples were cut from pieces of the relevant parent metal with wire snips. No account was taken of sample shape, which naturally tended to be "irregular". It was noticed that a given sample, which may have been put through several complete thermal cycles, retained its original shape. Tests were done in a flow of argon, directly from the bottle with no drying train and it appeared that an oxide film formed on the sample during heating, which was sufficient to support the liquid phase when it formed, with little or no distortion of shape. Since the shape of the solidified sample was not more rounded than the starting shape, it was concluded that surface tension was not involved. An inflection in both heating and cooling curves was noticed when testing the Analar lead. The sample was cut from foil, which for convenience, was stood on edge in the crucible. It was considered that the inflections were caused by at least some collapse of the sample during thermal cycling, although it still retained foil geometry at the end of several runs. These observations confirmed that thought needed to be given to the size, shape and method of preparation of samples.

Experiments with pure zinc.

The equipment was capable of handling sample weights of up to 200mg. It was decided to prepare four samples of pure zinc, with approximate weights of 10, 50, 100 and 200mg. Suitable starting pieces were cut from a block of pure zinc. By alternately using wire cutters and emery paper, the small samples were ground into roughly hemispherical

shape, with the intention that the flat base would be placed in contact with the bottom of the crucible when setting up an experiment. As the samples were being shaped, they were regularly weighed on a microbalance. Four acceptable samples were produced with weights of, 12, 66, 93 and 170mg.

The other important variable requiring study was the rate of heating (or cooling) through the phase change region. It was decided to examine the effect of ramp rates of 0.2, 1, 2, 5, 10 and 20°C/min.

Each sample was subjected to several test runs in a set routine, as follows. All components of the equipment were switched on and allowed to warm-up for forty minutes. A steady flow of cooling water for the furnace was activated and the flow of argon gas through the experimental chamber, direct from the cylinder, was set at 30 l/hr. The balance was zeroed with an empty alumina sample crucible. The sample was carefully positioned in the centre of the crucible base, and the furnace raised to the start position. Using Trace, the required test programme was entered. Typically, the cycle of the furnace was as follows,

ambient temperature to 400°C at 20°C/min., hold for 5min,

400 to 450°C at the required heating rate, hold for 5min,

450 to 400°C at the required cooling rate, hold for 2min,

cease recording data and allow free cool to ambient temperature.

It must be emphasised that the temperature programme applies to the furnace, so the sample temperature lagged behind the programmed temperature during heating and cooling.

When the set cycle was completed, the equipment automatically stopped recording data and stored the data already collected as a file in the default data area, ready for analysis.The furnace was allowed to cool to near ambient temperature and another experiment, with a different ramp rate, was immediately performed. For the slowest ramp rates, slight modifications to the regular cycle were made, in order to save time. The full cycle time varied between forty minutes at the 20°C/min. ramp rate, and seven hours at the 0.2°C/min. ramp rate. Typically, three test runs were made in a day. The equipment responded extremely well to the demands, no problems arose, and a high level of confidence in the sensitivity and reproducibility of the data was engendered.

Using the plot function of Trace, the data was manipulated and a trace plotted. For each experimental run, the scales of the axes were adjusted to maximise display of the arrest points on both heating and cooling. The trace was then plotted, and measurements taken directly from the print-out. A typical trace, showing the various measurements made, is illustrated in Figure 23 (page 53). For reference purposes, in addition to the detail graph, graphs of microvolts vs temperature and microvolts vs time, from ambient to maximum temperature and down to the stop temperature, were also plotted. An explanation is now given of the extraction of data points from each graph.

T_1 is the first indication of the occurrence of a thermal event, during either heating or cooling. In all of the graphs produced, the onset of melting is gradual, that is, represented as a curved line running from the baseline into the arrest line. In contrast, the cooling arrests, at all but the fastest rates, are sharply defined, ie, T_1 and T_2 are

coincident. This behaviour was expected from a consideration of first principles, as explained later in the Chapter 6. The generally accepted definition of the melting or solidification point is the "isothermal" arrest temperature. The quotes are because the measured arrest will only be isothermal under very specific test conditions, but may be very close to isothermal and represented by a straight line. T_2 is the manifestation of those arguments, and is determined from the graph by a simple construction. During the manipulation of the data and graph plotting using Trace, it is possible to obtain T_2 and have it entered on the screen plot for recording purposes. The onset T_1 is difficult to judge, and is not available within Trace.

All the other data taken from a graph were considered to be of value when making the final comparisons to establish the conditions for the optimum experimental technique. It was assumed that geometric symmetry about a zero baseline would represent an experiment under ideal conditions. The results are presented in Tables 3, 4, 5 and 6.

Analysis of results

It is useful to begin by considering the cycle of events occurring in the environment chamber during a test run.

During heating, the environmental cup wall is heated by radiation from the furnace wall and convection. Crucible and platform are, in turn, heated by radiation and convection. Gas flow improves uniformity of heating. The sample is heated mainly by radiation from the crucible wall, with some conduction through the crucible base. The platform and crucible base may be slightly cooler than other regions of the sample due to gas impingement and being sheltered from radiation.Thus the first melting is likely to occur near a free surface or in the body of the sample. The necessary latent heat of fusion is supplied by conduction through the sample, so there is a delay before the thermocouple detects the thermal event. Thus, the heating curve shows a gradual run into the arrest line, which indicates progressive melting. The change would be sharper at slower heating rates and more gradual at higher heating rates. The temperature required is that for the onset of melting and , as discussed earlier, Porter and Easterling (8) explain that T_1 on a heating curve correctly indicates the solidus temperature.

On cooling, heat is extracted from the sample by conduction through the crucible base and platform at a faster rate than is lost generally by radiation and convection. Thus, the first solid to form is on or near the bottom of the sample. The thermal event occurs close to the thermocouple, and is detected early. This gives a sharp change in the cooling curve as it runs into the arrest line. It must be noted that some undercooling will occur due to the need for nucleation. Thus, taking T_2, the arrest temperature from a cooling curve, is the most reliable indication of the liquidus temperature.

The above remarks apply to samples of sufficient size to have good contact with the crucible base and develop thermal gradients when melting first occurs, say, 50-200mg. Small samples, say, 5-10mg, lying flat on the crucible base, should display very little lag and show sharp curve changes, both on melting during heating and solidification during cooling.

The two sets of results summarised in Table 7, which were selected for particular

Rate	Onset T_1 °C		Onset T_2 °C		Peak μV		Area μV.°C		End °C		Range °C		Base line μV	
°C/min	heat	cool	heat	cool	heat	cool	heat	cool	heat	cool	heat	cool	heat	cool
0.2	418.4	418.6	418.7	418.6	4.5	5.3	6	6	421	416	2.5	2.0	3	3
1	418.2	418.3	418.7	418.3	9.8	10.3	30	26	424	413	6	5	1	0.5
2	417.0	418.1	418.6	417.9	14.5	15.8	76	71	427	409	10	9	0	-2
5	418.8	418.4	420.0	417.7	24.5	23.5	147	165	432	404	12	14	1	-2
10	416.4	418.1	419.1	416.6	22.5	26.0	147	299	429	395	13	23	5	-3
20	417.3	416.5	419.3	415.8	22.0	30.0	143	390	430	390	13	26	4	-6

Table 3 DTA results for zinc, 12mg sample.

Rate	Onset T_1 °C		Onset T_2 °C		Peak μV		Area μV.°C		End °C		Range °C		Base line μV	
°C/min	heat	cool	heat	cool	heat	cool	heat	cool	heat	cool	heat	cool	heat	cool
0.2	418.4	418.7	418.7	418.7	13.0	13.5	12	13	422	415	3.7	3.7	6	7
1	417.7	417.9	418.2	417.9	32.1	31.4	72	71	427	409	9	9	-1	-1
2	417.5	417.7	418.1	417.6	45.0	43.8	158	151	431	404	14	14	-2	-2
5	418.6	417.9	420.7	417.5	55.0	70.0	203	436	432	392	14	26	-2	-2
10	419.1	418.1	420.3	417.7	55.0	83.3	199	542	433	392	14	26	0	-2
20	418.1	416.9	419.4	415.1	51.0	91.0	181	585	431	390	13	26	0	-4

Table 4 DTA results for zinc, 66mg sample.

Rate	Onset T_1 °C		Onset T_2 °C		Peak μV		Area μV.°C		End °C		Range °C		Base line μV	
°C/min	heat	cool	heat	cool	heat	cool	heat	cool	heat	cool	heat	cool	heat	cool
0.2	417.6	418.3	418.0	418.3	18	18	36	36	422	414	4	4	0	0
1	417.5	417.9	417.9	417.9	38	38	209	190	429	428	11	10	0	0
2	417.4	418.0	418.6	418.0	56	56	420	420	432	433	15	15	-3	-3
5	418.0	417.8	419.5	417.8	87	87	914	1349	439	387	21	31	-3	-2
10	417.7	417.5	419.0	417.1	64	110	416	1705	431	386	13	31	-5	-5
20	418.5	417.5	419.8	416.0	87	113	957	1695	440	387	22	30	-4	-6

Table 5 DTA results for zinc, 93mg sample.

Rate	Onset T_1 °C		Onset T_2 °C		Peak μV		Area μV.°C		End °C		Range °C		Base line μV	
°C/min	heat	cool	heat	cool	heat	cool	heat	cool	heat	cool	heat	cool	heat	cool
0.2	418.3	418.5	418.6	418.5	25	25	75	63	424	414	6	5	-2	0
1	417.7	418.3	418.7	418.3	54	55	378	358	432	405	14	13	-2	0
2	417.7	418.0	418.6	418.0	72	77	540	809	432	397	15	21	-10	-7
5	417.5	417.5	419.0	417.5	76	117	608	1931	433	384	16	33	-5	0
10	418.6	417.3	419.2	417.1	75	145	600	2465	433	383	16	34	-10	0
20	419.4	417.7	420.7	416.9	70	140	525	2170	435	386	15	31	-10	0

Table 6 DTA results for zinc, 170mg sample.

consistency, clearly demonstrated the high levels of sophistication and performance of the equipment. Also, the levels of sensitivity, accuracy and reproducibility claimed by the makers, were all confirmed. Initially accepting T_2 cooling as a good representation of the the solidification temperature of the zinc samples, the range of that value, across the widely varying experimental conditions was only 4°C. Omitting the experiments conducted at rates of 10 and 20°C/min., brought the range in T_2 (cooling) down to 1°C. Now, looking in more detail at the results.

It is stated in the equipment manual that a ramp rate of 5°C/min. should be "slow enough" to avoid hysteresis when seeking transition points. Although the results were close to confirming that statement, it became clear that the slower rates were more suitable for precise measurements. Workers in the field quote rates as low as 0.5°C/min., but using less sophisticated equipment. Thus, it was useful to observe that 2°C/min. was sufficiently slow for acceptable performance, since some of the alloys to be tested had long solidification ranges, rendering thermal analysis very time consuming.

The results clearly showed that there was some flexibility in optimum sample weight, within the range, 50-100mg. The instrument was set-up and calibrated for general use, with an alumina powder standard, contained in an alumina crucible. The crucible weight was 136mg and the alumina powder weight was 31mg. Assuming that the ideal test sample weight would give rise to a heat capacity equal to that of the standard, that sample weight, S, may be calculated as follows,

$$S = 31 \times C_{Al} / C_{Zn} \text{ mg}$$

where C_{Al} is the specific heat of alumina, and C_{Zn} is the specific heat of zinc.
Therefore,

$$S = 31 \times 1.087 / 0.386 \text{ mg}$$
$$= 87\text{mg}$$

This endorses the observations made earlier.
Similarly, for aluminium test samples, $S = 31 \times 1.087 / 0.899 = 37\text{mg}$

Decisions

1. For a given event, either T_1 or T_2 could be reliably measured, but on scientific grounds (to be explained later). T_1 on the heating curve, would be recorded as the solidus, and T_2 on the cooling curve as the liquidus.
2. A sample, prepared with a flat base, weighing 90+/- 10mg would be adopted for the zinc rich alloys and would be used in subsequent trials with the aluminium rich alloys.
3. The measured value of the solidification temperature for zinc to be used for the preparation of the experimental alloys of 418.1°C would be accepted as a calibration point against the known temperature for high purity zinc of 419.6°C (57).
4. The existing calibration was acceptable for the full range of alloys to be tested after several runs with samples of the aluminium to be used for the preparation of experimental alloys gave a solidification point of 660.0°C against the known value for pure aluminium of 660.4°C (57)

Weight mg	Rate °C/min	Onset T_2 °C		Peak μV		Range °C		Baseline μV	
		heat	cool	heat	cool	heat	cool	heat	cool
66	0.2	418.7	418.7	13	13	4	4	6	7
	1	418.2	417.9	32	31	9	9	-1	-1
	2	418.1	417.6	45	44	14	14	-2	-2
93	0.2	418.0	418.3	18	18	4	4	0	0
	1	417.9	417.9	38	38	11	10	0	0
	2	418.6	418.0	56	56	15	15	-3	-3

Table 7 Selected DTA results for zinc

Trials with alloys

Several zinc-aluminium binary alloys were selected for testing on the basis of distinct solidification features, such as a wide solidification range. Trial DTA experiments were made on samples containing 3, 10 and 30% aluminium. In each case, the traces clearly indicated thermal events on heating and cooling, allowing starting temperatures for the events to be precisely measured. When compared with liquidus, solidus and eutectic temperatures taken from the binary diagram due to Elliott (36), most matched exactly, and all were within one degree. Figure 24 illustrates the features of the trace for the 3% aluminium alloy.

4.2 Preparation of experimental alloys.

In order to identify each experimental alloy, the initial letter of each component was used, together with the nominal amount. For example, Z30A is the binary alloy with 30% aluminium, Z30A1S is the equivalent ternary alloy with 1% silicon and Z30A1CM1S is the equivalent complex alloy with 1% copper, 0.02% magnesium and 1% silicon.

For the binary system, compositions were selected at appropriate intervals, to fully explore the melting and solidification behaviour of alloys ranging from zinc rich to aluminium rich. For the ternary system, the approach was to take the binary compositions 30%, 50% and 70% aluminium and investigate the effect of additions of silicon on each of the three base alloys. It was judged to be of most value, for each group of ternary alloys, to maintain the ratio of zinc to aluminium constant with increasing additions of silicon. The intention was to analyse the results when graphically represented on a vertical section plot.

As mentioned previously, a prime objective of the work was to obtain scientific information of immediate practical, industrial benefit. Thus, logical follow-on investigations were planned to determine the effect of copper and magnesium additions on the behaviour of the zinc-aluminium-silicon ternary alloys. The whole scheme should become clear on studying Table 8, which gives the nominal compositions together with the designation mark of each alloy.

Melts were prepared by foundry staff with considerable experience of melting and casting zinc-aluminium alloys. The well established technique involved melting in a clay - graphite crucible in a natural gas fired furnace. For each alloy, the pouring temperature was set at 50°C above the estimated liquidus temperature. During melting, care was taken to avoid the melt rising above that temperature at any time, except in certain cases , to be mentioned later. For the zinc-rich alloys, the weighed amounts of zinc and aluminium were melted together in the crucible. If required, silicon was added as a 50/50, aluminium/silicon hardener. Understandably, there are difficulties with dissolving the silicon hardener, but a technique based on successful experience was used. The main features of the technique were to add fragmented hardener to the melt and stir with a silica rod, remove visible undissolved hardener, further fragment, put back in the melt and repeat the operation.

For high aluminium alloys, the aluminium and if required the silicon hardener were melted first, the temperature reduced, and the zinc added. With those alloys, considerable

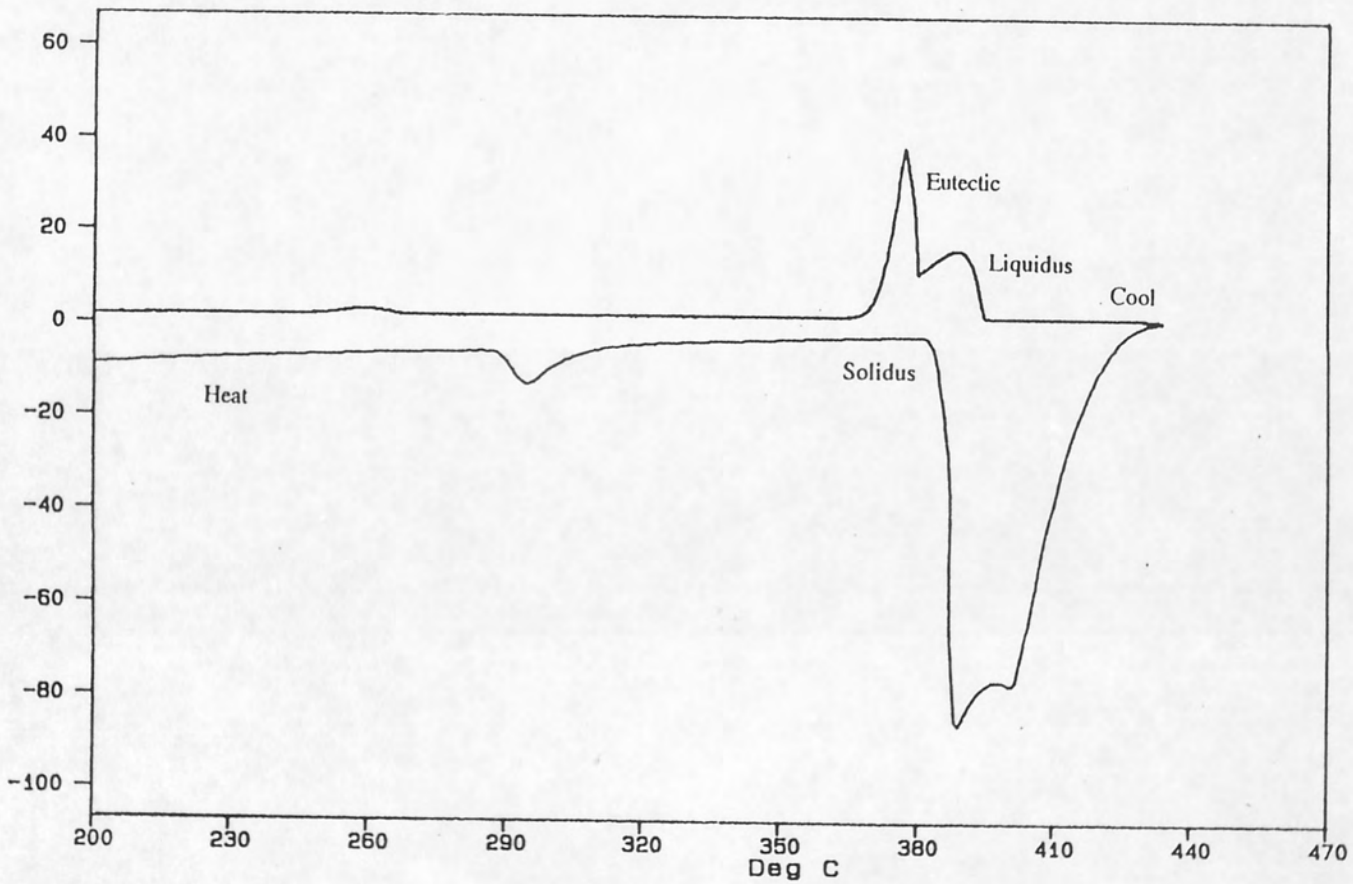

Figure 24 DTA trace for Z3A alloy.

Alloy type	Compositions %
Binary	Zn + 0.5, 3, 5, 10, 15, 25, 30, 40, 50, 60, 70, 80 Al
Ternary	Zn 30Al + 0.25, 0.5, 0.75, 1.0, 1.5, 2, 3, 5 Si Zn 50Al + 0.5, 1.0, 2.5, 5.0, 7.5, 10 Si Zn 70Al + 2.5, 5.0, 7.5, 10, 12.5, 15, 20 Si
Quasi - commercial	Zn 30Al 1Cu 0.02Mg + 0.25, 0.5, 1.0, 1.5, 2.0 Si Zn 30Al 2Cu 0.02Mg + 0.25, 0.5, 1.0, 1.5, 2.0 Si Zn 50Al 1Cu 0.02Mg + 1, 2, 3, 5, 7.5, 10 Si Zn 50Al 2Cu 0.02Mg + 1, 2, 3, 5, 7.5, 10 Si Zn 70Al 1Cu 0.02Mg + 2.5, 5, 7.5, 10, 15 Si Zn 70Al 2Cu 0.02Mg + 2.5, 5, 7.5, 10, 15 Si
Commercial	ZA8, ZA12, ZA27 see Table 4 Alloy3, Zn 4Al 0.03Mg Alloy5, Zn 4Al 1Cu 0.05Mg

Table 8 Nominal compositions of alloys tested

care was taken to control the loss of zinc by vaporisation.

For alloys requiring the addition of copper, a 40% copper- aluminium hardener was added to the melt, with vigorous stirring, just before pouring.

For magnesium-containing alloys, the pure metal was added immediately after the pouring temperature had been reached, followed by a quick stir to avoid vapour loss, and pouring.

No flux was used during melting. With most alloys, the thin layer of slag which formed on the melt caused no problems. In the higher aluminium alloys, the slag was occasionally "sticky" due to the presence of oxide. That slag was removed by scraping, just before pouring.

Before the start of the project, careful consideration was given to the problem of making such a small, but representative sample of each alloy, for the DTA work. It was the writer's long standing association with powder metallurgy that inspired the idea of "shotting" each melt. Assuming that a melt is homogeneous after careful control of procedure and adequate stirring, pouring into a bath of water would give a high enough quench rate to freeze the chemical state of the liquid metal. With most alloys, the effect of pouring into water was to produce some shot, but mainly a tangle of stringers. However, within the stringers were droplet shaped pieces of metal that proved to be ideal for shaping into DTA samples. The premise that the frozen droplets were representative of the melt was put to the test on several occasions by repeat testing of randomly selected droplets from a given alloy. The high degree of reproducibility was quite remarkable.

The chemical analyses of all the alloys made and tested, are given in Table 9 in the Appendix.For the binary alloys, and a few of the ternaries, the small slab cast from each melt was analysed. For most of the alloys, the sample for chemical analysis was taken from shotted material. As a check, for about a dozen alloys, both types of analysis sample were taken. In each case, the differences between the two sets of analysis results were small enough to be ignored.

4.3 Foundry cooling curves.

It is accepted that for pressure die and permanent mould castings, the cooling rates are very fast, and create far from equilibrium microstructures. But the cooling rates of sand castings could compare with those imposed on the samples during thermal analysis. After some personal enquiries to foundrymen and researchers, and an exploratory literature search, no specific information was obtained on the cooling rates experienced by the zinc-aluminium based alloys during casting. Thus, it was decided to make some exploratory experimental determinations using one alloy. It seemed appropriate to select a zinc rich alloy, which on cooling from the molten state, solidified in two stages, for example, as primary crystals followed by a eutectic. On that basis, the 90% zinc, 10% aluminium composition was selected.

After considering the types of commercial castings produced, it was decided to study the cooling of the molten alloy after casting into each of four, cylindrical moulds, namely,

1. 80 mm diam. sand

2. 80 mm diam. thin walled steel tube, lagged with Kaowool

3. 80 mm diam. thick walled iron, chill mould

4. 40 mm diam. sand

As a sighting shot, the lagged mould was tried first since it was suspected that the cooling rate of the sand casting might be too fast to handle experimentally. This prediction, fortunately, was subsequently proved to be wrong.

The set-up for each experiment is shown in Figure 25. The thermocouple was Type K, mineral insulated, positioned in the mould in a thin walled, stainless steel sheath. The cold junction oven was controlled at 45°C. A Tekman TE 200, millivolt, chart recorder was calibrated before each experiment, using a Time Electronics Ltd. device.

About 2kg of alloy was melted and the temperature adjusted to 720°C before pouring into the mould.

The chart recording of temperature vs time gave a much clearer depiction of arrests than anticipated, as illustrated by Figure 26.

4.4 Fluidity spiral tests.

A foundryman must ensure that the molten metal completely fills the mould. With relatively low melting point alloys, such as those of zinc base, which are often used for complex castings, rapid filling of the mould cavity is essential. Thus, it was decided to measure the fluidity of a small selection of alloys, to acertain whether any significant differences existed.

A well established method of assessing fluidity is the Spiral Test using a sand mould. Since the pouring temperature is important to the flow of molten metal in a mould, it was decided to pour each alloy being tested, from fifty degrees above its determined liquidus temperature.

4.5 Optical and electron metallography

It was anticipated that the extent of optical metallography would be limited, because of the availability of an SEM, with the benefit of good image contrast in the type of alloys under investigation. Thus all samples were mounted in conducting Bakelite, in preparation for polishing on wet, rotating carborundum papers and diamond paste impregnated cloth covered wheels. Samples were finished either on a one micron diamond wheel, or by hand pad with Sylvo polishing fluid.

The optical microscope used was a Reichert - Jung, Polyvar.

The scanning electron microscope used was a Cambridge S90B, fitted with a K E Developments, backscattered electron detector and an Oxford Instruments AN 10000, energy dispersive, X-ray analyser.

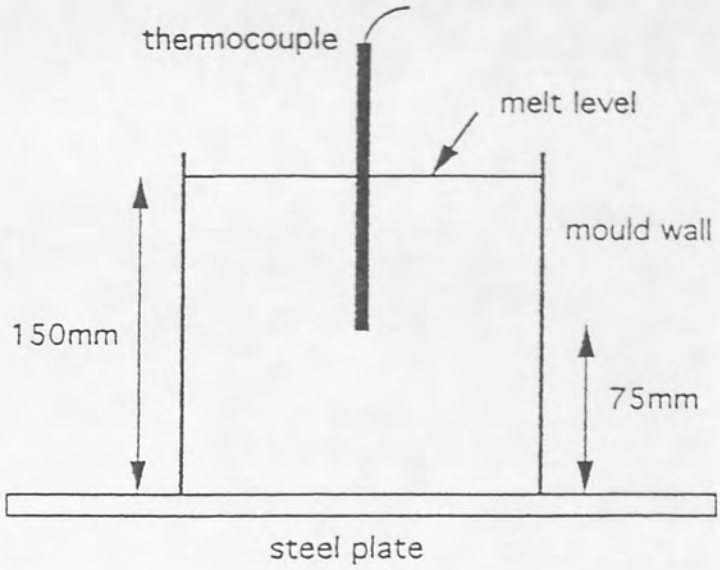

Figure 25 Set-up for foundry cooling curves

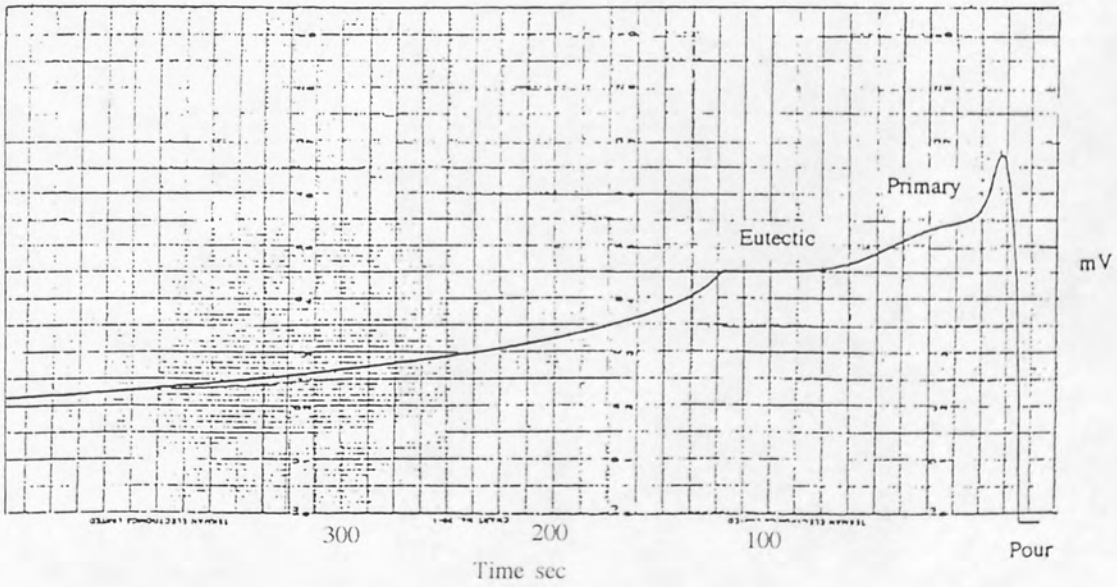

Figure 26 Portion of cooling trace for chill casting.

5. EXPERIMENTAL RESULTS

5.1 The alloys tested

Each of the alloys studied was chemically analysed by an established, specialist laboratory, CLS Ltd., Birmingham. The analysis results are presented in Table 9 in the Appendix.

5.2. Binary zinc-aluminium.

Having established an experimental technique using pure zinc with the STA 1500, the zinc-aluminium binary system was selected as a means of assessing the suitability of the equipment for phase diagram determination. Initially, alloy compositions were chosen for test to give data at 10% intervals between the two pure metals, with some extra alloys for more detail in the zinc-rich, eutectic region. The results, including solidification ranges, are compared with published values (36) in Table 10. As a further illustration of those results of particular interest, the liquidus and solidus values obtained from DTA traces are presented graphically in Figure 27.

A metallographic examination of the 5% aluminium alloy after DTA, clearly revealed the presence of a zinc-rich primary phase. This confirmed the presence of a small primary phase arrest, seen earlier on the DTA cooling curve for that alloy. As a consequence, alloys were prepared for testing with analysed compositions of 4.81, 5.15 and 5.39% aluminium. DTA traces indicated the presence of a primary phase in the 4.81 and 5.39% aluminium alloys, and this was subsequently confirmed by metallographic examination. The DTA trace from the 5.15% aluminium alloy showed eutectic solidification only. During a very thorough metallographic examination of the DTA sample, no primary phase was seen.

In the aluminium-rich alloys, the expected solid phase changes were not clearly defined on DTA traces. Thus, additional tests were made on samples containing 80% aluminium, using techniques aimed at emphasising any solid phase thermal events. No clarification was obtained and comment is made later in the Discussion.

5.3 The ternary and complex alloys.

The results of the investigation into the Zn-Al-Si ternary system and the effects of copper and magnesium additions, are presented graphically in Figures 28, 29 and 30. Although a full set of data was taken from the DTA trace for each sample, it was decided to restrict the presentation to the liquidus and solidus values. The graphs represent vertical sections of the ternary system with a constant ratio of zinc to aluminium as the silicon content increases. Each graph shows the liquidus (L_c) and solidus (S_c) obtained from a DTA cooling curve and the solidus (S_h) from a heating curve. Features of particular interest are the precise location of a eutectic trough and the slope of the liquidus from zero silicon, which is relatively steep in the zinc-rich region and lessens in slope in the proportion of 18 to 11 to 8 for the 30%, 50% and 70% aluminium alloys, respectively. Also, in each case, the 1% copper with magnesium additions uniformly lower the liquidus by 5 or 6°C and the higher copper addition of 2% gave a further, slight reduction in the liquidus

position. More significantly, the 1% copper with magnesium additions proportionately reduce the silicon content of the eutectic by approximately 12%, 18% and 17% for the 30%, 50% and 70% aluminium alloys, respectively. The 2% copper addition causes a further, small reduction in the silicon content of the eutectic by 5% and 2% for the 50% and 70% aluminium alloys respectively, but by a surprising 100% in the case of the 30% aluminium alloy

To help with the analysis of the results, isotherms were constructed on each graph, and the silicon content at the intersection with the liquidus on either side of the eutectic trough, was recorded. The results, together with the precise position of the eutectic trough are given in Table 11.

A contour diagram of the liquidus surface projection is shown Figure 31.

5.4 Electron metallography.

It was considered unnecessary, and indeed would have not been feasible, to make a detailed metallographic examination of each sample tested. Thus, samples were selected for examination on the basis of one or more of the following criteria,

* the DTA trace showed exactly what was theoretically expected
* a feature of the DTA trace was anomalous
* seek evidence to confirm a difference between two DTA traces

A common feature of all the samples examined was the presence of macro-porosity. As explained earlier, when each sample became molten during a test, a cocoon of oxide retained the shape of the solid. Thus, it was inevitable that some shrinkage porosity would arise in the sample during solidification. That feature of samples after DTA was useful during subsequent SEM examination, when seeking phases representing the last liquid to solidify . A typical macro-structure is shown in Figure 32.

The benefits of atomic number contrast when using the backscattered electron imaging technique were evident from the examination of the first samples. Also, the general area SEM analyses correlated well with the known chemical analyses. The results of the electron metallographic examination of selected samples are shown in Figures 33 to 42.

Z30A, DTA trace Figure A1, Appendix.

The DTA cooling trace showed a primary phase solidification arrest at 507°C, an inflection at about 440°C, an arrest at 380°C and last liquid to solidify at about 370°C.

An electron image of the structure is shown in Figure 33. A general area analysis gave 71Zn 29Al 0.4Fe. The main feature of the structure is the presence of heavily cored primary α crystals, the dark centre of one analysed at 49Zn 51Al. The mottled, lenticular shaped region at the centre of the photograph, which analysed at 97.5Zn 2.5Al, represents the last liquid to solidify as the zinc rich eutectic of $\beta + \eta$, which on further cooling transformed to $\alpha + \eta$. The adjacent, white, oval shaped region indicates where β phase formed at about 440°C (accepting the existence of a peritectic reaction), and later transformed to $\alpha + \eta$. One of the several fine needles which were observed during microscopical examination was analysed to give the composition 15Zn 63Al 22Fe.

Z30A2S, DTA trace Figure A2, Appendix.

The DTA cooling trace showed a small primary phase solidification arrest at 529°C, a very well defined arrest at 490°C, an inflection at about 440°C and last liquid to solidify at about 390°C.

As can be seen in Figure 34, more than half of the cross section contains aluminium-rich α primary dendrites, but the alloy composition is on the silicon side of the eutectic trough. Of the several long needles in the structure, one analysed at 95Si 3Zn 2Al, clearly a primary silicon rich phase. The end of the needle can be seen at the centre of the right hand edge of Figure 35. An analysis of the core of the primary dendrite near the centre of Figure 35, gave 44Zn 56Al, confirming it as the aluminium-rich α phase. An adjacent mottled region, marked **x**, analysed at 84Zn 16Al representing the formation of β phase during solidification. An adjacent white area marked **o**, analysed at 99.5Zn 0.5Al, representing the last liquid to solidify, as the zinc rich eutectic. The chunky, black script-like phase, at the top left of the micrograph, analysed at 64Si 24Al 12Zn, confirming that it is the silicon-rich primary phase.

Z50A5S, DTA trace Figure A3, Appendix.

The DTA cooling trace showed a small, primary phase solidification arrest at 557°C, a well defined arrest at 523°C, an inflection at about 460°C and a last liquid to solidify at about 420°C.

A general area analysis of the field shown in Figure 36, gave 50Zn 44Al 6Si. The large primary dendrites have a distinctive pattern of black and white layers. Analysis of a white layer gave 52Zn 48Al. The structure is a manifestation of the presence of a miscibility gap in the particular region of the phase diagram, giving rise to a characteristic form of decomposition of the primary α phase on cooling. This type of structure was seen in several samples and will be explained in Chapter 6. The grey angular constituent, at the edge of a pore on the right of Figure 37, analysed at 87Si 6Al 7Zn, representing the silicon-rich primary phase.

Z70A10S, DTA trace Figure A4, Appendix.

The DTA cooling trace showed a small, primary phase, solidification arrest at 610°C, a well defined arrest at 547°C, an inflection at about 540°C and last liquid to solidify at about 492°C.

A general area analysis of the field shown in Figure 38, gave 64Al 21Zn 15Si. The black, cube shaped constituent had the composition 97Si 2Al 1Zn, confirming that it was the silicon-rich primary phase. The α phase in the surrounding α + Si eutectic was clearly cored, as particularly well illustrated at the bottom left of the micrograph. A dark, aluminium-rich region, which analysed at 78Al 22Zn, immediately surrounds the black cubic silicon-rich particle. The image becomes lighter in colour, moving away from the particle, as the concentration of zinc increases. An analysis of the light region gave 52Al 48Zn.

Z50A2CM1S, DTA trace Figure A5, Appendix.

The DTA cooling trace was one of the most eventful produced during the programme of experiments. There was a sharp, primary arrest at 540°C, an inflection at about 530°C, an arrest at 487°C, an inflection at about 455°C, a small arrest at 392°C and last liquid to solidify at about 372°C.

A general area analysis gave 59Zn 38Al 1.7Cu 1Si. A range of microstructural features are illustrated in Figure 39. Clearly shown are heavily cored primary α dendrites, several interdendritic phases, fine needles and porosity. The needle at the lower centre of the micrograph analysed at 58Al 20Fe 13Zn 7Si 1.5Cu. Analysis of the white irregular interdendritic phase near the centre of Figure 40 gave 87Zn 12Cu 1Al, representing the last liquid to solidify as the zinc rich-eutectic. The adjacent, angular grey phase gave an analysis of 58Cu 27Al 15Zn.

Z50A2CM5S, DTA trace Figure A6, Appendix.

The DTA cooling trace showed a small primary arrest at 565°C, a well defined arrest at 510°C, an inflection at about 445°C and last liquid to solidify at about 370°C.

A general area analysis gave 52Zn 41Al 5.7Si 1.6Cu. One of the large black, irregular or sometimes script-like constituents of the structure seen in Figure 41, analysed at 98Si 1.5Zn, clearly indicating the primary silicon phase. One of the several long, fine needles evident in the structure, analysed at 64Al 21Fe 8Zn 7.5Si. In an interdendritic region, detailed in Figure 42, the white, outlined region in the centre of the micrograph, analysed at 88Zn 11.6Al 0.4Cu, indicating the last liquid to solidify, ie the ternary eutectic. An adjacent, mottled region, marked **x**, analysed at 81Zn 17Al 2Cu.

5.5 Foundry experiments

As explained in Chapter 4, cooling curve arrests were readily identified on the chart recorder traces. Thus, for each casting, the start temperatures of primary solidification, eutectic formation and the solid phase change were estimated. The results obtained from the ingot cooling experiments are presented in Table 12.

The mould used to produce spiral castings by the method described in Chapter 4, placed "pips" on the top of the spiral at two inch intervals. Thus the length of each spiral, in inches, was easily measured.

The results obtained from the spiral casting tests are given in Table 13.

5.6 Dendrite arm spacing

The availability of a range of cast structures, solidified under closely controlled conditions, provided the opportunity to examine the effect of composition on dendrite arm spacing. Accordingly, suitable micrographs were selected, measurements were made in at least two areas of each, and the average dendrite arm spacing was estimated. The results are given in Table 14.

Al%	STA liquidus and solidus °C			Elliott liquidus and solidus °C	
	L_c	S_h	S_c	L	S
0.5	416	404	388	416	393
3.0	394	382	367	397	382
5.0	381	382	364	382	382
10.0	423	380	364	420	382
18.1	463	381	367	466	390
24.7	493	429	370	494	440
30.0	507	440	370	508	442
39.9	536	451	380	539	451
50.0	562	473	417	564	467
59.6	586	501	440	586	504
70.0	605	539	480	608	540
80.0	624	580	525	626	580

Table 10 Liquidus and solidus values for binary alloys

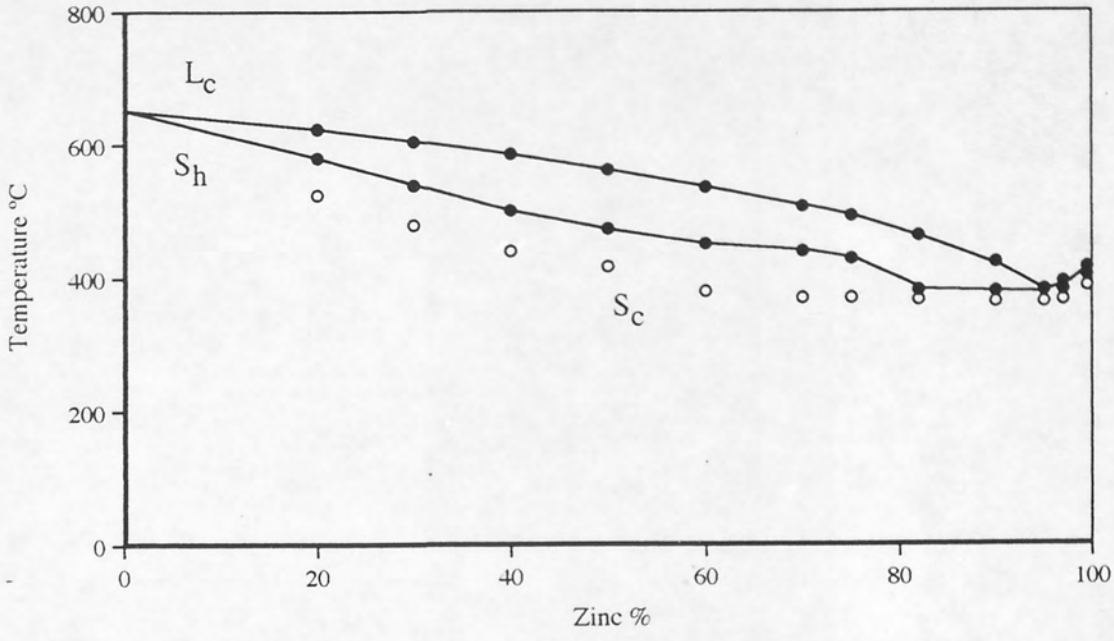

Figure 27 Experimental results for liquidus and solidus of binary

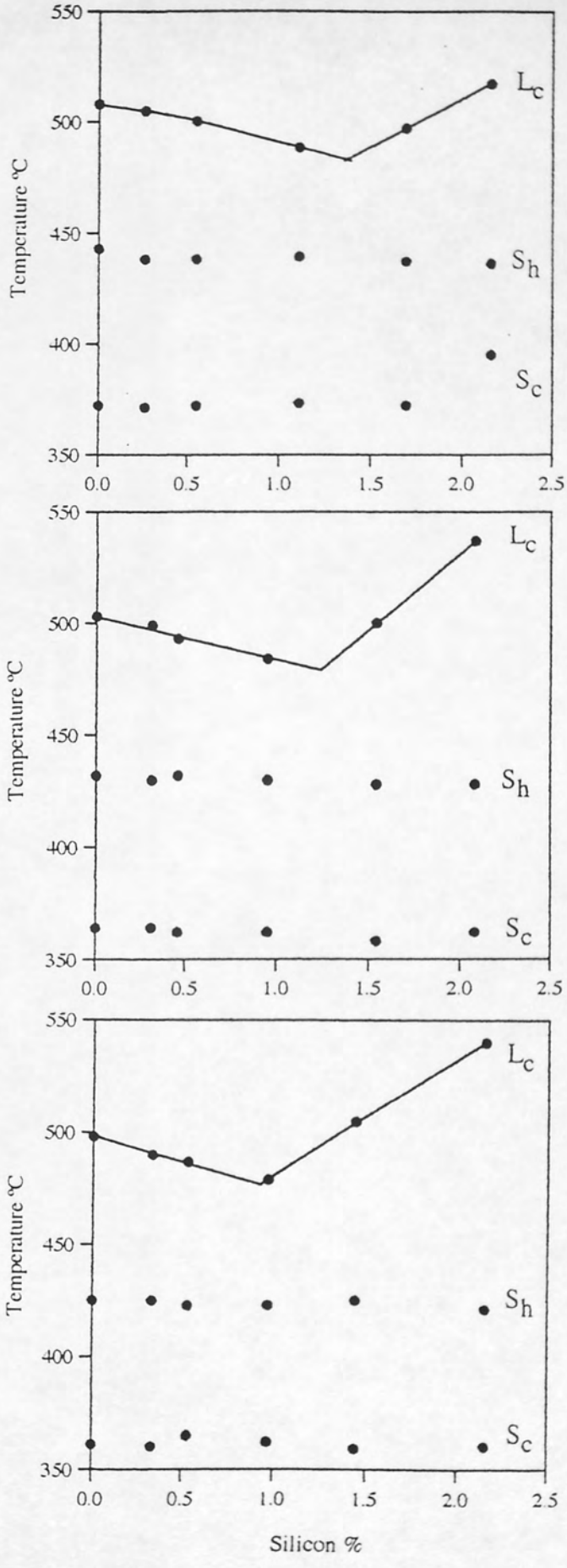

Figure 28 Vertical sections, 30% aluminium.

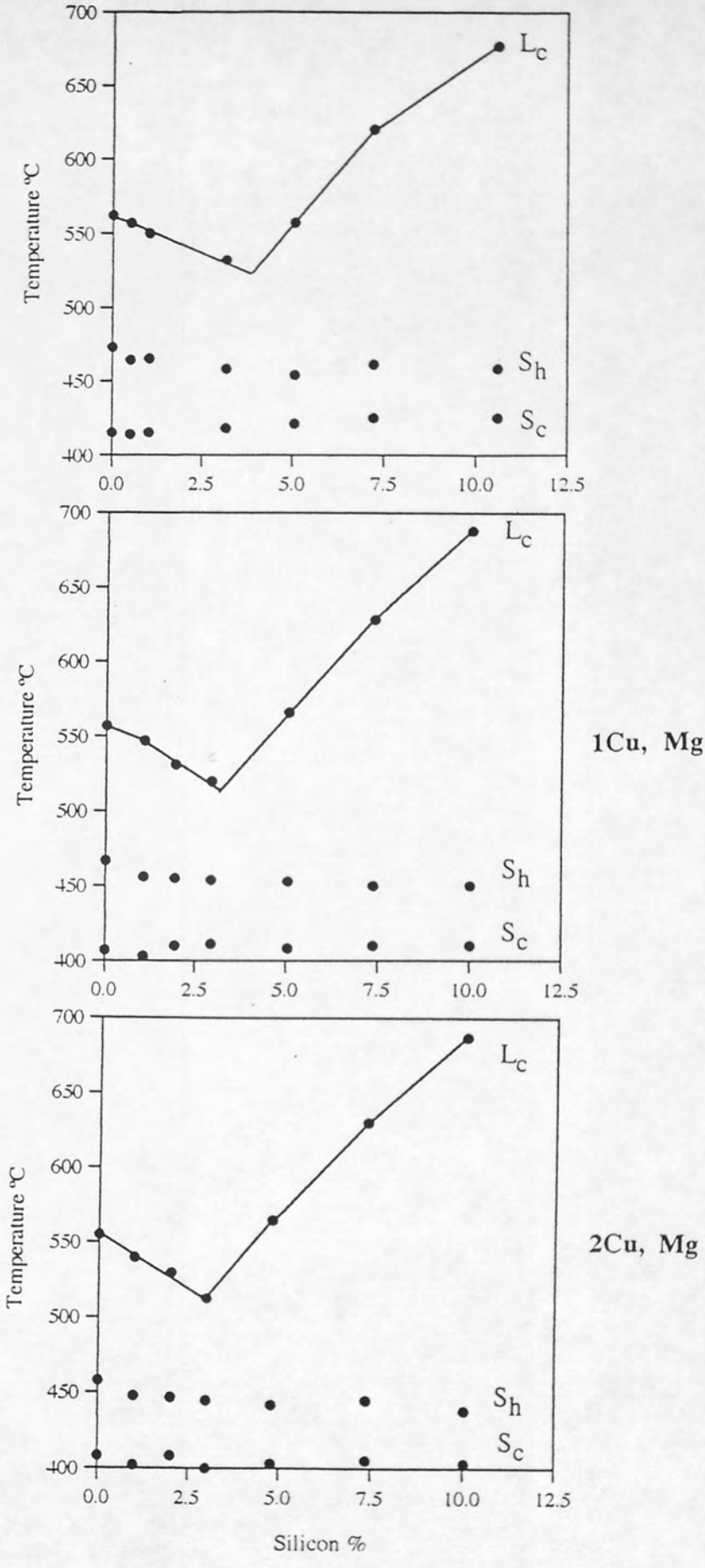

Figure 29 Vertical sections, 50% aluminium.

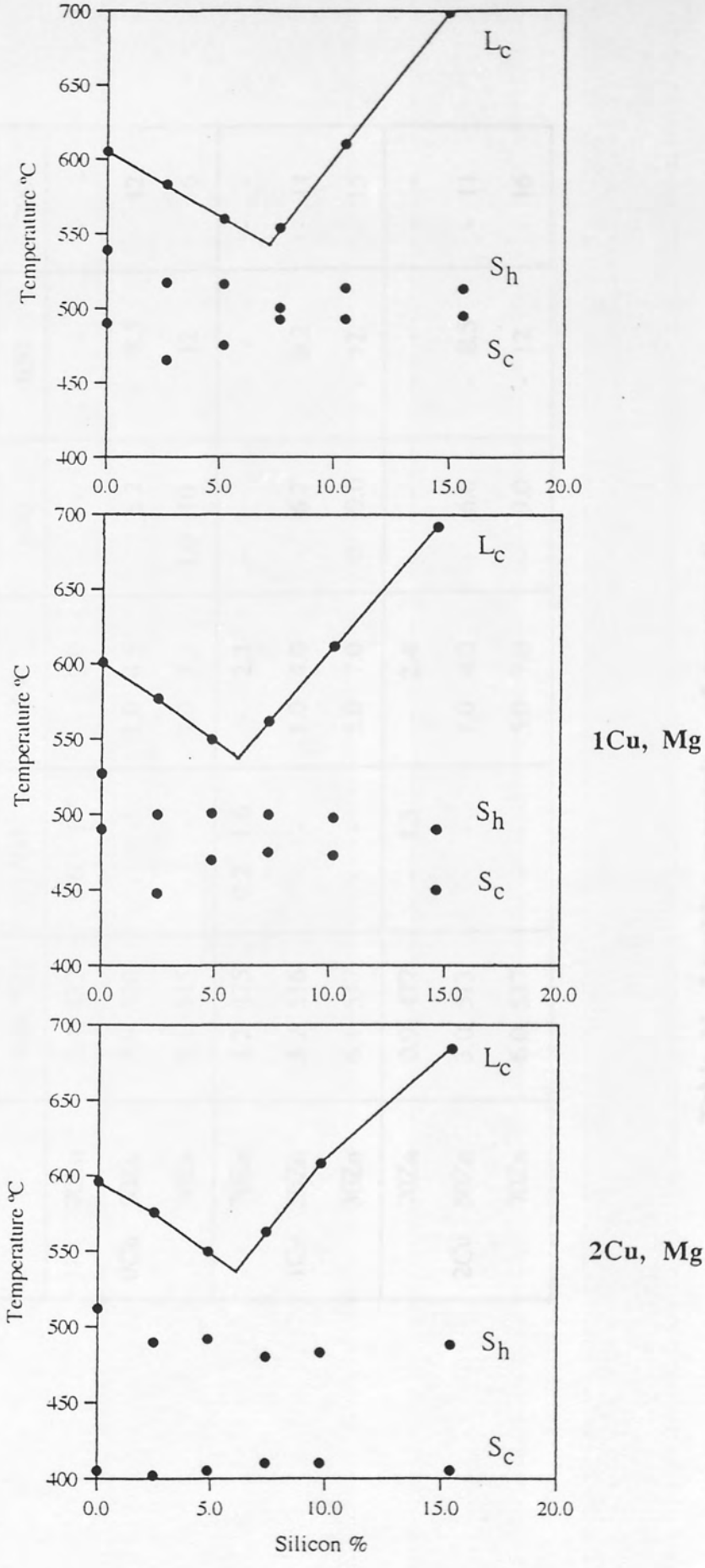

Figure 30 Vertical sections, 70% aluminium.

Alloy		Eutectic	Silicon % at temperature ℃				
		%Si, ℃	500	550	600	650	700
0Cu	70Zn	1.4, 482	0.6 1.7	- 2.9	- -	- -	- -
	50Zn	3.9, 520	- -	1.0 4.5	- 6.2	- 8.5	- 12
	30Zn	7.1, 545	- -	7.0 7.3	1.0 10	- 12	- 16
1Cu	70Zn	1.2, 475	0.2 1.6	- 2.3	- -	- -	- -
	50Zn	3.2, 516	- -	1.0 4.0	- 6.2	- 8.2	- 11
	30Zn	6.1, 537	- -	5.0 7.0	0 9.0	- 12	- 15
2Cu	70Zn	0.9, 477	- 1.3	- 2.4	- -	- -	- -
	50Zn	3.0, 513	- -	1.0 4.0	- 6.0	- 8.5	- 11
	70Zn	6.0, 537	- -	5.0 7.0	- 9.0	- 12	- 16

Table 11 Liquidus comparison of ternary alloys

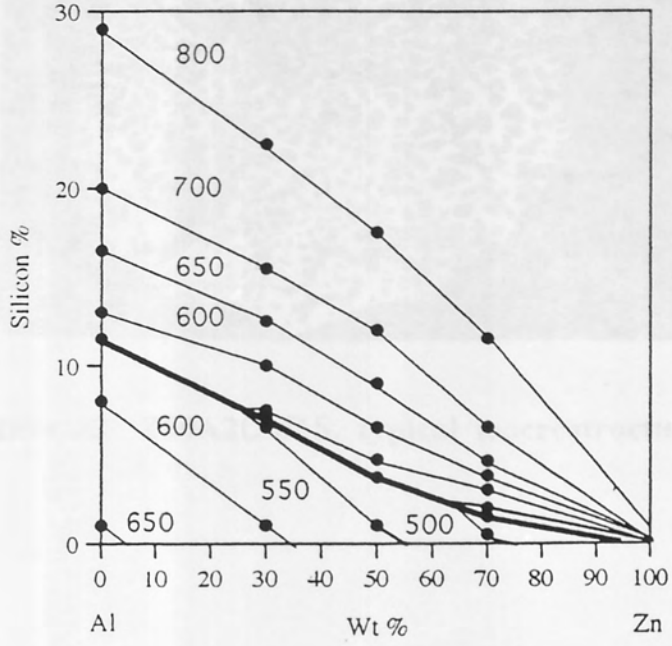

Figure 31 Liquidus surface contours of ternary.

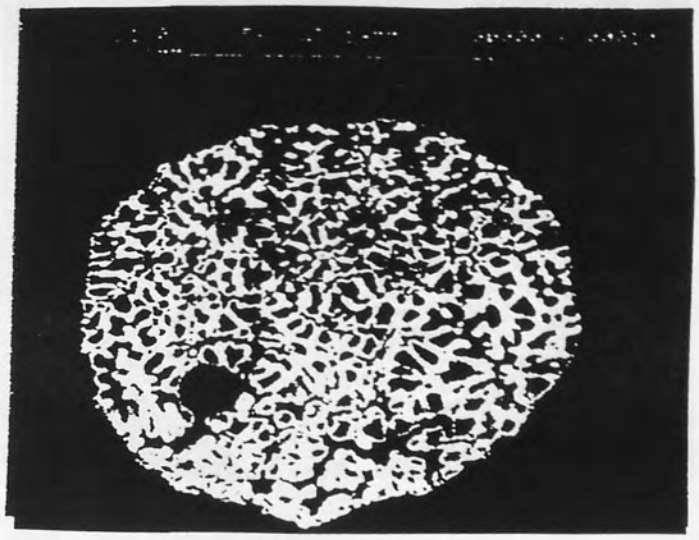

Figure 32 Z50A2CM1S, typical macrostructure

Figure 33 Z30A, structure reflects DTA trace

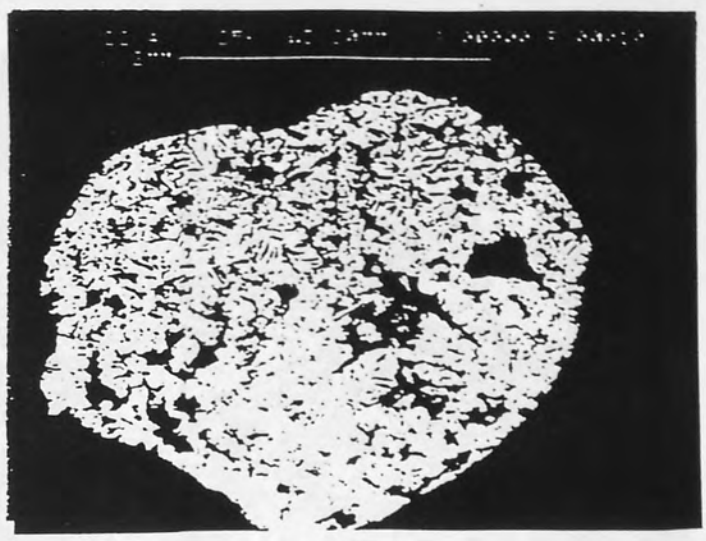

Figure 34 Z30A2S, macrosegregation of silicon

Figure 35 Z30A2S, general structure

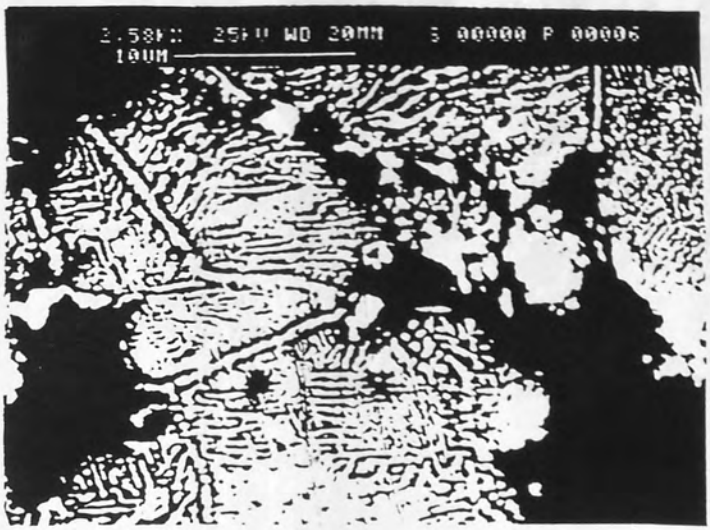

Figure 36 Z50A5S, decomposition of primary phase

Figure 37 Z50A5S, primary silicon

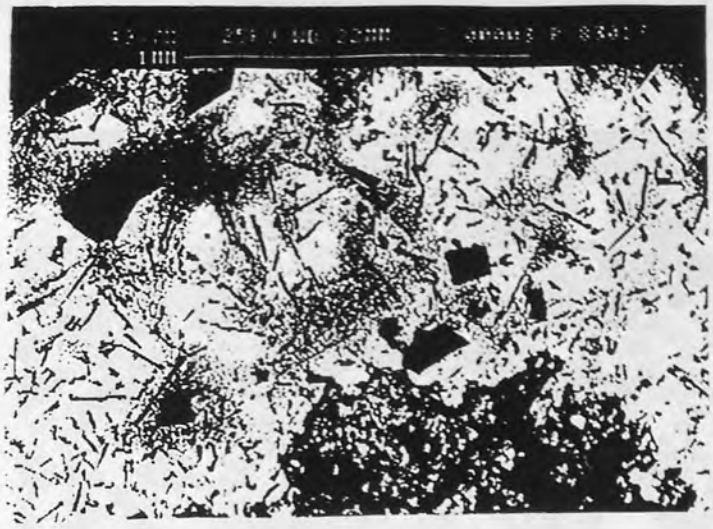

Figure 38 Z70A10S, cored hyper-eutectic

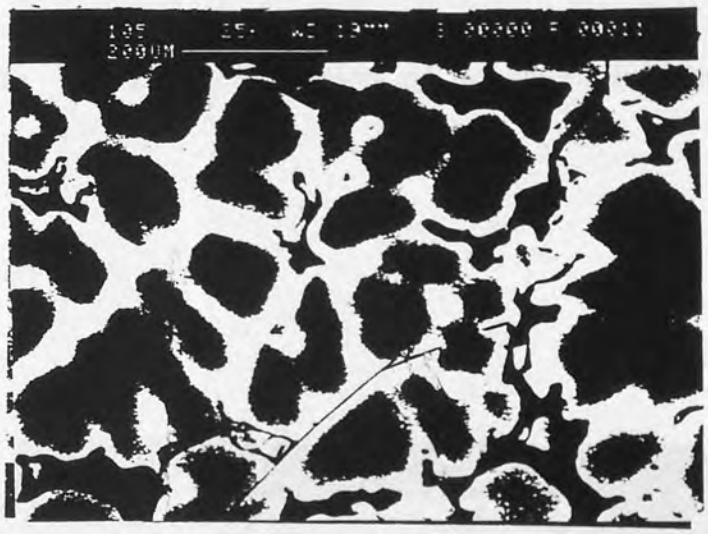

Figure 39 Z50A2CM1S, cored primary

Figure 40 Z50A2CM1S, T phase

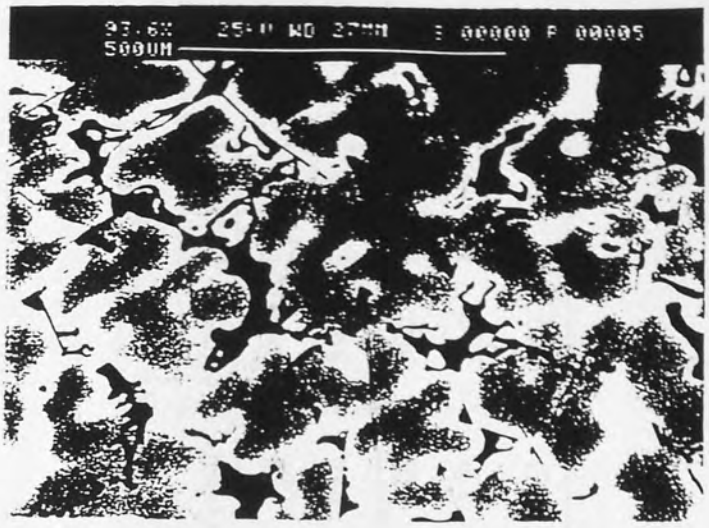

Figure 41 Z50A2CM5S, needles of intermetallic compound

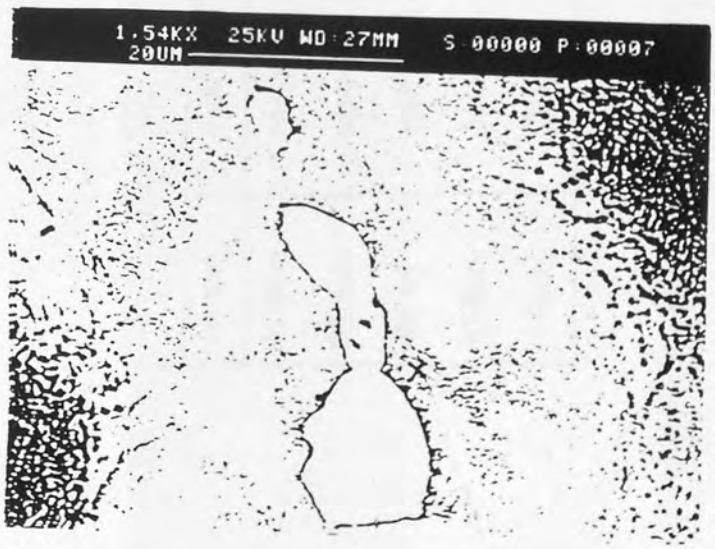

Figure 42 Z50A2CM5S, decomposition of zinc rich phases

Mould		Cooling rate, °C per min.			Arrests °C		
size mm	type	liquid	pasty	solid	primary	eutectic	solid
80 diam	Kaowool	8	2	2	428	386	277
80 diam	sand	17	3	3	434	390	277
80 sq.	chill	137	27	10	436	386	267
40 diam	sand	48	8	9	428	387	277
3 diam	STA	2	2	2	423	380	266

Table 12 · Results from foundry cooling curves.

Alloy	Length inch
zinc	>60
aluminium	43
Z30A	20
Z30A1.5S	22
Z30A1CM	34
Z30A1CM1S	29
Z30A2CM	34
Z30A2CM1S	28
Alloy 3	41
ZA27	34

Table 13 Fluidity spiral results.

Alloy	Dendrite arm spacing µm
Z30A	130
Z30A0.25S	110
Z30A2S	60
Z30A1CM0.5S	100
Z30A2CM	100
Z50A	190
Z50A0.5S	200
Z50A5S	120
Z50A2CM1S	120
Z50A2CM5S	100
Z70A	220
Z70A2.5S	220
Z70A10S	220
Z70A2CM2.5S	215

Table 14 Dendrite arm spacing in samples after DTA

6. DISCUSSION

6.1 Thermal analysis.

The STA 1500 equipment is marketed mainly for the thermal analysis of ceramic materials, and the Aston unit was purchased for that purpose. However, following an enquiry, it was decided to make some exploratory tests on metals, without changing the equipment set-up, but with thorough consideration of the experimental method. Fortunately, the preparation of samples, the experimental technique and the method of interpreting the results were well chosen, and came together to create a very encouraging overall picture. It quickly became clear that excellent results could be obtained from tests designed to explore the solidification characteristics of a family of zinc base alloys, the physical properties of which were being studied by a colleague. The novel aspects of the thermal analysis experimentation are discussed below.

The initial experiments with commercially pure zinc demonstrated remarkable levels of sensitivity, accuracy and reproducibility. Optimum experimental conditions were established, but it was noticeable that even if conditions were well away from optimum, the quality of the results was still very high and based on past experience, valid.

It is generally accepted by research metallurgists using thermal analysis that heating and cooling rates of 1°C per minute, or less, are necessary for accurate results. The makers of the STA 1500 offer the observation that 5°C per minute is "slow enough" to avoid hysteresis problems when studying transformations. Indeed, the writer obtained acceptable results with that rate of cooling, although it became clear that 2°C per minute was the optimum cooling rate. In choosing the optimum rate, account was taken of the total time of a test run. Understandably, alloys with a relatively high melting point coupled with numerous phase changes on heating and cooling took a long time to test. However, with a 10°C per minute heating rate and 2°C per minute cooling rate, it is possible to complete such a test in a "working day" of eight hours. It was pleasing to find at a later stage that the chosen cooling rate of 2°C per minute was similar to that experienced by a sand casting in the foundry. The choice of 10°C per minute for the heating rate is worthy of comment. The emphasis was to be put on the cooling curve for the determination of the phase change temperatures, with an initial reservation on the solidus. As mentioned earlier, Porter and Easterling (8) observed that, based on thermodynamic first principles, the solidus is more reliably obtained from a heating curve. A further comment was that the rate of heating could be relatively fast, compared with cooling, without compromising the accuracy of the result. Thus, the approach of the writer was to select as fast a heating rate as possible, in order to keep the total test time to a minimum. It was useful to find, confirming the Porter and Easterling observation, that the solidus of an alloy was satisfactorily determined with a heating rate as high as 10°C per minute.

6.2 The binary alloys.

The STA 1500 was first characterised and calibrated with commercially pure zinc, then the experimental assessment programme was extended into the zinc-aluminium binary system, with the added possible benefit of gaining new information. Indeed, a Keynote

speaker at the 1985 ILZRO Conference, when referring to the acknowledged need of foundrymen for more basic scientific information on the widely used complex alloys, commented that even the binary system was not fully understood. As testing progressed it became clear that the STA 1500 was excellent for the study of melting and solidification, fortunately the focus of the project, but as anticipated, not so well suited to the study of solid phase transformations.

For the specific compositions tested, there was very close agreement between the determined liquidus (cooling), and solidus (heating), and the accepted values, published by Elliott (36). In the zinc-rich alloys, the solid state transformations were clearly defined on both heating and cooling, by DTA curves, with a hysteresis gap of about 25°C. In all cases, an average value agreed reasonably well with the published equilibrium temperature values. In the aluminium-rich alloys, the solid state transformations were poorly defined on DTA traces. In particular, the α / $\alpha + \eta$ boundary was barely indicated on a heating curve and not registered at all on the subsequent cooling curve. For interest and to broaden experience with the STA 1500, a programme of experiments was planned with an 80% aluminium alloy, with the object of locating that phase boundary. A variety of techniques were used, for example, very slow heating and cooling rates, isothermal treatment above and below the likely boundary temperature, testing a sample after rapid cooling and aging, and so on. After a week of testing, no progress had been made, and bearing in mind the original decision to concentrate the study on the melting and solidification behaviour of the alloys, the programme was abandoned. However, the subject remains of great interest, and further study may well be included in a future project.

The writer's results were compared with data taken from the generally accepted equilibrium phase diagram, due to Elliott (36), as shown in Table 10. The liquidus points obtained from DTA cooling curves were in excellent agreement with the published values, with a high proportion being identical. The solidus points obtained from STA heating curves also show good agreement, with the largest difference being two degrees.

Solidification range

The freezing, or solidification range of an alloy is of prime importance in the foundry. In the absence of other information, taking the temperature difference between liquidus and solidus from an equilibrium diagram may be of some use. However, as clearly demonstrated by the results presented here, the solidification range of an alloy during continuous cooling, even at relatively a slow rate, may be much greater than the value at equilibrium. The DTA results, given in Table10, agree well with the long established binary equilibrium diagram. Additional information, presented in Table 15, arose when comparing for each alloy, the equilibrium freezing range, L - S_h, with the continuous cooling freezing range L - S_c. Looking at the extension in freezing range values during continuous cooling, moving through the compositions from 0.5% aluminium, there was a sharp increase between 18% and 25% aluminium and the higher level was then maintained up to 80% aluminium. It is likely that the actual change in the level of freezing range extension occured at or near to 25% aluminium, that is, the composition of the β

Al%	STA liquidus and solidus °C			Solidification ranges °C		Extension °C
	L	S_h	S_c	$L-S_h$	$L-S_c$	S_h-S_c
0.5	416	404	388	12	28	16
3.0	394	382	367	12	27	15
5.0	381	382	364	0	17	17
10.0	423	380	364	43	59	16
18.1	463	381	367	82	96	14
24.7	493	429	370	64	123	59
30.0	507	440	370	67	137	70
39.9	536	451	380	85	156	71
50.0	562	473	417	89	145	56
59.6	586	501	440	85	146	61
70.0	605	539	480	66	125	59
80.0	624	580	525	44	99	55

Table 15 Solidification ranges of binary alloys.

phase, if the existence of a peritectic reaction is accepted, or the sharp change in slope of the solidus, in the non-peritectic phase diagram.

The eutectic reaction

During sample preparation, an attempt was made to prepare what is regarded as an alloy of exactly eutectic composition, namely, one containing 5% aluminium. Although the analysis confirmed that composition, some primary crystal formation was evident from the DTA cooling curve. Metallographic examination of the DTA sample revealed the presence of some globular zinc-rich primary phase. Further DTA samples were prepared with compositions bracketing the eutectic composition.The cooling curve results, coupled with very thorough metallographic examination of the DTA samples, established the eutectic at 5.2% aluminium, rather than the 5.0% generally accepted. The practical value of this new piece of information may be limited, but it should be of interest to researchers. Certainly, the sensitivity of the STA 1500 equipment was further demonstrated.

The peritectic reaction

As discussed in Chapter 2, although good evidence was presented during the decade following the year 1960, for the existence of a peritectic reaction at about 25% aluminium, that evidence is still being questioned. It was not an objective of the writer to study that particular aspect of the zinc-aluminium binary system, but having obtained the DTA data, it seemed sensible to make an examination.

The DTA trace for the 25% aluminium alloy is shown in Figure 43. On heating, the two solid-state phase change boundaries were indicated by a sharp arrest at 280°C and a slight inflection at about 300°C. The solidus was sharply defined at 429°C, which correlated closely with the β to $\beta + L$ phase boundary in the Elliott phase diagram, Figure 44. Uncharacteristically, the arrest line was curved and the "nose" was rounded. These features suggested that the initial formation of liquid was followed by a reduction in the rate of endothermic phase change. At about 470°C on the heating curve, a strong endothermic event was indicated, completing the phase change, as indicated by the rapid return of the trace to the baseline. The cooling trace indicated the start of primary crystal formation at 493°C, which correlated well with the Elliott phase diagram. At about 465°C an inflection in the curve showed the beginning of a strong, exothermic event, correlating well with the DTA heating curve, and the eutectic solidification was clearly indicated on the trace at 380°C. The two solid phase boundaries were well defined with an inflection at 320°C and an arrest at 260°C. Now, the previously published evidence put the peritectic reaction at a temperature of 443°C. The completion of a peritectic reaction requires atomic diffusion and mass transfer, and the sample environment was being heated at 10°C per minute. However, it was still difficult to accept a temperature lag of 22°C. Also, the DTA determined solidus for the 30% aluminium alloy was 440°C and for the 40% aluminium alloy 451°C, precluding the possibility of a peritectic reaction at a temperature near to 470°C. Comparing the DTA traces for those alloys, with that of the 25% aluminium alloy, each trace showed the arrests and inflections described earlier, occurring at closely similar

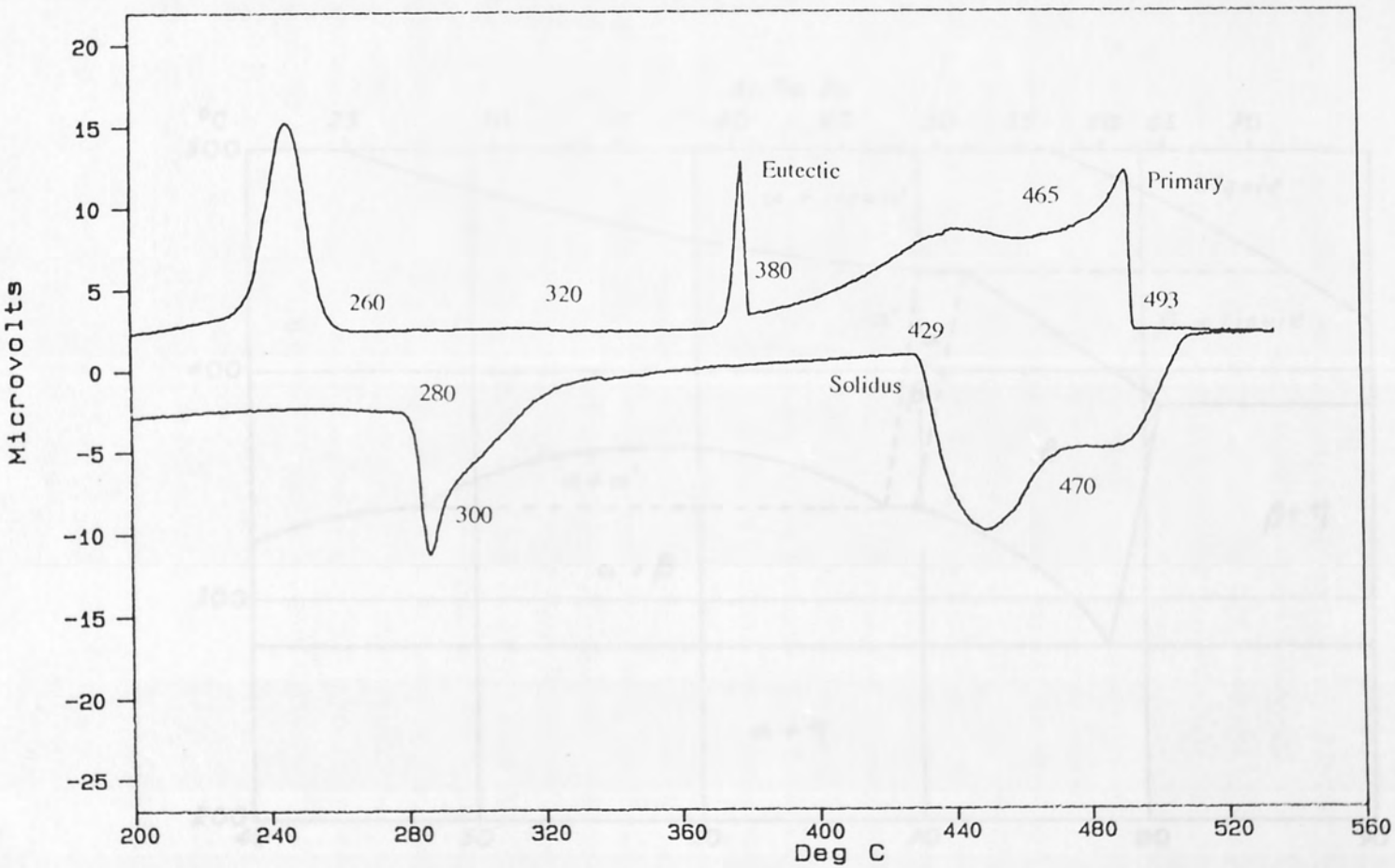

Figure 43 DTA trace for Z25A alloy

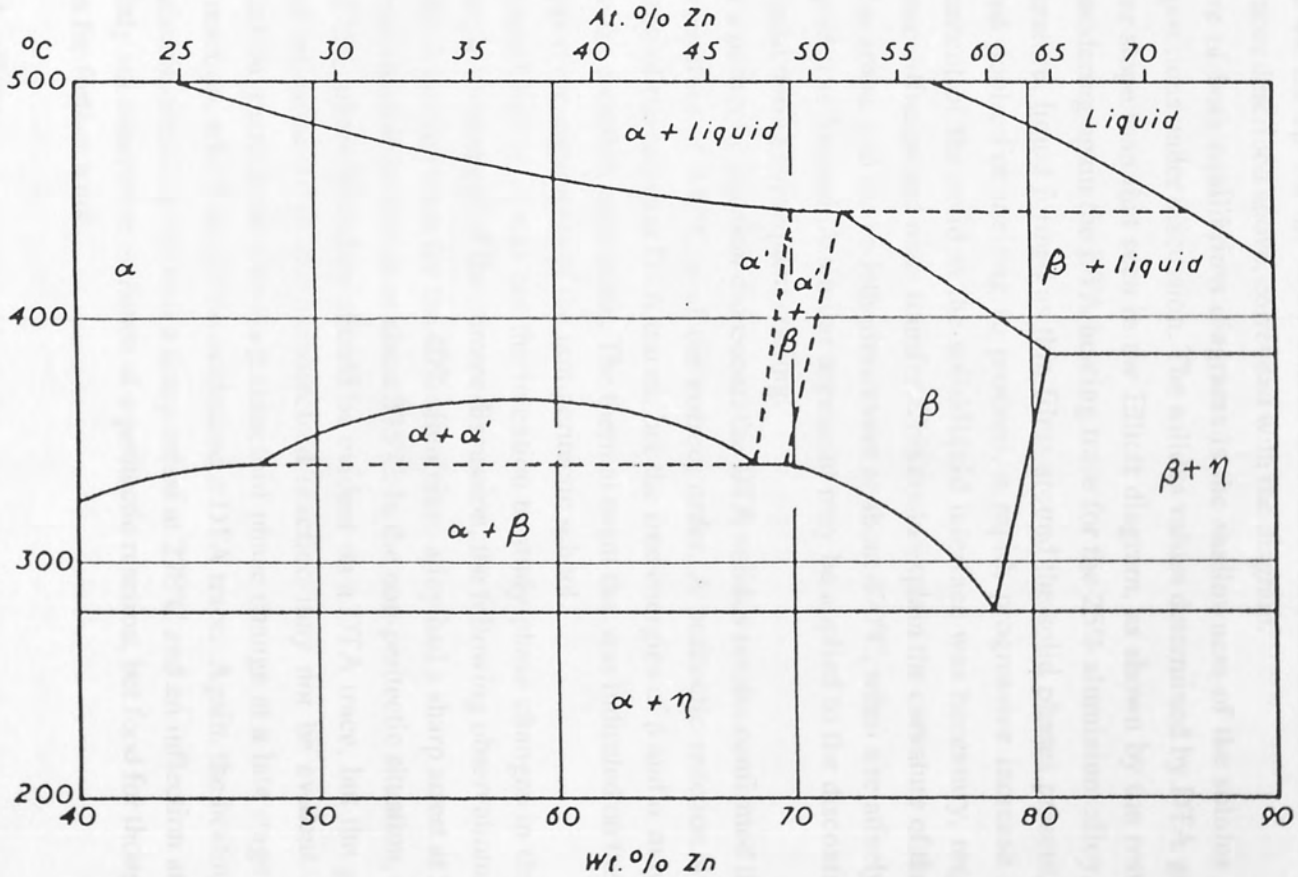

Figure 44 Central region of binary diagram

temperatures.

The non-peritectic diagram may be visualised by taking out the dotted boundary lines in Figure 44. Except for the super solidus thermal event, the arrests and inflections on the DTA traces described above, correlated with the diagram.

A feature of both equilibrium diagrams is the shallowness of the solidus in the range of compositions under discussion. The solidus values determined by DTA gave an even shallower slope than that seen in the Elliott diagram, as shown by the results in Table 10. Considering again the DTA heating trace for the 25% aluminium alloy, at the solidus temperature, liquid formed as thin films around the solid phases present, or in small scattered pools. For melting to proceed, a rapid, progressive increase in the aluminium content of the solid at the solid/liquid interface was necessary, requiring extensive atomic diffusion and mass transfer. This could explain the curvature of the trace after the solidus arrest, and the endothermic event at about 470°C, when a relatively large amount of liquid was formed. A similar argument may be applied to the discontinuous formation of solid during subsequent cooling.

Thus, if a peritectic reaction did occur, the DTA solidus results confirmed that the proposed temperature of 443°C is of the correct order. A peritectic reaction was not indicated on any of the relevant DTA traces, but the free energies of β and α may be so similar as to make detection impossible. The thermal event that was indicated on the traces appears to support the arguments of the non-peritectic school.

As indicated earlier, it was not the intention to study phase changes in the solid state. However, in the context of the current discussion, the following observations are of interest. The DTA heating trace for the 40% aluminium alloy had a sharp arrest at 278°C, and a slight, endothermic inflection at about 335°C. In the non-peritectic situation, during heating, the 275°C phase boundary should be evident on a DTA trace, but the gradual compositional adjustments of the monotectoid reaction may not be evident. In the peritectic situation, there is an α to $\alpha + \beta$ eutectoid phase change at a late stage of the monotectoid reaction, which should be evident on a DTA trace. Again, the heating trace for the 50% aluminium alloy showed a sharp arrest at 278°C and an inflection at about 345°C. Certainly not conclusive evidence of a peritectic reaction, but food for thought and a good reason for further work.

Commercial alloys.

Alloys 3 and 5 gave very similar DTA traces. Comparison with interpolated values from the equivalent experimental binary alloy tests showed that :

* liquidus values agreed within two degrees
* solidus (heating) was 20°C lower
* solidus (cooling) was 10°C lower
* solid state transformations agreed within two degrees

The trace for Alloy ZA8 was similar in shape to that of the 10% aluminium, experimental binary alloy tested. More precisely :

* liquidus was exactly the same
* solidus (heating) was 9°C lower

* solidus (cooling) was 9°C lower
* solid state transformations agreed within two degrees

The shape of the trace for ZA12 was also similar to that of the 10% aluminium experimental binary alloy, except for an additional thermal arrest at just above 400°C. More precisely, when compared with the experimental alloy :

* liquidus was 4°C lower.
* solidus (heating) was 7°C lower
* solidus (cooling) was 10°C lower
* heating arrest at 406°C compared with an inflection at about the same temperature
* cooling inflection at about 402°C compared with a similar event at about 407°C
* solid state transformations agreed

The endothermic event in the commercial alloy at just above 400°C was very marked on the DTA heating trace. On the the trace for the comparable experimental alloy, there was a barely evident inflection at a similar temperature.

The trace obtained for the ZA27 alloy, shown in Figure 45, was quite different from that of the 30% aluminium binary alloy, Z30A, but was very similar to that for Z30A2CM. A detailed comparison of the results for ZA27 with those for Z30A2CM gave the following:

* liquidus was 13°C lower
* solidus (heating) was 4°C lower
* heating inflection at about 477°C, was 15°C higher
* cooling inflection at about 463°C, was the same
* cooling arrest at 383°C, was the same
* cooling arrest at 376°C, was the same
* solidus (cooling) temperature, was the same
* solid state transformation temperatures, were the same

With so many similarities in the DTA traces, it was surprising to see that the liquidus of ZA27 was 13°C lower than that of Z30A2CM. The distinct, twin arrests near the eutectic temperature, confirm the effect of the concentration of copper in the zinc-rich liquid during cooling. It is important to note that the effect was not seen in alloys containing only 1% copper.

The solidus temperature for both Alloy 3 and Alloy 5 was 20°C lower than the equivalent, experimental binary alloy. Considering impurity levels, when seeking an explanation for such a large discrepancy, the zinc and aluminium used to prepare the experimental alloys was obtained from the firm that supplied the commercial alloys for remelting. Also, it is very unlikely that possible small differences in melting and casting pratice, will affect impurity levels in this type of alloy. Based on the writer's findings, the copper in Alloy 5 may lower the liquidus, but should not affect the solidus. Thus, the significant difference, relative to solidus temperature, between the commercial alloys and the equivalent experimental alloys seems to be the magnesium content. Alloys 3 and 5 contain deliberate magnesium additions of 0.05% and 0.04%, respectively, while magnesium was not detected during the analysis of the experimental alloys. Now, magnesium in amounts much less than those quoted above, is known to have a marked effect on mechanical properties (23). The zinc-magnesium binary phase diagram (38)

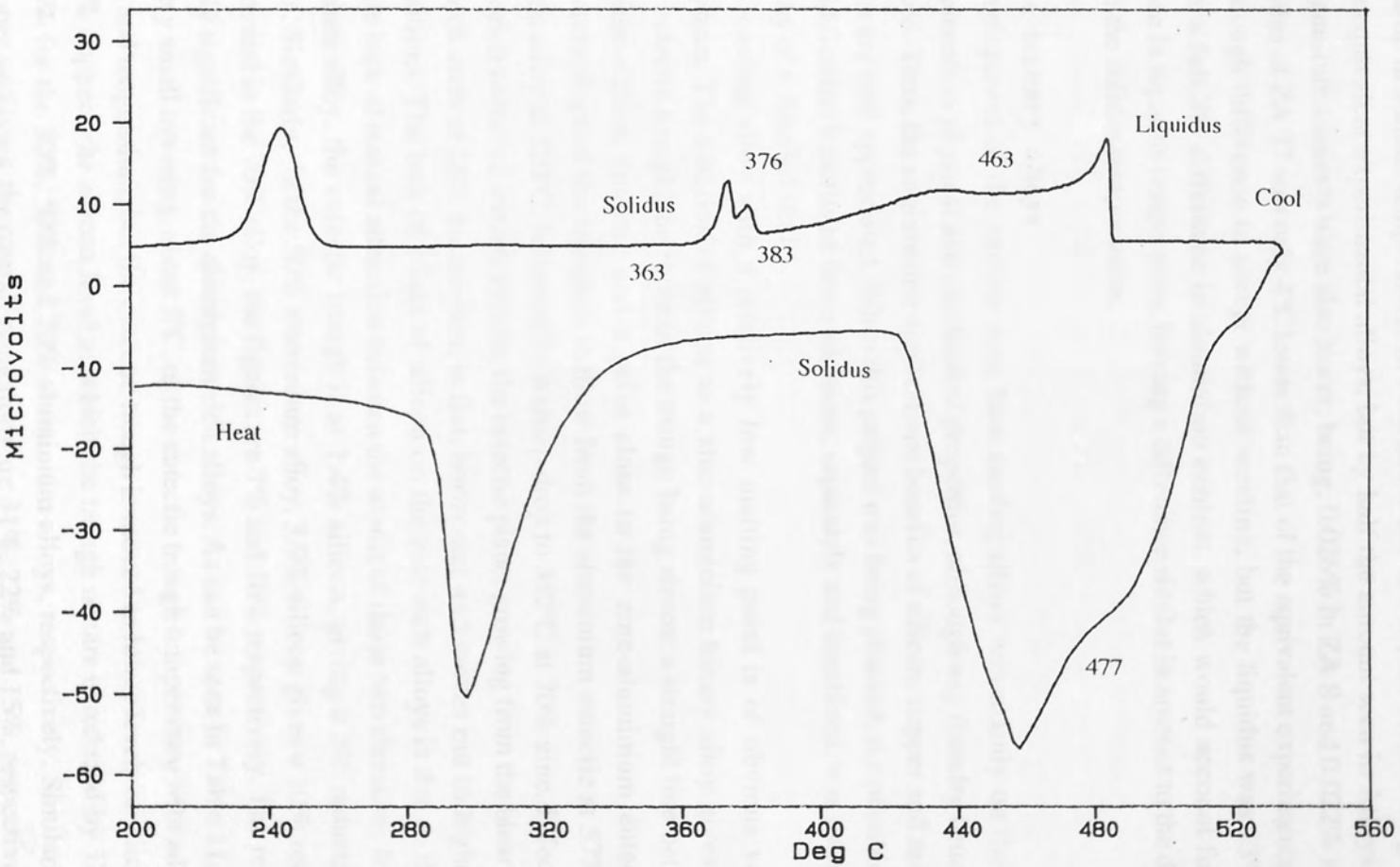

Figure 45 DTA trace for ZA27 alloy

gives the solid solubility of magnesium in zinc as 0.1% maximum, a eutectic at 3% magnesium 364°C and between 75 and 100% zinc there is a strong tendency for the formation of intermetallic compounds. Perhaps an intermetallic compound is responsible for the drop in solidus temperature. In both ZA 8 and ZA 12, the solidus is again lower than the equivalent experimental alloys, but by half the amount seen in Alloys 3 and 5. The magnesium contents were also lower, being, 0.026% in ZA 8 and 0.022% in ZA 12. The solidus of ZA 27 was only 4°C lower than that of the equivalent experimental alloy, a small enough difference to accept without scrutiny, but the liquidus was 13°C lower. There is a full 3% difference in aluminium content, which would account for an 8°C difference in liquidus temperature, leaving a difference similar in amount to the difference between the solidus temperatures.

6.3 The ternary alloys

The development of the various zinc base casting alloys was mainly on the basis of improvements in physical and mechanical properties, although any foundry benefits were publicised. Thus, the engineering applications benefits of silicon, copper and magnesium additions are well appreciated. When this project was being planned, the possible melting and solidification benefits of those additions, separately and combined, was considered to be worthy of a detailed study.

A casting alloy with a relatively low melting point is of obvious value to a foundryman. The addition of silicon to a zinc-aluminium binary alloy gives rise to a ternary eutectic trough, the route of the trough being almost a straight line between the aluminium-silicon eutectic and a point close to the zinc-aluminium eutectic. The temperature slope of the trough is shallow from the aluminium eutectic at 577°C to the 50% zinc alloy at 520°C, followed by a sharp drop to 382°C at 70% zinc. Effectively, in the zinc-rich corner of ternary system, the eutectic plane, growing from the binary eutectic line which ends at 18% aluminium, is flat, horizontal and moves out to higher silicon compositions. The lack of effect of silicon on the zinc-rich alloys is due to the almost complete lack of mutual attraction between the atoms of those two elements. In the 30% aluminium alloy, the eutectic trough is at 1.4% silicon, giving a 5% reduction in the liquidus. Similarly, in the 50% aluminium alloy, 3.9% silicon gives a 10% reduction in liquidus, and in the 70% alloy, the figures are 7% and 10% respectively. The reduction is certainly significant for the aluminium-rich alloys. As can be seen in Table 11, there is a relatively small lowering, about 5°C, of the eutectic trough temperature with additions of copper and magnesium, but the eutectic trough is moved to lower levels of silicon. Thus, with 1% copper , the silicon level at which the trough occurs is reduced by 12%, 18%, and 14% for the 30%, 50% and 70% aluminium alloys, respectively. Similarly, for the 2% copper additions, the overall reductions are 31%, 22% and 15%, respectively. There is no commercial value in these effects, due to the low cost of silicon, but there is a possible benefit in melting practice. Silicon is normally added to melts using a 50/50 aluminium - silicon alloy, but there is still a problem of ensuring complete solution of the silicon. Thus to achieve a particular objective by alloying with silicon, the less silicon required, the better from an alloy preparation viewpoint.

As mentioned earlier, the eutectic trough runs from aluminium-silicon binary at 12.6% silicon 577°C to a ternary eutectic point very close to the aluminium-zinc eutectic at 380°C and probably containing less than 0.05% silicon. The presence of a eutectic in a binary system indicates liquid immiscibility, ie repulsion of the two constituents when alloyed, and in thermodynamic terms, ΔH_{mix} is much greater than zero. Manipulating the data in Table 2, the size difference between aluminium and silicon atoms is 17% at room temperature and increases to 18.5% at 600°C, while the equivalent figures for zinc and silicon are 11% and 13% (12% at 400°C). Accepting that a size difference greater than 15% promotes incompatibility in an alloy lattice, the figures suggest a much greater likelyhood of repulsion between aluminium and silicon atoms than between those of zinc and silicon. The effect of a difference in crystal system is probably similar and minimal for each pairing, that is, FCC vs diamond and CPH vs diamond. It follows that differences in electronic structure must provide an explanation for the observed alloying behaviour. Aluminium and silicon are somewhat similar in electronic structure and on coming together, silicon contributes an extra electron per atom to the alloy lattice. Zinc and silicon are quite different in electronic structure and silicon contributes two extra electrons to the alloy lattice. The greater instability of the zinc-silicon pairing is probably due to a large increase in the configurational entropy of mixing.

Liquidus surface.

As mentioned in Chapter 2, Mey and Hack presented results for the Zn-Al-Si ternary system in a paper (40). Some of those results were also reproduced in the latest edition of the ASM Handbook (38). Care was needed when comparing the results with those of the writer, because atomic percent and K were used in the paper to represent composition and temperature respectively, but weight percent and °C in the ASM Handbook. Also, on the ternary liquidus surface projection in the ASM Handbook, the value attributed to each isotherm is in K, but labelled °C. It eventually became evident that there was good agreement between the published liquidus surface projection and that presented in Figure 31. The detailed appraisal of the region near the ternary eutectic led Mey and Hack to state that the point lies at 656.9K and 0.8722 at% zinc and 0.0006 at% silicon. Although impressed by the presumed accuracy, it is surprising that Mey and Hack make no comment about the temperature, which is several degrees higher than the widely accepted (and confirmed by the writer) value for the binary eutectic. The writer made a sketchy extrapolation of the eutectic trough in an enlarged version of Figure 31, and estimated the ternary eutectic point at a more reasonable value of about 650K. Again, accepting that the silicon content of the eutectic is very small, the suggested zinc content of 93.8 wt% is a full 1% lower than the widely accepted value for the binary eutectic, which seems unlikely, but again no comment from Mey and Hack.

Understandably, the liquidus surface from the silicon-zinc side of the phase diagram plunges very steeply from about 800°C at 5% silicon towards the 420°C level in the zinc corner. There is an important practical consequence of that feature of the ternary system. A steep liquidus slope beyond the eutectic severely limits the silicon content of any alloy being commercially developed, because of unacceptably high melting point and

long freezing range. The slope of the liquidus becomes much shallower in the 70% aluminium region of the alloy system, with little further change in slope as the composition moves towards the aluminium-silicon axis. As can be seen in Table 11, additions of copper, magnesium, have a slight effect on the liquidus slope at 30% aluminium, but no effect at 50% and 70% aluminium.

Solidification ranges.

Looking at the results for the 30% and 50% aluminium alloys, there seemed to be little effect of silicon addition on the equilibrium solidus, S_h and the continuous cooling solidus, S_c. In fact, when plotted in Figures 28, 29 and 30, for each series of alloys, the solidus lines are virtually horizontal and straight. However, in the 70% aluminium series of alloys, both solidus lines fall sharply with small additions of silicon, and undulate as silicon progressively increases. Of course, there are no fundamental reasons why the solidus lines should be horizontal or straight. During the solidification of a ternary alloy, in contrast to a binary alloy, there is still one degree of freedom when the eutectic starts to solidify and both compositional and temperature changes occur as the remaining liquid "runs down" the eutectic trough. Also, as mentioned in an earlier argument, silicon will have more effect on the solidification characteristics of the aluminium-rich alloys than on the zinc-rich alloys. Since solidification range is of particular interest, and to take account of the variations referred to above, it was decided to make comparisons on the basis of average values, near to and on either side of the eutectic trough. For the plain ternary alloys, the equilibrium solidification ranges, $L\text{-}S_h$, closely matched those of the equivalent zinc-aluminium binary alloy, with the 50% zinc alloys giving 65°C, and the other two alloy series, each giving 55°C. However, the solidification range extension on continuous cooling, $S_h - S_c$, progressively reduced as the aluminium content of the alloy increased, being, 66, 40 and 23°C, for 30%, 50% and 70% aluminium, respectively.

In each alloy series, additions of copper and magnesium, had little effect on the solidus values or the solidification range extension, with one exception. In the 70% aluminium series of alloys with 2% copper and a small amount of magnesium, as silicon increases, the solidification range extension remained constant at about 75°C, compared with about 20°C for all the other 70% aluminium based alloys. It is difficult to explain that behaviour, since, as mentioned in an earlier argument, a copper addition is expected mainly to affect the solidification characteristics of the zinc rich alloys.

As explained in Chapter 2, foundrymen were pleased to work with the original, zinc rich zinc-aluminium alloys, due to ease of handling and low processing costs. Design engineers welcomed the developments leading to alloys with higher aluminium contents, due to much improved physical and chemical properties. However, are the improved properties at the expense of good foundry behaviour and if so, does the research reported here offer possible solutions? Foundry problems with the higher aluminium alloys are not acute, because ZA 27 is widely used and the recently introduced Super Cosmal alloy (60% aluminium), is gaining in popularity. When considering the behaviour of an alloy in the foundry, melting temperature, solidification range and erosion/corrosion of equipment by the molten metal, are important. The molten high

aluminium alloys do react more with iron base moulds and handling equipment, putting up costs, but the problem is not serious (23). Only the possible attack on equipment is significant in pressure die casting, but all three are important in sand and gravity die casting. The alloy melting temperature increases with increasing aluminium content, again putting up foundry costs. Based on the writer's results, consideration could be given to the use of a silicon addition to the higher aluminium alloys, aiming to give a composition at the ternary eutectic trough and a melting point reduction of 50-70°C. A particular problem with sand and gravity die casting is underside shrinkage, which is more prevalent in alloys with long solidification ranges. As explained at the start of this section, the solidification range of ternary alloys, of compositions near to that of the eutectic trough, reduce progressively with increasing aluminium content, as demonstrated by a fall from 121°C at 30% aluminium, to 78°C at 50% aluminium. This provides further encouragement for a consideration of silicon additions to the higher aluminium commercial alloys.

6.4 Metallography

The observed structure in the binary alloy Z30A (Figure 33), correlated well with the information obtained from the DTA cooling trace. The primary α phase starting to form at 507°C was, as expected in this type of alloy, heavily cored. Within the dendrite arms was the characteristic pattern indicating the decomposition of the primary α phase on cooling to ambient temperature. This type of structure was demonstrated even more clearly in the Z50A5S sample, and will be explained in that context. Regarding the needles observed in the structure, iron is a commonly occurring impurity in both commercial purity aluminium and zinc, and needles containing iron commonly occur in the structures of these alloys. A conversion of the weight percentage composition of the needle analysed, to atomic proportions, gave the possible compound formula of $Fe_2Al_{10}Zn$. The diameter of the electron beam is of the same order as the width of the needle, so the inevitable overlap into the matrix affects the analysis result, in this case, the recorded levels of zinc and aluminium. Also, the electron beam may penetrate the needle and again incorporate elements from the matrix into the analysis. If the chemical analysis of the needle was critical, steps could have been taken to minimise the beam overlap, but in the context of this research, it was considered to be acceptable to make slight adjustments to the recorded analysis based on experience. Thus, the estimated atomic composition of the needle was $FeAl_4$. It is generally accepted by workers studying aluminium alloys, that the needles commonly seen in microstructures are an intermetallic compound with the formula $FeAl_3$. However, an intermetallic compound can exist over a range of composition, so the needle analysed by the writer, and deemed to have the composition $FeAl_4$, is almost certainly the compound frequently noted by other workers, and described as $FeAl_3$.

Again, with the alloy Z30A2S (Figures 34 and 35), the microstructural features correlated well with the information obtained from the DTA cooling trace. At the planning stage of the project, the writer was concerned about two possible problems with the melting and solidification of some of the alloys. These were, incomplete solution of

silicon during preparatory melting, and the likelihood of gravity segregation in the liquid or semi-liquid states. Considerable evidence emerged during the project to confirm that complete solution of silicon had been achieved when preparing the alloys. However, metallographic examination of the Z30A sample suggested that macro-segregation of silicon had occurred during the DTA test, to give the anomalous structure shown in Figure 34. Of the many samples examined, no other showed any sign of silicon segregation. The levels of zinc and aluminium in the analysis of the silicon needle were initially considered to be the contribution from beam overlap with the matrix, as explained above. However, a colleague (58) has observed similar levels of those metals, appearing consistently in calibrated SEM analysis of primary silicon crystals in zinc-aluminium alloys, even with special precautions taken to avoid beam overlap.

The metallographic features seen in the DTA sample of alloy Z50A5S (Figures 36 and 37), were those expected for the near equilibrium solidification of an alloy of the specified composition, and reflected the phase change indications on the DTA cooling trace. The phase contrast afforded by the back scattered image technique, again clearly demonstrated the decomposition of the primary α phase. For compositions in the central region of the constitutional diagram, aluminium and zinc atoms are miscible in the liquid state and form an ideal (or near ideal) solution, where the heat of solution, $\Delta H_{mix} = 0$. A single solid solution forms on solidification but on further cooling, atomic repulsion arises, ie $\Delta H_{mix} > 0$. A more stable form of the solid is a mixture of two solid solution phases, α' richer in aluminium and α'' richer in zinc than the original α phase. The two phases are of similar crystal structure, namely FCC, with slightly different lattice parameters. In the electron micrograph, Figure 37, the aluminium-rich α' phase appears as the black irregular lines, and the compact eutectic like pattern arises due to the restriction in diffusion distances as the temperature falls. Smallman (59), implies that a miscibility gap in a binary alloy system is caused by a size difference between the constituent atoms of greater than 15%. Table 2 shows that the size difference between aluminium and zinc atoms at room temperature is about 9% and taking into account the expansivities, the difference becomes less at higher temperatures. However, the solid state incompatibility of the zinc and aluminium atoms must be due to the considerable differences in electronic structure and the mismatch in favoured crystalline form.

Regular involvement with the behaviour of binary eutectics, can result in the misguided view that all eutectic solidification is invariant, in phase rule terms. However, when ternary eutectics solidify, the temperature falls and there is a change in composition. The coring of the α phase in the ternary eutectic was clearly illustrated in the microstructure of alloy Z70A10S, as seen at the bottom left of Figure 38. The black square shaped phase is primary silicon, and the first eutectic deposited alongside appears relatively dark, indicating a high content of aluminium. In the micrograph, moving away from the primary silicon, the eutectic becomes lighter in colour, indicating a relative increase in zinc content as the composition follows the eutectic trough with falling temperature, towards the zinc corner of the phase diagram. It is interesting to note that the angular, sometimes script like shape of the silicon in the eutectic manifests well ordered growth, demonstrating ample "room to grow" in the liquid during the solidification of this

particular alloy sample. In contrast, in the Z70A2.5S sample (no illustration presented here), the constrained growth of the eutectic gave rise to globular shaped silicon in the eutectic.

Heavily cored primary dendrites and evidence of primary α phase decomposition were seen again in the microstructure of alloy Z50A2CM1S (Figures 39 and 40). Of special interest were the adjacent phases in the centre of the field of view in Figure 40. The white phase, with an analysis of 87Zn,12Cu,1Al, was judged to be the the last liquid to solidify, ie a ternary eutectic, with the black rim indicating the rejection of aluminium from the η phase during cooling to ambient temperature. Although a substantial copper content was anticipated, the exceptionally high level is probably due to SEM beam overlap into the adjacent, copper-rich phase. Several workers, including Koster and Moeller (60) have observed that in copper-containing zinc-aluminium alloys, the copper concentrates with zinc in the last liquid to solidify. When examining copper-containing zinc-aluminium alloys, they identified an intermetallic compound with an ordered BCC structure based on the CsCl type, isomorphous with the well documented Cu_3NiAl_6 compound which they called T phase. Moeller gave a composition range for the T phase as, 56/58Cu 10/30Zn. The grey, copper rich phase in Figure 40, analysis 58Cu 27Al 15Zn, was considered to be the T phase.

A conversion of the weight percentage composition of the needle analysed in alloy Z50A2CM1S, gave the atomic proportions $Fe_2Al_{10}ZnSi$. Making allowances for beam overlap with the matrix, the estimated atomic composition of the needle is $FeAl_4$, which compares well with the observations made about the needle in the microstructure of alloy Z30A.

The microstructure of alloy Z50A2CM5S (Figures 41 and 42) was very similar to that of alloy Z50A2CM1S, described above, but there were some specific features to warrant inclusion in the results selected for presentation. Of particular interest was the multiphase region, marked **x** in Figure 42, with the analysis 81Zn 2Cu 17Al. This was judged to be the ternary eutectic identified by Koster and Moeller (60) and others working in the same field. They gave the composition as 89Zn 7Al 4Cu.

A conversion of the weight percentage composition of the needle analysed in alloy Z50A2CM5S, gave the atomic composition as $Fe_4Al_{20}Si_2Zn$. Allowing for electron beam overlap with the matrix, the atomic composition of the needle was estimated as Fe_2Al_5Si. At the level of silicon in the alloy, it would be expected to find evidence of the presence of the intermetallic compound FeSi in the microstructure. Thus, the needle analysed is considered to be a combination of FeSi and $FeAl_4$ intermetallic compounds.

Dendrite arm spacing

Although the dendrite arm spacing exercise was limited in scope, the results presented in Table 14, were sufficiently consistent to warrant analysis. In the binary system, the effect increasing aluminium content from 30% to 50% and 50% to 70%, was to give an increases in dendrite arm spacing of 50% and 15%, respectively. In the ternary system, the effect of silicon depended on whether the alloy was of hypo- or hyper-eutectic composition. In hypo-eutectic alloys, silicon reduced dendrite arm spacing by 15% at

30% aluminium, but had no effect at either 50% or 70% aluminium. In the hyper-eutectic alloys, silicon reduced dendrite arm spacing by 50% at 30% aluminium, 30% at 50% aluminium and had no effect at 70% aluminium. Regarding the effect of copper, it would be unwise to attempt a quantitative analysis with so few results, but there is evidence that in both binary and ternary alloys, a copper addition reduced the dendrite arm spacing.

The solidification front of a pure metal is planar. When an alloy starts to solidify, the front is planar but quickly becomes irregular due to the consequenses of the transverse (parallel with the front) diffusion of rejected solute atoms in the liquid. There may also be a disrupting effect from thermal gradients developing in the liquid, near the advancing front. The disruption of the front, results in a cellular mode of solidification. In the majority of cases, growth of the cells is accelerated in the direction of the advancing solidification front, producing arms which in turn begin to branch. In other words, cellular growth changes to dendritic growth. According to Porter and Easterling (8), the reasons for the change from cellular to dendritic growth are not fully understood, but it is possibly associated with the occurrence of constitutional supercooling in the liquid between the cells, causing interface instabilities. They go on to propose that the eventual dendrite arm spacing in an alloy casting, is that which reduces constitutional supercooling in the intercellular liquid to a very low level. Support for that view is offered by the observation that dendrite arm spacing decreases with increasing cooling rate, which gives less time for lateral diffusion of rejected solute atoms.

Accepting the comments of Porter and Easterling and incorporating personal perceptions in an attempt to explain the results, there are three factors which are important in the determination of dendrite arm spacing,

* the temperature at which solidification starts
* the solidification range
* the rate of cooling

In the case under consideration, the cooling rate was fixed and common to all alloys, and the solidification ranges were similar. Thus, the temperature at which solidification of the dendrites started was the main factor controlling dendrite arm spacing, the implication being, the lower the temperature the smaller the spacing. The results for the binary alloys support the proposal, since the start of solidification was 508°C for the 30% aluminium alloy, 562°C for the 50% alloy and 605°C for the 70% alloy. The results for the hyper-eutectic ternary alloys also give support, because solidification now starts with primary silicon and the dendrites of α solid solution start to form at the much lower eutectic temperature. Finally, as became clear during the DTA work on the binary system, copper addition lowers the liquidus, ie the start of solidification of the primary dendrites.

Metallographic summary

In all the microstructures examined, the formation temperatures of the phases identified could be located on the relevant DTA cooling curve. Again, in all cases, even when solidifying at the slow rate of 2°C per minute, the aluminium-rich α phase was heavily cored, both as primary and as a component of the eutectic. The cast structure became coarser, as assessed by dendrite arm spacing, as the aluminium content increased. In

general, silicon addition reduced dendrite arm spacing in the zinc rich alloys and in the 50% aluminium alloys if the resulting alloy composition was hypereutectic. Silicon addition had no effect on dendrite arm spacing of the 70% aluminium alloys. The smallest dendrite arm spacing observed was 60 μm, in the 30% aluminium 2% silicon alloy. In every case, there was evidence that the α phase had decomposed on cooling to room temperature, in accordance with the known presence of a miscibility gap in the alloy system. The fine needles observed in several samples were deemed to be an intermetallic compound of probable composition, $FeAl_4$. In the complex alloys containing 2% copper, there was evidence that copper concentrated in the zinc-rich, last liquid to solidify. In one sample, the copper rich T phase was identified and in another, a copper containing ternary eutectic phase.

6.5 Foundry experiments.

Cooling curves

The requirement was to produce cooling curves for several different types of casting, in order to gain "some idea" of the rates of temperature change at the various stages in the cooling of an ingot. Fortunately, considerable care and some expert advice were taken when designing, setting-up and executing the first experiment, namely, the 80mm diameter Kaowool insulated casting. The outcome was good and further successful experiments were done. Although the results presented in Table 12 were obtained from single experiments, performed on different days, it was considered worthwhile to go beyond the planned superficial analysis.

The combination of a Type K mineral insulated thermocouple, supported by a thin-walled stainless steel sheath, proved to be sufficiently sensitive to clearly depict thermal arrests. It was suspected that using a sheath, which was of course necessary to prevent corrosive attack from the melt, would render the system too insensitive. After each test run, it was possible to cut out the sheath from the solidified melt. There was no visible evidence of corrosion, and after a rub with fine emery paper, the sheath could be used again.

For reasons given earlier, there was limited interest in the solid phase transformations and it was assumed that an arrest would be difficult to detect on the type of cooling curve to be used. In the event, with very careful inspection of each curve, it was possible to determine the start temperatures of solid phase changes. Apart from the chill casting, the results were very consistent and in each case about 4°C above the accepted equilibrium value.

Of immediate interest in the results from the first experiment, was the surprisingly slow, 3°C per minute cooling rate recorded during the pasty stage of ingot solidification. Even so, the liquidus and solidus temperatures were both 10°C above the accepted equilibrium values. Interestingly, the Kaowool-insulated mould produced an ingot cooling rate in the pasty stage of 2°C per minute, identical to that used for the DTA experiments. The estimated liquidus and solidus temperatures were still above the accepted equilibrium values, this time by 5 and 6°C, respectively. The 40mm diameter sand casting solidified at three times the rate of the 80mm casting, with liquidus and

solidus temperatures again higher than the equilibrium values by 5 and 7°C, respectively. When molten metal is poured into a mould, heat is lost from the centre, mainly by conduction through the metal to the outer surface of the ingot, then into the mould material. A relatively small amount of heat is lost by radiation. Conduction through the metal is rapid, but the thermal gradient at the metal-mould interface is invariably steep, mainly due to the air gap created by the solidifying shrinkage. Thus, the rate of heat transfer into the mould, normally controls the rate of cooling of an ingot. When comparing the rates of cooling of two different-sized ingots of similar shape, the main factors are the heat content of the metal and the outer surface area of the ingot. In the case being considered, the heat content of the smaller ingot is one quarter of that of the larger, and the outer surface area is one half. In theory, the ratio of the cooling rates should be four to one, so the observed ratio of about three to one is reasonably explained.

The cooling rates for the chill casting, when compared with the sand castings, strikingly demonstrated the effect of a massive chill. The cooling rate in the pasty stage was almost an order of magnitude faster than that of the similar sized sand casting. Even so, the liquidus temperature was the highest recorded, at 13°C above the accepted equilibrium value. The solidus temperature was similar to that obtained from the cooling curves of the other castings, at 6°C above the accepted equilibrium value.

Comment was made in Chapter 4 about the lack of cooling rate data for ingots. However, although the size and shape of the castings do not match particularly well, it is interesting to compare the results in Table 12 with those published by Barnhurst et al (60). Barnhurst and his fellow workers did a wide ranging study on the sand casting of plates in three commercial alloys, namely, ZA8, ZA12 and ZA27. They studied how the variables of size, pouring temperature and the use of chills affected cooling rates, thermal gradients, solidification times and microstructure. Taking the results for a 1inch thick plate in alloy ZA8, using graphite chills, the cooling rate during solidification was 32 °C per minute, which compared with the 27°C per minute for the 80mm square chill casting. A similar plate with no chills, gave a cooling rate during solidification of about 10°C per minute, which compared with the 8°C per minute for the 40mm sand casting. Finally, although credibility is further stretched, Barnhurst quotes solidification times for sand cast, one inch thick plates in alloy ZA27 of about 10 minutes, which compares well with about 12 minutes for the 40mm sand casting.

Because it became clear after just two experiments that the original objective of the foundry cooling curves would be more than adequately fulfilled, it was decided not to resolve the problem of the somewhat elevated arrest temperatures. It was, however, realised that the most likely cause of the inaccuracy was the lack of sensitivity in the temperature recording. If accurate arrest temperatures had been a requirement, the millivolt scale of the recorder would have been "backed off" to take the first arrest temperature to almost a full scale deflection. A similar adjustment would subsequently be made to improve the accuracy of measurement of the lower temperature arrests.

Fluidity spirals

Good fluidity of a molten metal and the ability to completely and quickly fill a mould are

very important to a foundryman. Unfortunately, in the development of casting alloys, the prime considerations are to improve the physical and chemical properties of the product. Although the performance of a new alloy in the foundry is eventually investigated, poor fluidity is unlikely to preclude commercial use. Indeed, poor fluidity would be taken into consideration at the casting design stage and in particular, when deciding on the degree of super heat to be applied to the molten alloy prior to casting. Predicting the fluidity of a new alloy is very difficult due to the complexity of the controlling factors. The speed and efficiency of filling a mould with molten metal from a feeder head, will depend on the temperature and heat capacity of the mould, together with its volume, shape and inner surface condition. Additional critical factors related to the molten metal are, the hydrostatic head, degree of superheat, density, viscosity, surface tension and mode of solidification. Illustrating the complexity of the situation, other factors relating to the molten metal are, oxidizability and chemical and physical reactions with the mould surface.

Several Eastern European workers have derived equations, as reviewed by Korol'kov (61), to allow calculation of the fluidity of an alloy of known composition and physical properties. From these equations, the properties considered to be most relevant are:

of the mould

* temperature
* hydrostatic head
* size of feed channel

of the liquid metal

* degree of superheat
* specific heat
* density
* latent heat of fusion

Constants are included in some of the equations to account for other "thermophysical properties" of the mould and liquid metal, which are not named. As Korol'kov implies, fluidity equations have been successfully applied to alloys of similar composition, mainly ferrous, but the possibility of a generally applicable formula is very remote, due to the extreme complexity of the situation. The writer is unaware of any activity in the field, but this may be another topic for the attention of expert computer programmers.

Inevitably, the approach to the practical problem of how to compare the fluidity of different alloys, involved the development of a standard mould, standard melting and casting procedures and a means of estimating the "degree of fill" achieved by each alloy. A widely accepted mould design is a narrow channel spiral, the filled length of spiral being taken as the measure of fluidity. When comparing results from different sources, the main concerns are the degree of superheat applied to the liquid metal in each case and the type of mould used. Most workers employ a sand mould, but a preheated cast iron mould is also used.

One objective of the research was to study the effects of silicon addition on the melting and solidification characteristics of zinc-aluminium alloys. Having completed a

scientifically based investigation, it was considered necessary to make sure that the addition of silicon did not dramatically reduce fluidity. The alloys chosen for fluidity testing were from the 30% aluminium series, in order to allow a comparison of the results with those available for well established commercial alloys. As can be seen in Table 13, the results from the "siting shots" with the pure metals, zinc and aluminium, posed no problems of interpretation. Pure metals have high fluidity due to a very short freezing range (no pasty stage), and a tendency to "skin solidification", where the molten metal flows freely through the channel formed by the solid chill layer on the mould cavity surface. Compared with aluminium, zinc has the additional benefits of a much greater hydrostatic head (2.4 x density) in the feeder, and a lesser problem of oxide interference with flow.

In foundryman terms, the 20in spiral length from the 30% aluminium alloy was good fluidity, and compared well with the results of Barnhurst et al (61). An addition of 1.5% silicon had little effect on fluidity. Rather surprisingly, the addition of 2.5% silicon doubled the fluidity. With only single experimental results, allowance must be made for possible experimental error, but that would not fully account for the 22in increase in spiral length. One factor may be the much increased heat content of the higher silicon alloy, due to the 50°C higher liquidus temperature. Also, silicon is known to increase fluidity when added to aluminium.

Figure 46 was taken from an interesting book by the Russian worker, Korol'kov (62p), which is a review of research into "The casting properties of metals and alloys". In the chapter on "Fluidity of metals and alloys", much is made of the observation that the fluidity of an alloy in a binary system correlates with its position in the phase diagram. Thus, according to Korol'kov, pure metals, eutectic alloys and intermetallic compounds have high fluidity but the addition of a solute to a pure metal progressively reduces fluidity, and alloys with large freezing ranges have poor fluidity. For all the results presented, fluidity was assessed using a preheated cast iron mould and the superheat for each alloy was 5% of the liquidus temperature. For the zinc-aluminium series, the mould was preheated to 330°C. The 30% aluminium alloy gave a spiral length of 28in, somewhat longer than that achieved with the alloy Z30A, presumably due to the preheated mould. The most interesting aspect of Figure 46 is the very low fluidity of the alloys with 10%, 15% and 25% aluminium. Although the author of the publication makes explanatory comments about the results for all the other binary systems featured, he makes no reference at all to Figure 46! Do the results further confirm the unusual solidification characteristics of those alloys, due to the shallow slope of the solidus (not actually shown in the figure), or is it evidence of a peritectic reaction?

As stated earlier, the objective was to check the comparative position of the experimental alloys, rather than making an accurate determination of fluidity. Thus, it would be inappropriate to prepare a detailed discussion of the results obtained from single experiments.

Additions of copper and magnesium appear to give some improvement in fluidity. The further addition of silicon slightly reduces fluidity. But the silicon-containing complex alloys show better fluidity than the plain binary alloy.

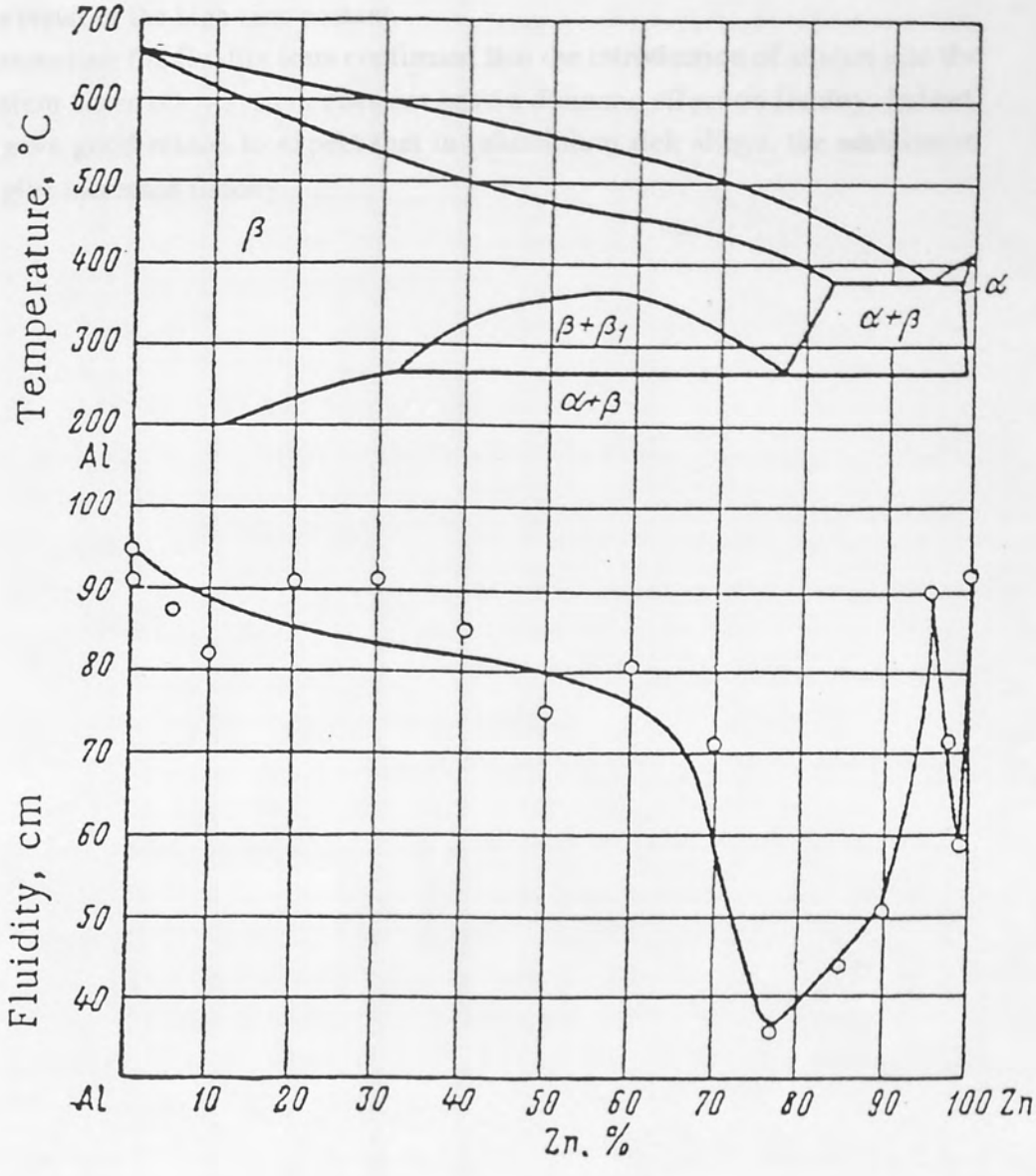

Figure 46 Effect of alloy composition on fluidity

The two commercial alloys fit well into the pattern of results with ZA 27 giving the same spiral length as the Z30A2CM alloy. Alloy 3, demonstrated particularly high fluidity, as a result of the high zinc content.

To summarise, the fluidity tests confirmed that the introduction of silicon into the 30% aluminium based alloy system does not have a dramatic effect on fluidity. Indeed, the results gave good reason to expect that in aluminium rich alloys, the addition of silicon will give increased fluidity.

7. CONCLUSIONS

1. The STA 1500 is excellent for the study of the melting and solidification characteristics of metals and alloys, using the technique of DTA, with the proviso that representative samples no greater than 200mg in weight are obtainable. Using a sample of around 90mg in weight, extremely high levels of accuracy, sensitivity and reproducibility were demonstrated. For solid state reactions, suitability is strictly limited.
2. The eutectic in the zinc-aluminium binary system occurs at 5.2% aluminium rather than 5.0% which is widely accepted.
3. The position of the eutectic trough in the zinc-aluminium-silicon system was determined, and follows a line defined by the following points, 30% Al, 1.4% Si, 482°C; 50% Al, 3.9% Si, 520°C; 70%Al, 7.1% Si, 545°C.
4. The addition of 1% copper reduces the silicon content at the eutectic trough by about 15% at each of the three aluminium levels and 2% copper reduces the silicon content at the eutectic trough by 36% at 30% aluminium, 23% at 50% aluminium and 16% at 70% aluminium.
5. A 1% copper addition has little effect on solidification characteristics of ternary alloys, but a 2% addition extends the solidification range and gives rise to the formation of copper rich, low melting point phases and compounds.
6. In all the DTA samples after solidification at 2°C per minute, the microstructure could be correlated with the data obtained from the relevant cooling curve.
7. In the copper-containing samples, there was evidence that the residual liquid became rich in copper and on solidification formed either a ternary eutectic or the T phase.
8. The dendrite arm spacing in ternary alloy samples after DTA decreased with decreasing aluminium content from 220μm at 70% to 130μm at 30%.
9. The dendrite arm spacing was directly related to the temperature at which the dendrites started to solidify, manifested by the smallest arm spacing recorded as 60μm in the 30% aluminium 2% silicon, binary alloy.
10. The cooling rates at the centre of a 1kg casting of alloy Z10A, were determined as; sand mould 3°C per minute, Kaowool insulated mould 2°C per minute and chill mould 27°C per minute.
11. Addition of 1 or 2% copper with magnesium to the 30% aluminium, ternary alloy gave an improvement in fluidity from a 20 inch to a 34 inch spiral length, and the equivalent commercial alloy, ZA27, also produced a spiral length of 34 inch.
12. Addition of 1% silicon to either of the ternary, copper-magnesium containing alloys reduced the fluidity spiral length by 5 inch.

8. SUGESTIONS FOR FUTURE WORK

1. Further experimentation with the STA 1500 to find a technique for the study of solid phase transformations, following on from the writer's exploratory work.
2. Join the world wide (mainly UK and USA) quest to determine the absolute melting points of metals. The writer was asked to contribute in 1995 with the results from zinc. The writer also has results (not reported here) for tin, copper, antimony and bismuth.
3. Explore further the effect of silicon on fluidity to include the 50% and 70% aluminium alloys.
4. Examine the effect of melt superheat on the fluidity of selected ternary alloys.
5. Check the results reported by Korolkov (60) for binary alloys, especially near the peritectic reaction.
6. Establish the present position regarding a formula for the calculation of fluidity, and if there is an opening, seek the co-operation of a computer programmer.
7. Make use of the STA 1500 in providing castings which have been subjected to controlled cooling and make a more detailed study of dendrite arm spacing.

9. REFERENCES

1. Tetrode H, Ann. Physik, 1912, 38, 434.
2. Debye P, Ann. Physik, 1912, 39, 789.
3. Mott N F, Proc Roy Soc, 1934, (146), 465.
4. Mott N F, Gurney R W, Trans Farad Soc, 1939, (35), 364.
5. Fowler R H, Guggenheim E A, Statistical Termodynamics, 1939, Cam Univ Press.
6. Gamertsfelder C, J Chem Phys, 1941, (9), 450.
7. Lumsden J, Thermodynamics of Alloys, 1952, The Institute of Metals.
8. Porter D A, Easterling K E, Phase Transformations in Metals and Alloys, 2nd Ed, 1992, Chapman and Hall.
9. Cahn R W, Nature, 1978, (273), 491-492.
10. Mackenzie J K, Mott N F, Melting and Crystal Structure, 1952, Oxford Uni Press.
11. Cotterill R J M, Kristensen W D, Jensen E J, Phil Mag, 1973, (27), 623.
12. Cotterill R J M, Kristensen W D, Jensen E J, ibid, 1975, (31), 245.
13. Frenkel J, Kinetic Theory of Liquids, 1946, Oxford Clarendon Press.
14. Gorecki T, Z Metallkunde, 1974, (65), 426.
15. Gorecki T, ibid, 1976, (67), 269
16. Gorecki T, Scripta Met, 1977, (11), 1051.
17. Fukushima, Ookawa, J Phys Soc Japan, 1955, (10), 970.
18. Ramachandrarao, Cantor, Cahn, J Mat Sci, 1977, (12), 2488.
19. Jackson K A, Liquid Metals and Solidification, 1958, Cleveland, Ohio, ASM.
20. Miller W A, Chadwick G A, 1967, Acta Met, (15), 607.
21. Dulong P L, Petit A, Ann. Chim (Phys), 1818, 7, 142.
22. Kubaschewski O, Alcock C R, Metallurgical Thermochemistry, 1979, Pergamon Pr.
23. Goodwin F E, Ponikvar A L, (Ed), Engineering Properties of Zinc Alloys, 1988, ILZRO Inc., USA.
24. Rosenhain W, Archbutt S L, Phil Trans Roy Soc, 1911, (211), 315.
25. Bauer O, Vogel R, Int Z Metall, 1916, (8), 101.
26. Hanson D, Gayler M L V, J Inst Met, 1922, (27), 267-306.
27. Tanabe T, ibid, 1924, (32), 415-453.
28. Isihara T, ibid, 1925, (33), 73-90.
29. Owen E A, Pickup L, Phil Mag, 1935, (20), 761-777.
30. Fink W L, Willey L A, Trans Inst Min Met Eng, 1936, (122), 244-265.
31. Gayler M L V, Sutherland E G, J Inst Met, 1938, (63), 123.
32. Ellwood E C, ibid, 1940, (66), 87-96.
33. Ellwood E C, ibid, 1951-2, (80), 217-224.
34. Presnyakov A A, et al, Russian J Phys Chem, 1961, (35), 6, 632-633.
35. Goldak G R, Par J G, J Inst Met, 1963-4, (92), 230-233.
36. Elliott R P, Constitution of Binary Alloys, 1965, McGraw Hill
37. Peng Q F, et al, Trans. Am Foundry Soc, 1991, 99, 199-202.
38. Alloy Phase Diagrams, 1992, Handbook Vol 3, ASM.
39. Zahra A, Zahra C Y, Ciach R, J Thermal Anal, 1983, (26), 303-305.

40. Mey S A, Hack K, Z Metalkd, 1986, (77), 7, 454-459..
41. Philips H W L, Inst Met Nom., 1959, (25).
42. St Claire Deville H, Caron H, Compt Rend Ac Sc, 1857, 45. 163.
43. St Claire Deville H, Caron H, ibid, 1863, 57. 740.
44. Winkler C, J Prakt Chem, 1864, 91, 193.
45. Vigouroux E, Compt Rend Ac Sc, 1896, (123) 115.
46. Moissan H, Siemens F, Ber deut Chem Ges, 1904, (37), 2086-2089.
47. Jette E R, Gebert E B, J Chem Phys, 1933, (1), 753-755.
48. Thurmond C D, Kowalchik M, Bell Systems Tech J, 1960, 39, 169-204.
49. Trumbore F A, ibid, 1960, (39), 205-233.
50. Charsley E L, Warrington S B, (Eds), Thermal Analysis Techniques and Applications, 1992, Special Pub, 117, Roy Soc Chem.
51. Chalmers B, Quarrell A G, (Eds), The Physical Examination of Metals, 1960, Edward Arnold.
52. Todor D N, Thermal Analysis of Minerals, 1976, Abacus Press.
53. Mackenzie R C, Farquharson K R, Cong Geol Int, Algeria, 1952, 18, 183.
54. Russell T F, J I S I, 1939, 139, 147.
55. Handford C, ibid, 178.
56. Masing G, Ternary Systems, 1944, Reinhold Pub Syst, USA.
57. Metals Data, 1992, Goodfellow, Cambridge Science Park.
58. Murphy S, private communication, 1995, Aston University.
59. Smallman R E, 1970, Modern Physical Metallurgy, Butterworths.
60. Koster W, Moeller K, Z. Metallkunde, 1947, 34, 206-207.
61. Barnhurst R J, Gervais E, Bayles F D, AFS Trans, 87th Meet, 1983, 91, 569-584.
62. Korolkov A M, Casting Properties of Metals and Alloys, 1963, Consultants Bureau, USA.

10. APPENDIX

Table 9 Chemical analyses of alloys tested.

Alloy identity	Composition wt % (rem Zn)			
	Al	Si	Cu	Mg
Z05A	0.49			
Z3A	3.02			
Z4.8A	4.81			
Z5A	4.98			
Z5.2A	5.15			
Z5.4A	5.39			
Z10A	9.98			
Z18A	18.08			
Z25A	24.72			
Z40A	39.86			
Z60A	59.57			
Z80A	80.03			
Z30A	30.0	0.01		
Z30A025S	30.2	0.26		
Z30A05S	30.1	0.55		
Z30A075S	30.1	0.81		
Z30A1S	30.0	1.11		
Z30A1.5S	29.8	1.69		
Z30A2S	29.6	2.16		
Z30A3S	29.1	3.59		
Z30A5S	28.7	5.22		
Z30A1CM	29.61	0.03	0.99	0.023
Z30A1CM025S	29.79	0.31	0.98	0.023
Z30A1CM05S	29.17	0.46	1.00	0.023
Z30A1CM1S	29.58	0.95	1.01	0.022
Z30A1CM1.5S	29.30	1.54	1.10	0.022
Z30A1CM2S	29.40	2.08	1.05	0.022
Z30A2CM	29.80	0.03	2.08	0.023
Z30A2CM025S	29.22	0.33	2.09	0.022
Z30A2CM05S	29.41	0.53	2.09	0.022
Z30A2CM1S	29.13	0.97	1.97	0.022
Z30A2CM1.5S	29.32	1.44	1.98	0.023
Z30A2CM2S	29.35	2.15	2.11	0.022

continued over page

Z50A	49.76	0.03		
Z50A1CM	49.30	0.03	0.98	0.020
Z50A1CM1S	48.94	1.07	1.01	0.020
Z50A1CM2S	48.02	1.94	0.97	0.022
Z50A1CM3S	47.61	2.95	0.97	0.021
Z50A1CM5S	46.87	5.05	0.99	0.022
Z50A1CM7.5S	45.55	7.37	1.01	0.021
Z50A1CM10S	44.42	10.01	1.00	0.022
Z50A2CM	49.34	0.03	1.94	0.022
Z50A2CM1S	49.04	0.99	2.03	0.022
Z50A2CM2S	48.80	2.01	1.95	0.020
Z50A2CM3S	48.42	2.99	2.01	0.022
Z50A2CM5S	47.52	4.78	1.98	0.024
Z50A2CM7.5S	45.46	7.35	1.93	0.022
Z50A2CM10S	43.86	10.03	1.96	0.021
Z70A1CM	68.91	0.03	1.03	0.022
Z70A1CM2.5S	67.40	2.45	1.00	0.021
Z70A1CM5S	66.19	4.85	0.98	0.020
Z70A1CM10S	62.75	10.17	1.00	0.020
Z70A1CM15S	59.70	14.64	0.99	0.019
Z70A2CM	68.86	0.06	2.00	0.020
Z70A2CM2.5S	67.63	2.45	2.00	0.021
Z70A2CM5S	65.97	4.85	1.94	0.020
Z70A2CM7.5S	64.04	7.39	1.91	0.020
Z70A2CM10S	62.72	9.76	1.93	0.020
Z70A2CM15S	60.22	15.37	2.10	0.024
Alloy 3	4.30	0.01	0.013	0.049
Alloy 5	4.18	0.01	1.08	0.040
ZA 8	8.94	0.01	1.05	0.026
ZA 12	12.94	0.11	0.78	0.022
ZA 27	26.89	0.03	2.07	0.012

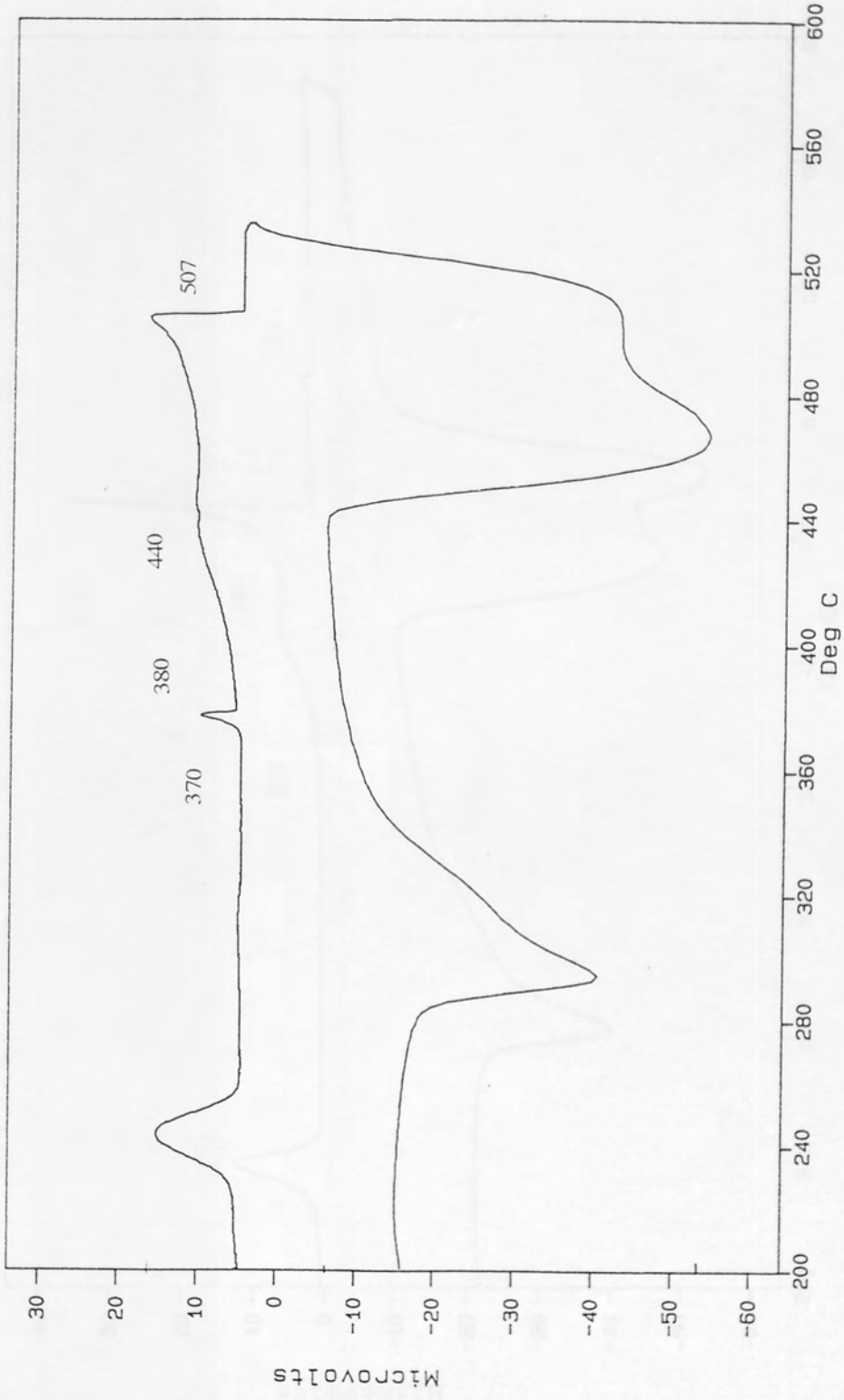

Figure A1 DTA trace for alloy Z30A.

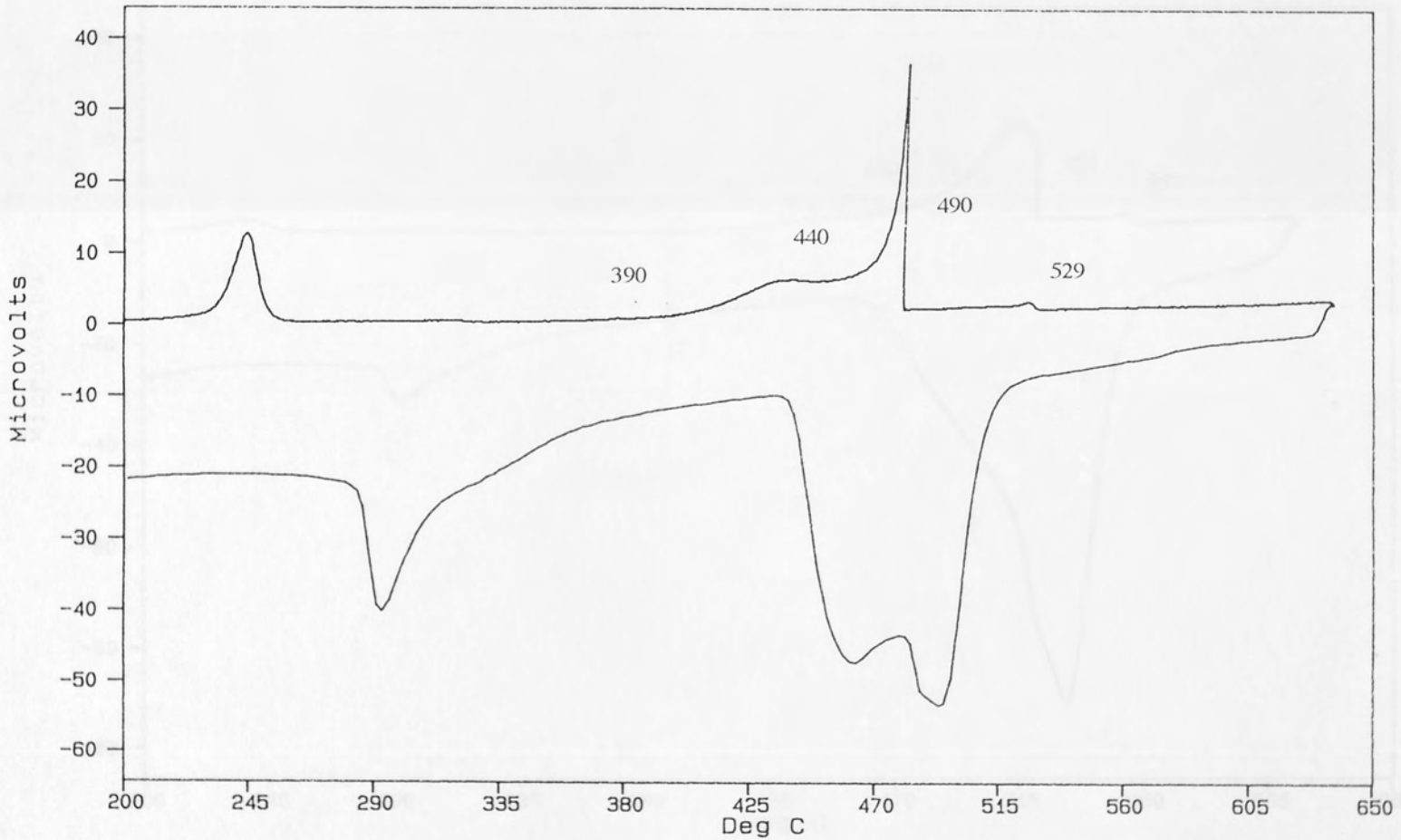

Figure A2 DTA trace for alloy Z30A2S.

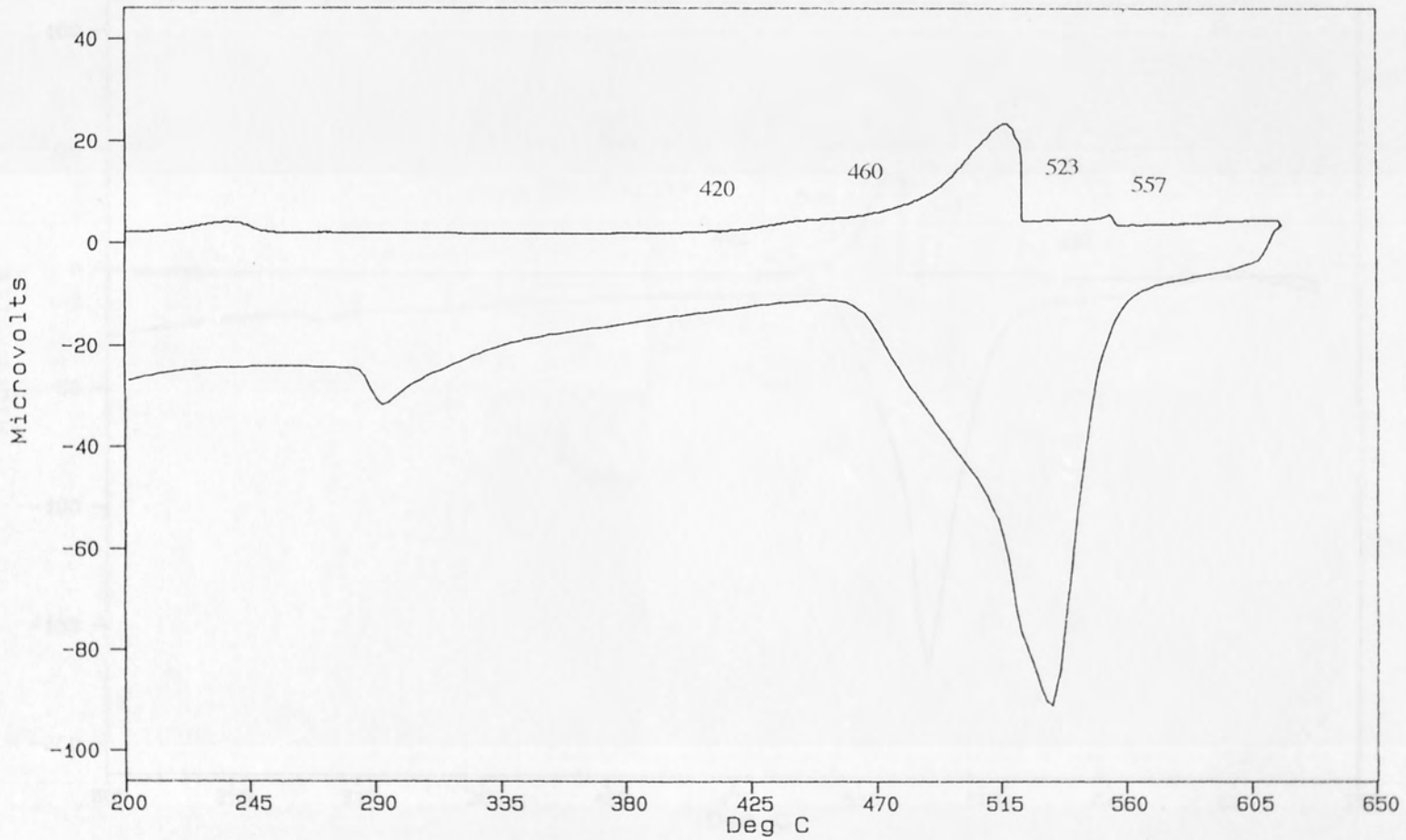

Figure A3 DTA trace for alloy Z50A5S.

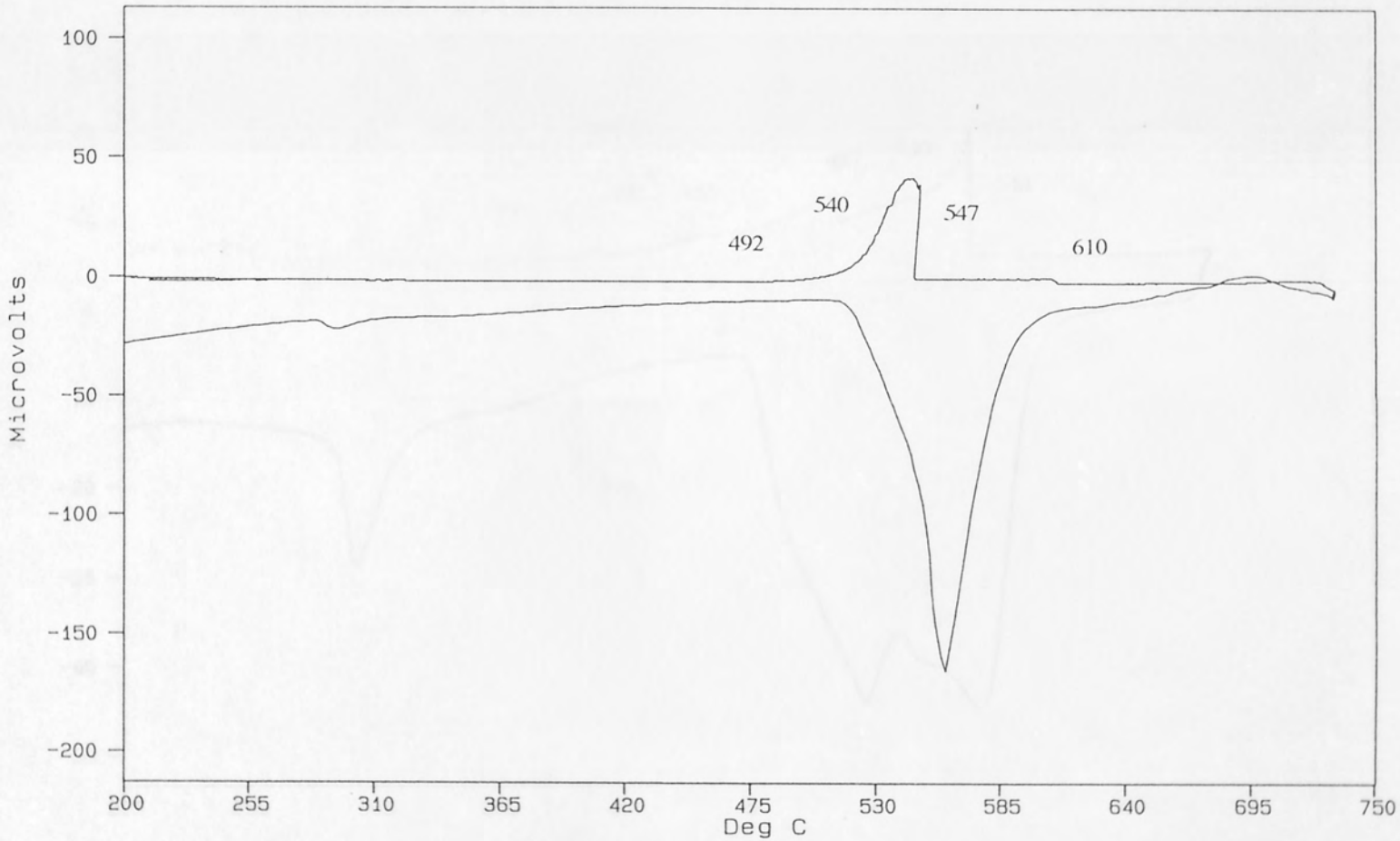

Figure A4 DTA trace for alloy Z70A10S.

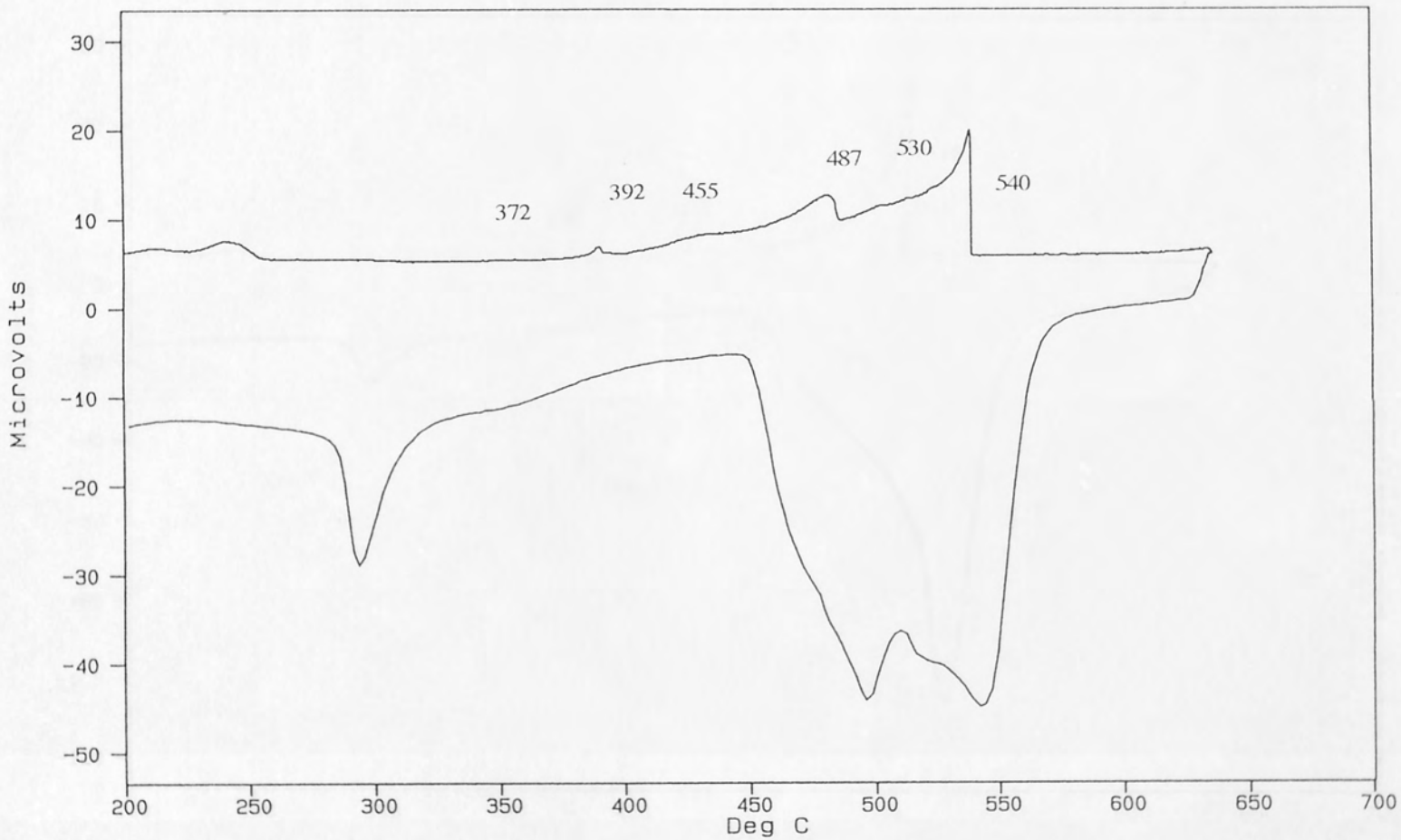

Figure A5 DTA trace for alloy Z50A2CM1S.

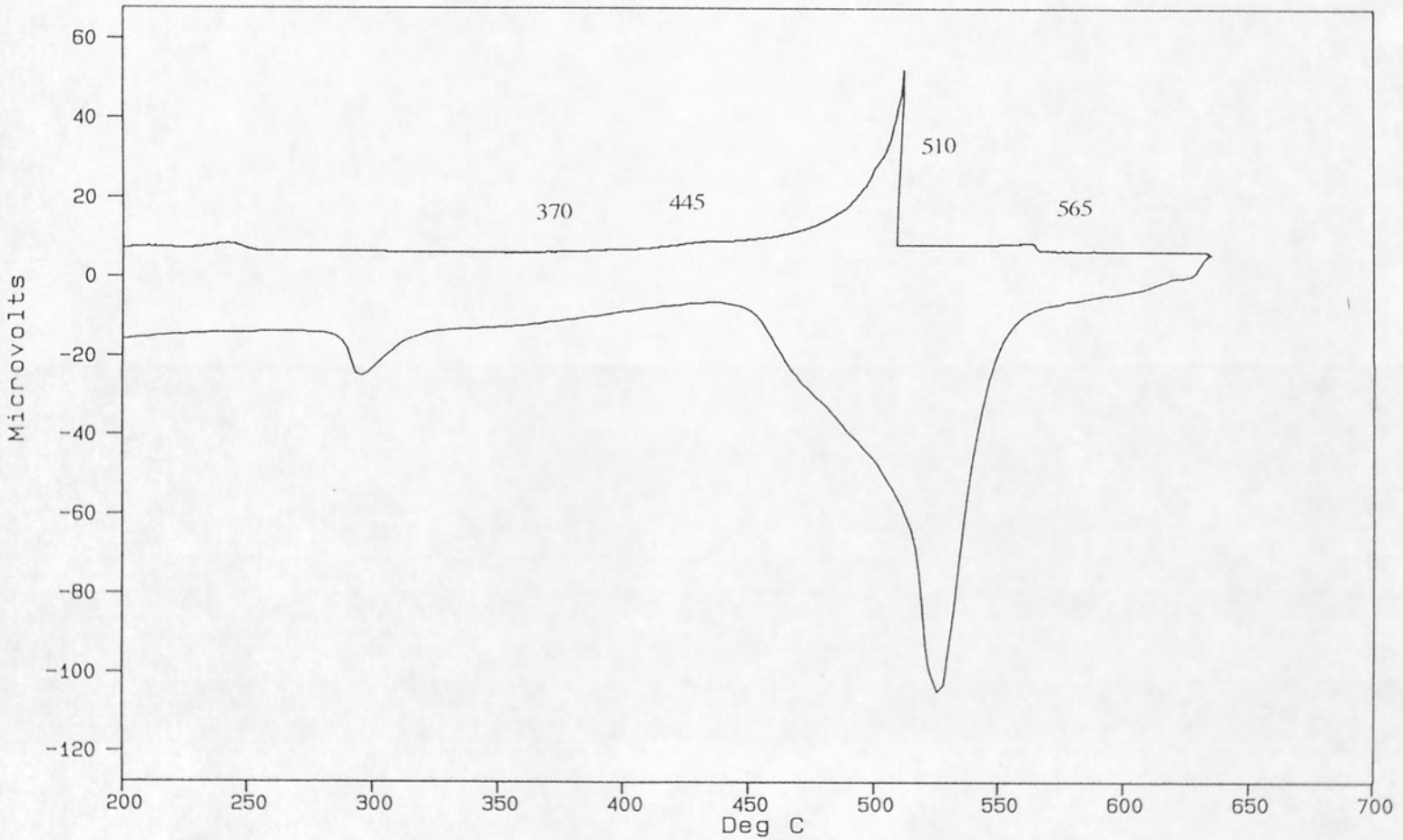

Figure A6 DTA trace for alloy Z50A2CM5S.